Theoretical and Experimental Studies of Ion Transport and Ion-Molecule Interactions

---

A thesis

submitted in partial fulfilment

of the requirements for the Degree

of

Doctor of Philosophy in Chemistry

in the

University of Canterbury

by

Richard W. Simpson

University of Canterbury

1988

The underlying physical laws necessary for the mathematical theory of a large part of physics and the whole of chemistry are thus completely known, and the difficulty is only that the exact application of these laws leads to equations much too complicated to be soluble.

Dirac (1929)

Contents

List of Tables

List of Figures

Abstract

Mobilities of positive and negative atomic ions in helium have been determined using both two- and three-temperature theories. These calculations require that an interaction potential be supplied which corresponds to the molecular ion HeX^+ or HeX^-, where X^+ or X^- is the ion of interest. The interaction potential must have the correct separation behaviour to spectroscopic states of the particles involved including ^1S He. Molecular orbital and valence bond methods have been employed to calculate interaction potentials for use in mobility calculations. A drift-tube mass spectrometer has been used for the experimental determination of ion mobilities in helium. These, and other experimental mobility data, have been compared to the calculated mobilities. The development of computer programs for mobility calculations, experimental control, data acquisition, and data analysis are described. An important feature of the ion mobility program used in this work is its ability to accept a tabulated interaction potential. This enables the result of an ab-initio calculation to be used directly in a mobility calculation. The differences between experimental measurements of the mobilities of ions of the same mass are explained in terms of differences in the ion neutral interaction potential. The mobilities of F^-, O^+, O^{+*}, B^+, N^+, F^+ and Li^+ ions in helium are calculated using the mobility program with ab-initio interaction potentials. Where two or more molecular states can arise from the spectroscopic states of helium and the ion involved, the ion mobility is determined from an average of the results of mobility calculations for each of the possible molecular states. An accurate measurement of the mobility of N^+ in helium from 35 Td to 140 Td has been made which agrees with an earlier mobility measurement. The rate constant for the reaction of positive helium ions, obtained from this work and subsequently measured independently, disagrees with previous work. Valence bond calculations are reported for a series of diatomic molecules and ions; the principal valence structures found correspond to those expected on the basis of traditional bonding theories.

The further application of the methods used and developed in this work is discussed.

Chapter 1

Introduction

The original objective of this work was to apply both experimental and theoretical methods to the development of a better understanding of gas phase ion mobility and, in particular, to the investigation of the effects of ion structure and excited ion states on gas phase ion transport. Experimental equipment, a drift tube mass spectrometer, and some quantum chemistry programs were already operational when I started, so it was logical to employ both of these techniques. This combination of experiment and theory led to a productive area of work, where the results of theoretical calculations answered questions posed by experimental measurements and *vice versa*. At the same time, an appreciation and respect of the limitations and strengths of experimental and theoretical techniques was developed.

The behaviour of ions in gases is an area of continuing interest. Models of the upper atmosphere, interstellar chemistry, lasers and many other areas of physical chemistry require quantitative information concerning the interaction between charged and neutral particles, often over a wide range of temperature or collision energy.

Experimental methods can provide the necessary data. Below about 900K, methods such as mass spectrometry, ion cyclotron resonance and flowing afterglow can provide information. At high temperatures, above 10^4K, crossed beam experiments yield results which can be unfolded to give the desired information. The energy gap between 900K and 10^4K is spanned by the results from drift tubes. However, there are limitations with experimental studies. Apart from the obvious limits on conditions, experiments may need to be modelled before the desired information can be extracted from the results, or else ambiguous or unusual results may pose further questions.

It has long been the aim of theoretical chemists to provide accurate molecular information without recourse to experimental measurements. However, this attitude has been largely superseded by a symbiotic relationship developing between theoretical and experimental chemists where the combination of diverse skills can be more informative than either approach alone. The experimental ambiguities or unknowns can be solved by theoretical methods, and

deficiencies in theoretical models are shown up by comparison with accurate experimental results.

The work described in this thesis is primarily concerned with the determination of the drift velocity, and hence mobility, of ions in drift tubes by both theoretical and experimental methods. The most successful theoretical descriptions of ion motion in a drift tube include the interaction potential that exists between a single ion and a buffer gas particle. This is the fundamental force governing the scattering collisions which occur as the ions move down the drift tube. A change in the interaction potential, if this was possible, would manifest itself as a change in the observed bulk ion drift velocity. The successful two-temperature theory by Viehland and Mason (1975, 1978) and the more accurate three-temperature theory (Lin et al., 1979) have both been used to calculate ion mobilities as a function of electric field strength (or more correctly, the electric field to gas number density ratio, E/N). Traditionally, such calculations have been limited to very simple systems, noble gas or alkali metal ions in noble gas buffers. In this work we have performed calculations of the mobilities of a variety of ions using ab-initio interaction potentials. The interaction potentials required were calculated or obtained from the literature.

Chapter 2 outlines the major developments of ion drift theory from the earliest kinetic theory, developed in the early years of this century, through to the most recent quantitative atomic ion-atomic buffer gas theory and beyond. The next two chapters describe the drift tube mass spectrometer used in the experimental work, and the computer programs developed to determine the mobility of an ion. In Chapter 5, the effect of ion structure on the measured ion mobility is discussed in terms of the results of some mobility calculations which use a model interaction potential. Following this chapter we report some accurate measurements of the mobility of N^+ in helium which helped resolve a problem posed during some theoretical calculations on the N^+-He system. Chapter 7 describes a comprehensive ab-initio study of the mobility of F^- in helium. A series of valence-bond calculations on fourteen electron diatomic molecules were performed. The results of this study, given in Chapter 8, include the principal valence structures which occur in the molecules studied. Both valence-bond and molecular orbital methods are used in Chapter 9 to calculate interaction potentials for the HeO^+ system. These are used to determine the ground and excited state mobilities of positive oxygen ions in

helium. Finally, Chapter 10 contains the results of a number of ab-initio mobility calculations for ions in helium including the first estimate of the mobility of B^+ and state-of-the art calculations for Li^+ ions in helium.

Chapter 2

Definitions and Theory of Ion Transport

2.1 Mobility

When an electric field, E, is applied to a collection of ions in a gas of uniform composition and temperature they rapidly accelerate and acquire an average velocity known as the drift velocity, v_d. This velocity is directly proportional to the magnitude of the field strength if the field is weak. The proportionality constant, K, is called the mobility of the ion:

$$v_d = K E \tag{2.1}$$

The drift velocity is a balance between the accelerating force of the field and the retarding force of collisions with buffer gas atoms or molecules and is analogous to the terminal velocity of a sky-diver. The mobility is a joint property of both the ions and the buffer gas. Ion mobilities are usually reported as a reduced mobility, K_0, (Ellis et al., 1976, 1978, 1984) defined by

$$K_0 = K \frac{p}{760} \frac{273.15}{T} = \frac{N}{N_0} K \tag{2.2}$$

where T is the buffer gas temperature and p is the gas pressure in torr. N_0 is the standard gas number density (at atmospheric pressure and 0 °C). Ion mobilities are usually reported in the units $cm^2V^{-1}s^{-1}$.

2.2 The Parameter E/N

When the field strength is raised, the mobility, K, is no longer a constant but usually depends on the ratio of the electric field strength, E, and the gas number density, N. This quantity is designated E/N and the unit normally employed is the Townsend (Td) where $1\ Td = 10^{-21}\ Vm^2$ (Huxley et al., 1966). It can be rigorously shown (McDaniel and Mason, 1973) that the reduced mobility is a function of only E/N and T for any given ion neutral system. Values of E/N below 5 Td are in the 'low field' region. This is where the energy

acquired from the field is small compared to thermal energies. When this criterion is reversed, that is, when the thermal energy is small compared with the energy the ions have acquired from the field, the field is described as 'high'. The region between these regimes is described as 'intermediate' or 'medium' field. Different theoretical treatments or approximations may be inappropriate in some of these field strength ranges (McDaniel and Mason, 1973). At low field strength the reduced mobility approaches a constant value. This can be extrapolated back to 0 Td to give the zero field reduced mobility, $K_0(0)$. Occasionally reduced mobilities have been reported as a function of the parameter E/p or E/p_0 where p_0 is the pressure 'reduced' to 0 °C:

$$p_0 = \frac{273.16}{T} p \tag{2.3}$$

If E/p_0 is given in units of $Vcm^{-1}Torr^{-1}$ then the conversion to E/N in Td units is given by

$$\frac{E}{N} = 2.828 \frac{E}{p_0} \tag{2.4}$$

2.3 Diffusion Coefficients

A localised collection of ions in a neutral gas will become dispersed by diffusion. The diffusive flow will be proportional to, but in the opposite direction to, the concentration gradient, ∇n, of the ions as described by Fick's Law of diffusion:

$$\mathbf{J} = -D \nabla n \tag{2.5}$$

Here **J** is the ionic flux density (the number of ions flowing in unit time through unit area normal to the direction of flow), n is the number density of ions, and D is the diffusion coefficient. D, like K, is a joint property of both the ions and the gas.

If a weak electric field is applied, a steady drift of the ions will occur along the direction of the field which is superimposed on the much faster thermal motion of the diffusing ions. The diffusion coefficient is directly related to the mobility in this situation (both quantities are a measure of the ease with which the ions can move through the gas) thus

$$\frac{qD}{K} = k_B T \tag{2.6}$$

Equation 2.6 is the Einstein (or Nernst-Townsend) equation; q is the ionic charge, k_B is Boltzmann's constant, and T is the gas temperature.

If the electric field is increased, the motion of the ions induced by the field becomes significant compared to thermal velocities and consequently diffusion takes place at different rates transverse and parallel (or longitudinal) to the field. The Einstein equation (2.6) is not valid in this region and the transverse and longitudinal diffusion coefficients, D_T and D_L respectively, increase rapidly. Diffusion coefficients are found to vary inversely with gas density, consequently diffusion coefficient data are usually presented as a product, DN.

2.4 Elementary Theories

2.4.1 Langevin Theory

Langevin published the first kinetic theory of gaseous ion mobility (Langevin; 1903, 1905). The mobility equation derived was

$$K = \frac{q\lambda}{m\bar{v}} \tag{2.7}$$

The mean free path length between collisions is λ, m is the mass of the ion, and $\bar{v}$ is the mean velocity. Mobility estimates using Equation 2.7 are high by a factor of four (Lin et al., 1974). This is principally due to the neglect of attractive forces acting between the charged and neutral particles. The original theoretical model was improved (Langevin, 1905) by including an inverse fourth power attraction with the original hard sphere repulsive potential. The attractive term is the point-charge - induced-dipole force. The interaction potential is described by

$$\begin{aligned} V(r) &= \infty && r \leq \sigma \\ V(r) &= \frac{-\alpha_p q^2}{8\pi\varepsilon_0 r^4} && r > \sigma \end{aligned} \tag{2.8}$$

where α_p is the neutral molecule polarisability, σ is the hard sphere radius, and ε_0 is the vacuum permittivity.

This interaction potential leads to the following expression for the mobility extrapolated to zero field strength:

$$K(0) = A(\lambda)\frac{27.1}{\sqrt{\mu\alpha_p}} \tag{2.9}$$

Here μ is the ion-neutral reduced mass in $gmol^{-1}$ and α_p is in $Å^3$. Values of the function $A(\lambda)$ have been tabulated (McDaniel, 1964). In Equation 2.9, λ is a dimensionless parameter and is not related to the path length between collisions. For the limiting case of a pure polarisation interaction potential, the Langevin theory reduces to the following expression for the mobility:

$$K(0) = \frac{13.876}{\sqrt{\mu\alpha_p}} \tag{2.10}$$

2.4.2 Free-Flight Theory

The free-flight theory by Wannier (1951, 1952, 1953) assumes the ion, in a gas subjected to an electric field, undergoes acceleration for a mean free time between collisions with gas particles. A fraction of the ions momentum is lost in each collision. A consideration of energy and momentum conservation averaged over all collisions leads to the "Wannier expression" for the mean kinetic energy, E_k, of the ions in the laboratory frame of reference as they move through a single component gas:

$$E_k = \frac{3}{2}k_BT + \frac{1}{2}mv_d^2 + \frac{1}{2}Mv_d^2 \tag{2.11}$$

Here m and M are the ion and neutral masses, respectively. The average ion energy is the sum of thermal energy, the energy the ions have acquired from the field in the direction of the field, and energy also acquired from the field by the ions but exhibited as random motion. In the centre-of-mass frame of reference the Wannier expression reduces to

$$E_{rel} = \frac{3}{2}k_BT + \frac{1}{2}Mv_d^2 \tag{2.12}$$

E_{rel} is the relative energy of the collision partners. Equation 2.12 suggests that the transport coefficients should be the same at values of T and E/N that lead to the same value of E_{rel}. It has been shown that this equation, based on a simple ion transport model, is accurate to within 10% (Viehland, 1981). Extension of the free-flight treatment to diffusion provides generalisations to the Einstein relation which agree with measured diffusion coefficients up to about 100Td

(McDaniel and Mason, 1973). The longitudinal and transverse diffusion coefficients, at field E, are given by

$$D_L(E) = D(0) + \frac{(M+3.72m)M}{3(M+1.908m)q}\frac{v_d^3}{E} \tag{2.13}$$

$$D_T(E) = D(0) + \frac{(M+m)M}{3(M+1.908m)q}\frac{v_d^3}{E} \tag{2.14}$$

Here D(0) is the zero field value obeying the Einstein relation.

2.4.3 One-Temperature Theories

Accurate treatment of ion mobilities requires solution of the Boltzmann equation. The Boltzmann equation for ions in a gas mixture is given by

$$\frac{\partial f_i}{\partial t} + v\cdot\nabla_r f_i + \frac{q}{m}E\cdot\nabla_v f_i = \sum_j \int\ldots\int [f_i(v')f_j(V_j') - f_i(v)f_j(V_j)]\, v_r\, I_s(\theta)\, d\Omega_{CM}\, d^3V_j \tag{2.15}$$

where the right hand side represents the source-sink terms due to collisions. The primes refer to velocities after collision and the summation is over all species of neutral molecules. The distribution functions, f_i and f_j, are normalised to the densities of ions and neutral molecules respectively:

$$\int f_i(v)\, d^3v = n$$
$$\int f_j(V_j)\, d^3V_j = N_j \tag{2.16}$$

The required ion drift velocity is given by

$$v_d = \frac{1}{n}\int v\, f_i(v)\, d^3v \tag{2.17}$$

However, the Boltzmann equation cannot be solved analytically.

Prior to 1975, the only satisfactory general solutions were those of Chapman and Enskog (Chapman and Cowling, 1970) and Kihara (1953) which were subsequently extended by Mason (1957). Details of the solution of the Boltzmann equation have been given (McDaniel and Mason, 1973). The Chapman-Enskog solution leads to an expression for the transport

coefficients in terms of the temperature, E/N, and the cross sections governing ion-neutral collisions. In the first approximation this reduces to

$$K = \frac{3q}{8N}\left(\frac{\pi}{2\mu k_B T}\right)^{1/2} \frac{1}{\Omega^{(1,1)}(T)} \tag{2.18}$$

where $\Omega^{(1,1)}(T)$ is the first of a family of integrals (McDaniel and Mason, 1973) that depend on the ion-neutral interaction potential.

The procedure for the solution of the Boltzmann equation involves transforming the equation into a set of coupled moment equations and then solving these coupled equations for the low order moments of interest. The one-temperature kinetic theories are so called because they use only a single temperature variable in the moment equations. One-temperature theories are accurate at low field but the power series expressions for the transport coefficients diverge at higher field strengths.

This theory has been used to fit (12,6,4) interaction potentials (Equation 2.19)

$$V(r) = \frac{\varepsilon}{2}\left[(1+\gamma)\left(\frac{r_m}{r}\right)^{12} - 4\gamma\left(\frac{r_m}{r}\right)^{6} - 3(1-\gamma)\left(\frac{r_m}{r}\right)^{4}\right] \tag{2.19}$$

to mobility data by varying the value of the three unknown quantities ε, γ, and r_m (Mason and Schamp, 1958). It has also been used in a calculation of the mobility of hydrogen ions in helium and hydrogen (Whealton et al., 1974) but the agreement with experiment, in this case, was poor.

2.4.4 Cold-Gas Kinetic Theories

At high field strengths the motion of the neutral gas molecules is negligible compared to the movement of the ions. If the thermal motions of the neutral gas molecules are totally neglected, the cold-gas approximation (Wannier, 1953), the Boltzmann equation is simplified and it is possible to accurately calculate the transport coefficients (Viehland, 1981) in this field strength region.

2.5 Monte Carlo Treatments

A computer simulation of the fate of an ion undergoing a large number of collisions with neutral gas molecules is termed a Monte Carlo study. The time intervals between collisions and the velocity changes occurring during collisions are chosen randomly from appropriate distributions. The time-averaged behaviour of the probe ion is equated with the ensemble average for the many ions in a real system to provide information on velocity distributions, diffusion coefficients, and the ion-neutral interaction potential. Theoretical details have been given by Lin and Bardsley (1977). The Monte Carlo method has been used to check the accuracy of drift theories and is a valuable complement to these methods but does not give the physical insight that the kinetic-theories provide.

2.6 Two-temperature Theory

The two-temperature theory of Viehland and Mason (1975, 1978) overcomes the high field divergence problems of the one-temperature theory. The essential difference between the one- and two-temperature theories of ion transport is the recognition, in the two-temperature theory, that the ions can have an effective temperature, T_{eff}, significantly greater than the neutral gas temperature, T:

$$\frac{3}{2}k_B T_{eff} = \frac{3}{2}k_B T + \frac{1}{2}Mv_d^2(1+\beta) \qquad (2.20)$$

The effective temperature characterises the mean ion energy in the centre of mass frame of the ions and neutrals (Freeman and Armstrong, 1985). Equation 2.20 is similar to the Wannier expression for E_{rel} (Equation 2.11) except for the correction factor β. In this theory the mobility of a swarm of atomic ions moving through a single-component atomic gas can be described, at all temperatures and field strengths, by

$$K = \frac{3q}{8N}\left(\frac{\pi}{2\mu k_B T_{eff}}\right)^{1/2}\frac{1+\alpha}{\Omega^{(1,1)}(T_{eff})} \qquad (2.21)$$

where μ is the ion-neutral reduced mass, α a second correction factor, and $\Omega^{(1,1)}(T_{eff})$ is the temperature-dependent momentum-transfer collision integral. The correction factors α and β

are normally less than 0.1 in magnitude and in the first approximation they are set to zero. The second approximation of the two-temperature theory estimates the correction factors by truncating the infinite summation expressions for these quantities after the first term (Viehland and Mason, 1978):

$$\alpha \approx \frac{m(m+M)}{(5(3m^2+M^2)+8mMA^*)}\left(\frac{10(m+M)}{5m+3MA^*}-\frac{5(m-M)+4MA^*}{m+M}\right)\frac{d\ln K}{d\ln(E/N)} \tag{2.22}$$

$$\beta \approx \frac{mM(5-2A^*)}{5(m^2+M^2)+4mMA^*}\frac{d\ln K}{d\ln(E/N)} \tag{2.23}$$

The quantities A*, B*, and C* in Equations 2.22 and 2.23 are ratios of higher order collision integrals (Hirschfelder et al., 1964):

$$A^* = \frac{\Omega^{(2,2)}(T_{eff})}{\Omega^{(1,1)}(T_{eff})}$$
$$B^* = \frac{(5\Omega^{(1,2)}(T_{eff})-4\Omega^{(1,3)}(T_{eff}))}{\Omega^{(1,1)}(T_{eff})}$$
$$C^* = \frac{\Omega^{(1,2)}(T_{eff})}{\Omega^{(1,1)}(T_{eff})} \tag{2.24}$$

The derivative in Equations 2.22 and 2.23 is given approximately by (Viehland and Mason, 1978)

$$\frac{d\ln K}{d\ln E/N} \approx \frac{(6C^*-5)(T-T_{eff})}{T_{eff}-(6C^*-5)(T-T_{eff})} \tag{2.25}$$

The collision integrals, $\Omega^{(l,s)}(T_{eff})$, that appear in the equations above are ultimately dependent on the ion-neutral interaction potential. Explicitly they are defined as (Hirschfelder et al., 1964)

$$\Omega^{(l,s)}(T_{eff}) = \frac{1}{(s+1)!}(k_B T_{eff})^{-(s+2)}\int_0^\infty E'^{(s+1)}\,Q^{(l)}(E')\exp\left(\frac{-E'}{k_B T_{eff}}\right)dE' \tag{2.26}$$

where the cross section $Q^{(l)}(E')$ is an integral of the classical deflection function $\chi(b,E')$

$$Q^{(l)}(E') = 2\pi\frac{2(1+l)}{(1+2l-(-1)^l)}\int_0^\infty [1-\cos^l\chi(b,E')]\,b\,db, \tag{2.27}$$

and b is the impact parameter, E' is the centre of mass energy and the deflection function $\chi(b,E')$ is

$$\chi(b,E') = \pi - 2b\int_{r_0}^{\infty}\left(1-\frac{b^2}{r^2}-\frac{V(r)}{E'}\right)^{-1/2}\frac{dr}{r^2} \qquad (2.28)$$

The lower integration limit r_0 in Equation 2.28 is defined as the outermost root of

$$1-\frac{b^2}{r_0^2}-\frac{V(r_0)}{E'}=0 \qquad (2.29)$$

From Equation 2.20, with β set to zero, it is clear that the two-temperature theory predicts, like the free-flight theories, that any combination of E/N and T with the same T_{eff} gives equivalent behaviour. The two-temperature theory can provide answers to most of the theoretical questions about gaseous ion transport. In the limit of low E/N the effective temperature, T_{eff}, becomes equal to the neutral gas temperature and the theory reduces to a one-temperature theory. It also has the correct limiting form at high field; becoming equivalent to a cold gas theory. The two-temperature theory is valuable because it provides accurate results for ion mobility over a wide range of E/N. However, it does suffer from some limitations. At high field strengths the convergence of the calculated mobility as a function of the level of approximation may be slow, but more seriously is the poor performance of the theory when it comes to describing ion diffusion. This latter deficiency is due to the single temperature describing the ion swarm. The diffusion coefficients are more intimately connected to the anisotropic nature of the ion swarm than ion mobilities and the use of a single ion temperature constrains the ion distribution to be isotropic.

The two-temperature theory has been used extensively to test potential functions by comparing calculated mobilities with experimental results (Gatland et al., 1977a and 1977b; Lin et al., 1979a; Lamm et al., 1981; Gatland, 1981; Viehland et al., 1981a)

2.7 Three-temperature Theory

The deficiencies of the two-temperature theory led to the development of a three-temperature kinetic theory (Lin et al., 1979b; Viehland and Lin, 1979) in which two temperature

variables are used to describe the ion temperature, both parallel, $T_{\parallel}$, and perpendicular, $T_{\perp}$, to the direction of the applied field thus allowing the ion distribution to become anisotropic. The third temperature is the temperature, T, of the neutral gas. This theory, like the one- and two-temperature theories, is based on solving the Boltzmann equation. As well as providing more acceptable estimates for the longitudinal and transverse diffusion coefficients than the two-temperature theory, the three-temperature theory has better convergence properties as the level of approximation is increased, especially for the high field ion mobility. It has been shown that the fourth approximation of this theory is of comparable accuracy to the best experimental measurements for both mobilities (1-2%) and diffusion coefficients (5-10%) (Lin et al., 1979b; Viehland and Lin, 1979). Although this theory leads to equations with no obvious physical interpretation it has been used with success to test the accuracy of proposed interaction potentials for ion neutral systems by comparing calculated transport properties with corresponding experimental quantities (Viehland and Lin, 1979; Viehland et al., 1981a; Viehland and Mason, 1984).

2.8 Direct Determination of Interaction Potentials

Both the two- and three-temperature theories described above have been used to obtain the ion-neutral interaction potential by an iterative inversion procedure using the experimental mobility (Viehland et al., 1976a and 1976b; Gatland et al., 1977a; Maitland et al., 1978; Gatland et al., 1978; Lamm et al., 1981; Viehland and Mason, 1981; Viehland, 1983; Kirkpatrick and Viehland, 1985). This method of obtaining an interaction potential does not presuppose any particular functional form. Each mobility measurement, $(E/N,K_0)$, is inverted to give a single point on the interaction potential, (r,V(r)). The basic assumption is that at any given electric field strength the collision scattering angle is largely determined by the interaction potential over a very small range of internuclear separation. The main limitation of this method is that very accurate mobility data is required, usually within 2%, to enable an interaction potential accurate to within 10% to be calculated. The other drawback is that the interaction potential obtained is often over a restricted range of internuclear separation corresponding to the possibly limited range of E/N at which mobilities were measured. This means that the potential

obtained cannot be used with confidence to predict the mobility outside the range of experimental measurements. However, the results of this procedure provide a valuable source of interaction potential data against which comparisons with ab-initio or otherwise determined interaction potentials can be compared.

2.9 Polyatomic Drift Theories

Theoretical analysis of molecular ion-neutral systems is more complex than atomic systems due to the presence of anisotropic interaction potentials and the possibility of energy being held in internal degrees of freedom. Early work (Mason et al., 1972) suggested a (12-4) displaced centre potential could represent the interaction of polyatomic ions with neutral molecules, thus:

$$V(r) = \frac{\varepsilon}{2}\left\{\left(\frac{r_m-a}{r-a}\right)^{12} - 3\left(\frac{r_m-a}{r-a}\right)^{4}\right\} \qquad (2.30)$$

where a is a rigid core. Other early attempts to understand polyatomic mobilities also attempted to rationalise experimental observations in terms of ionic size by comparison with the Langevin theory hard sphere predictions (Patterson, 1972; Lin et al., 1974).

Drift theories for polyatomic ion-neutral systems must be similar to atomic ion-neutral theories since the fundamental processes which occur are the same. An extension of the successful two- or three-temperature theories for atomic systems to polyatomic systems is therefore desirable. The Wang Chang, Uhlenbeck and de Boer equation (Wang Chang et al., 1964) is a generalisation of the Boltzmann equation for particles with internal degrees of freedom and can also account for inelastic collisions. It is the starting point for quantitative drift theories for polyatomic ion-neutral systems. However, theoretical progress in this area has been hampered by the difficulty in calculating the collision cross sections required for anisotropic interaction potentials and in estimating the energy contained in internal degrees of freedom. The first semi-classical kinetic theory of polyatomic ion mobilities was due to Viehland et al. (1981b) and was an alternative to time consuming classical trajectory studies. This theory is analogous to the two-temperature theory and leads to very similar equations for the ion temperature and mobility:

$$\frac{3}{2}k_B T'_{eff}\left(1+\frac{M\xi}{m}\right)=\frac{3}{2}k_B T+\frac{1}{2}Mv_d^2 \qquad (2.31)$$

$$K=\frac{3q}{8N}\left(\frac{\pi}{2\mu k_B T'_{eff}}\right)^{1/2}\frac{1}{\Omega'(T'_{eff})} \qquad (2.32)$$

In Equation 2.32 ξ characterises the fraction of energy lost to inelastic collisions and can be expressed as a dimensionless ratio of the collision integral for inelastic energy loss to that for momentum transfer. The collision integral in Equation 2.32, $\Omega'(T'_{eff})$, accounts for inelastic collision processes occurring with an anisotropic interaction potential.

The most recent drift theory for polyatomic ion-neutral systems (Viehland, 1986) is a rigorous classical treatment of non-vibrating (rigid-rotor) diatomic ions in atomic gases and the similar system of atomic ions drifting in a non-vibrating gas.

There have, as yet, been no quantitative calculations performed using any of these polyatomic theories.

Chapter 3

Experimental Apparatus and Procedure

3.1 The Drift Tube Mass Spectrometer

The drift-tube mass spectrometer (DTMS) used in this study has been described previously (Harland and McIntosh; 1983 and 1984; McIntosh, 1984) and is similar to the Georgia Institute of Technology drift tube (McDaniel and Mason, 1973). Briefly, the drift tube comprises eleven 1 cm gold-plated interlocking drift rings 5 cm in diameter enclosed in a temperature-controlled envelope. A movable electron impact ion source, which uses an electron-beam control grid and a two element plane lens, is enclosed in a stainless steel sleeve which is electrically biased according to its position within the drift tube. During operation the drift tube is pressurised with 0.2-0.5 Torr (27-67 Pa) of helium containing 0.04-1.0% of the sample of interest. He^+ ions formed in the helium buffer gas by 80 eV electron pulses of 2 μs duration, undergo dissociative charge transfer with the trace component. The resulting ions drift out of the ion source under the influence of an applied uniform electric field. The strength of this field is determined by the ratio E/N, where E is the electric field gradient in Vm^{-1} and N is the particle density in the drift tube in m^{-3}. After drifting from the movable ion source, down the field gradient, to the end of the drift tube they are gated before passing into a second vacuum chamber for mass analysis by an Extranuclear model 4-270-9 quadrupole mass filter and detected by pulse counting; the ions are sampled at 1 μs intervals and the mass-selected ion pulses accumulated for repeated scans. Total counting times per increment are typically 30-60 s The resulting arrival-time distribution of the ions is used to obtain the average drift time or provides the experimental data to which modelling calculations of arrival time distributions can be compared. A discussion of the theoretical modelling of the arrival time distribution is given in Section 4.3 of this chapter. The drift velocity of the ion being studied can be determined at each value of E/N by finding the slope of a mean drift time versus drift distance graph. Typically, eight to ten drift distances are used for each value of E/N. Electron and ion gatings

are achieved by the application of square-wave voltage pulses to override small blocking bias voltages on the electron beam control grid and the ion exit control grid. Figure 3.1 is a schematic diagram of the drift tube mass spectrometer used in this study:

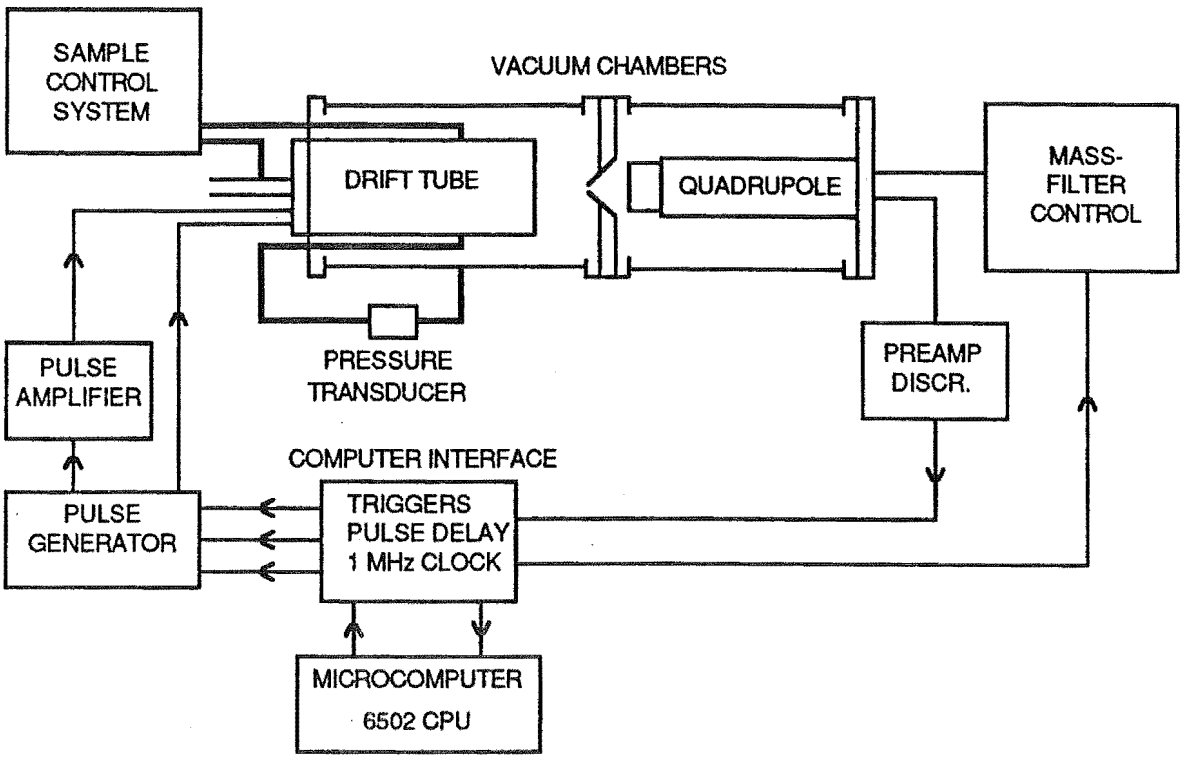

Figure 3.1 Schematic diagram of the computer-controlled drift tube mass spectrometer.

All the materials used to construct the drift tube were ultra-high vacuum (UHV) compatible. The two vacuum chambers were both 15 cm Varian stainless steel crosses sealed using Conflat flanges with copper gaskets. The chambers were partitioned by a gold plated skimmer. A 2 mm diameter orifice in the skimmer, positioned about 10 mm from the end of the drift tube, allowed particles to travel between chambers. The skimmer is insulated electrically from its support. Both chambers are pumped by 2000 $l s^{-1}$ (for helium) Varian 183-VHS-4 10 cm diffusion pumps using DC705 silicone oil, and separated from the chambers by liquid nitrogen traps (cryo-baffles). The vacuum chambers may be sealed from the pumps by Temescal gate valves. The mass spectrometer chamber backing pump is an Edwards EDM20 pump (300 $l min^{-1}$) and the drift tube chamber is backed by a 350 $l min^{-1}$ Ulvac rotary pump. A machine drawing of the drift tube is given in Figure 3.2.

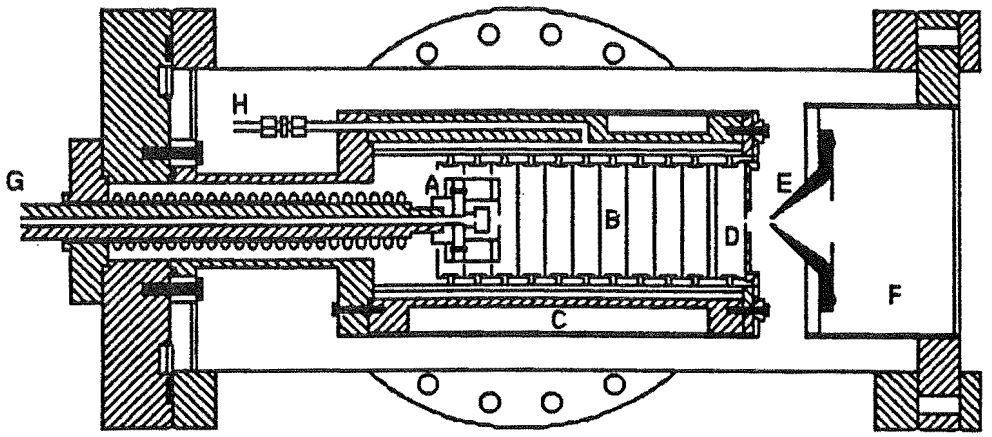

Figure 3.2 Machine drawing of the drift tube. A, movable ion source supported on a threaded rod; B, gold plated drift rings; C, drift tube vacuum envelope; D, gold plated ion exit plate; E, skimmer placed before the quadrupole assembly; F, mass spectrometer chamber; G, linear drive shaft for the ion source; and H, one of two diametrically opposite sample lines used for gas admission to the drift tube and drift tube pressure measurement.

The motor driven threaded support rod for the ion source may be used to position the ion source within the drift tube to better than ±0.1 mm by rotating a wheel on the end of the support assembly. A stainless steel bellows maintains the vacuum during the motion of the ion source. The whole ion source assembly, including the support rod and bellows may be removed from the drift tube for servicing by unbolting the small external flange. The seal between this flange and the main flange is maintained by a 1.0 mm diameter pure tin gasket. The movable ion source eliminated the so called 'end-effect' error which is always present in drift tubes having a fixed drift length. This error is a consequence of unknown electric field behaviour at the ion source and the exit orifice. The outer envelope of the drift tube, C, contains channels for water circulation which provide temperature control. Also, two embedded heaters enable the drift tube to be baked, if required, to outgas water and other impurities. Sample admittance and pressure monitoring tubes also pass through the envelope and open into the drift tube. The drift tube pressure is measured with an MKS Baratron capacitance manometer (310BM-10) with a 10 Torr head. The ring assembly, B, consists of

eleven 1cm gold plated stainless steel rings of 5cm internal diameter separated by ground glass ceramic insulators. The rings are interconnected by 1% tolerance 100 kΩ resistors. The gold plated exit plate is insulated from the drift tube envelope by a teflon disk. The potential between the exit plate and the final ring is half the potential drop between adjacent rings. The total voltage drop, V_r, across the ring assembly is given by

$$V_r = 10.5\ E \tag{3.1}$$

where E is the electric field required inside the drift tube in Vcm^{-1}. A 15 mm diameter molybdenum disc is recessed into the exit plate through which there is a 0.25 mm ion exit aperture. This is covered by a grid of 90% transmission, gold plated copper, electroformed mesh. A small bias, of opposite polarity to the ions, on this grid prevents the passage of ions from the drift tube providing the necessary ion gating facility for ion arrival time acquisition. Ions are formed in the ion source by impact of thermionically emitted electrons travelling perpendicular to the drift tube axis. The filament is spot welded onto molybdenum rods, housed inside a stainless steel shield and separated from the collision chamber by a grid and a mica insulator. An appropriate bias voltage on the grid enables it to be used as a control gate for the electron beam. The ion source is electronically insulated from the supporting rod by a glass ceramic spacer. The ion source has an electron trap for monitoring the electron current traversing the collision chamber, and two lenses for extracting the ions. The entire source is enclosed in a stainless steel sleeve maintained at a potential, V_t, which is proportional to its position along the electric field inside the drift tube:

$$V_t = E\ z \tag{3.2}$$

Here z is the distance from the sleeve to the exit plate. The gas temperature inside the drift tube is monitored by three thermocouples which are attached to the ninth ring (from the bellows end) of the drift tube, in the drift tube gas space, and on the drift tube envelope. These generally agree to within 1-2 °C. With the filament operating close to the ninth ring a localised heating of approximately 2 °C is observed. The voltages required for the correct field conditions are supplied by regulated power supplies.

During operation, typical pressures within the drift tube and quadrupole vacuum chambers were of the order of 10^{-7} Torr and 10^{-8} Torr respectively. The water moderated temperature inside the drift tube was usually close to 300 K.

3.2 The Computer, Computer Interface and Data Processing

The 6502 based microcomputer was originally an Ohio Scientific C1P but during this work was replaced by an APPLE II+ which was a more versatile machine in terms of graphics capabilities and disk operating system but had a slightly different clock speed of 1.023 MHz compared with the 1 MHz clock in the previous computer. The interface between the microcomputer and the drift tube mass spectrometer consists of six 6821 peripheral interface adaptors (PIAs) providing twelve 8-bit I/O ports. Three of these are used to provide a 24-bit counter to register the ion pulses. Another half PIA uses two bits to reset and latch the counter and two bits to control a pulse generator. A further two bits are combined with another half PIA to control a 10-bit D/A converter for use as a mass programmer. The last PIA is used to control two 8-bit D/A converters, and two 8-bit A/D converters. The interface system is shown schematically in Figure 3.3.

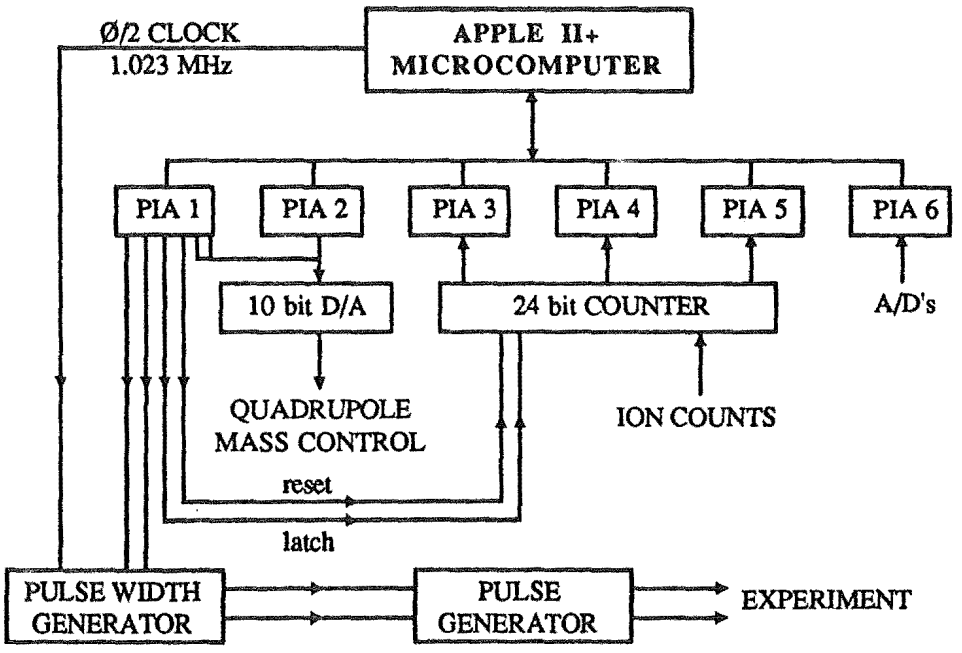

Figure 3.3 Schematic diagram of the computer interface system.

The triggering and synchronisation of the pulses and the collection of the ion counts is controlled by the computer using the program ATD. A discussion of this program and the associated machine code program, PULSEMC, is given in Chapter 4 and the programs are listed in Appendix B. Briefly, the program initiates the generation of TTL pulses from the computer which are converted into floating, variable width and height, positive or negative going, square-wave voltages which control the ion source control grid and the exit plate of the drift tube. The second pulse is delayed with respect to the first by a machine code delay of between 6 and 300 clock cycles. The computer is also used to issue reset- and latch-pulses to the ion counter and to read in the number of ion counts received. By varying the time between pulses and recording the ion signal as a function of drift time it is possible to build up an arrival time distribution. The microcomputer has other tasks to perform during the measurement of the mobility of an ion in the drift tube. As well as saving the experimental data on disk for subsequent analysis, it calculates the voltages required along the drift rings, at the ion source and at the exit orifice. This gives the required electric field gradient corresponding to the value of E/N at which the mobility is to be measured.

3.3 Gas Handling System and Materials

A schematic diagram of the high vacuum gas handling line used to purify, transfer and mix gases is given in Figure 3.4.

The line is evacuated by a 75 $l$min^{-1} Alcatel rotary pump backing a CVC 2.5 cm water cooled oil diffusion pump. A liquid nitrogen trap is used to prevent backstreaming of oil and to assist the removal of condensables. The pressure obtained in the main manifold is approximately 1×10^{-5} Torr. The sample bulbs and their associated connecting lines may be divided into two independent sections. Each section has its own pumping lines, attachment points for bulbs or cylinders, and a line to an MKS Baratron capacitance manometer, type 221AH-A-1000. This pressure gauge has a total pressure range of 1000 mbar. The attachment points are Quickfit ground glass fittings into which vials of liquid, additional gas bulbs, or gas cylinders may be fitted for the preparation of gas samples.

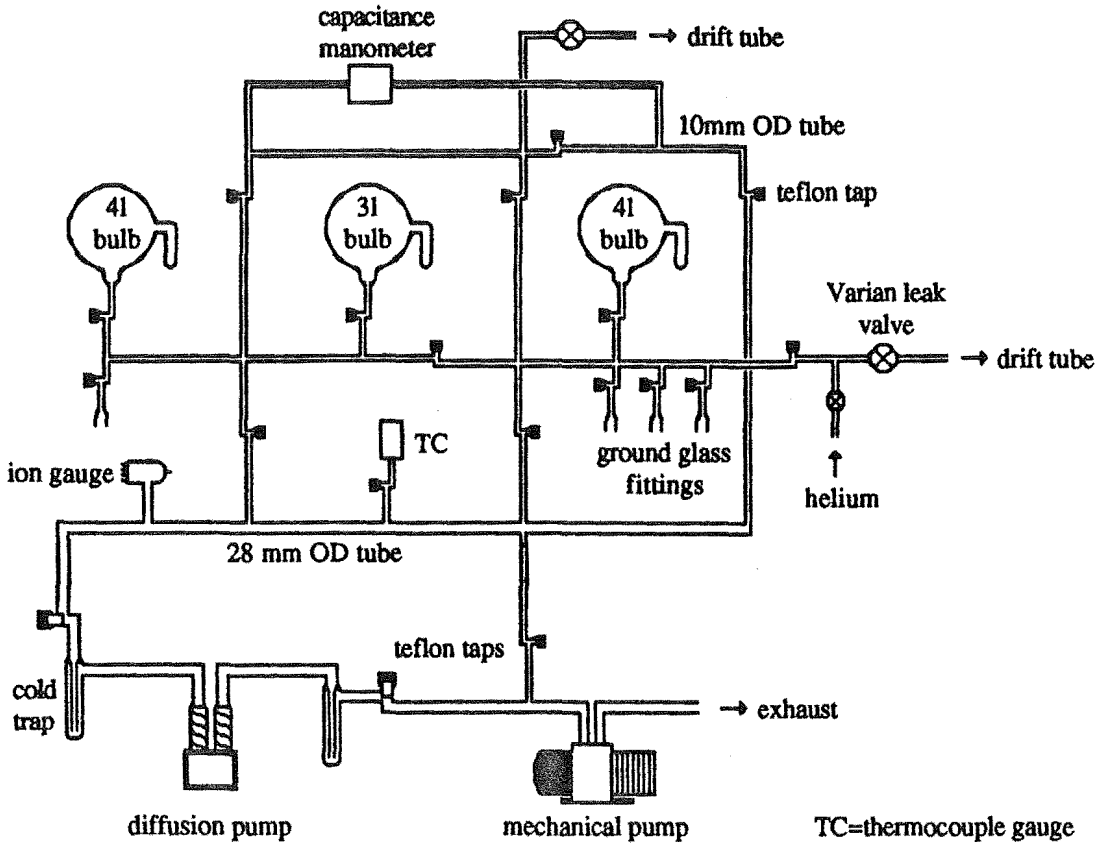

Figure 3.4 Gas handling system for the drift tube mass spectrometer.

The dilute gas mixtures of the sample of interest in helium were prepared on the vacuum line using the capacitance manometer to measure the required partial pressures in the following way. The evacuated bulb is flushed two or three times with helium, evacuating after each time, then the trace gas sample is added into the sample bulb to the desired pressure (2-10 mbar). The bulb is then sealed and the remaining trace gas in the line is pumped away. The helium buffer gas is then admitted to the line, to a pressure of several hundred millibars, before the tap to the sample bulb is opened slightly allowing the buffer gas in, but preventing the trace gas from diffusing out. As the helium in the line is consumed it is replenished until the total pressure in the line and bulb is 1000 mbar. The bulb is then sealed and the buffer gas in the line pumped away. Mixtures are left for several hours to ensure homogeneity before use. The gas mixture is admitted to the drift tube through a Varian variable leak valve (951-5106). This valve must be progressively opened during the course of the experiment to compensate for the diminishing sample gas pressure. Pressures in the drift tube can be maintained to within ±0.05%.

The helium gas used was commercial scientific grade with a purity of >99.995%. No impurities that could have unambiguously come from this helium were ever detected using the drift tube mass spectrometer. Commercial oxygen free nitrogen was dried by passing through a liquid nitrogen trap containing molecular sieves. Dimethyl ether was prepared by the reaction of 98% sulphuric acid on methanol at 135°C and the product purified by vacuum distillation. Ethylene oxide and acetaldehyde were vacuum distilled from B.D.H. reagent grade products. Spectroscopic-grade ethanol was used without further purification.

3.4 Modelling Arrival Time Distributions

The interpretation of the experimental arrival time distribution (ATD) is aided considerably by comparison with a calculated distribution. Ionic motion in drift tubes has been analysed mathematically by McDaniel and Mason (1973). This analysis, given a particular set of boundary conditions, leads to equations for the time evolution of the macroscopically observable ion distribution . The boundary conditions reflect the experimental apparatus, the initial distribution of the ions immediately after leaving the ion source, and the position where the ion density as a function of time is sampled. The transport equation obtained contains terms for longitudinal and transverse diffusion, and allows for reaction. The expressions used here are those derived for the Georgia Institute of Technology drift tube (Moseley et al., 1969; McDaniel and Mason, 1973. The Georgia Institute of Technology drift tube is constructed and operated in a similar manner to the instrument used in the present work. McDaniel and Mason's analysis (1973) has been extended to secondary ions (Snuggs et al., 1971) which are formed by charge transfer from primary ions. The unknown drift velocity in these equations may be determined by treating it as a parameter that is to be varied until the agreement between the calculated and experimental ATDs is satisfactory.

An expression for the number density of primary ions sampled on the drift tube axis, after passing through an exit aperture of area, a, as a function of time, t, and drift distance, z, is given by

$$n_A(z,t) = \frac{sa}{4(\pi D_L t)}\left(v_d+\frac{z}{t}\right) \exp\left[-\alpha t - \frac{(z-v_d t)^2}{4D_L t}\right] \left[1-\exp\left(\frac{-r_o^2}{4D_T t}\right)\right] \qquad (3.3)$$

All the ions are assumed to be introduced as a delta function burst with initial uniform surface density, s, through the ion entrance aperture of radius, r_o. No ions are produced by reaction in the drift space although some are lost by reaction with frequency α. The reaction frequency, α, is given by $\alpha=kN_r$ where k is a second order rate coefficient and N_r is the number density of the neutral reactant. The longitudinal and transverse diffusion coefficients, D_L and D_T, may be estimated by using the generalised Einstein relationships (Equations 2.13 and 2.14 respectively). From Equation 3.3 the drift velocity, v_d, of the primary ion can be found by comparing the calculated and experimental arrival time distributions. A thorough study of this equation in comparison with experimental measurements (McIntosh, 1984) has shown that, for most purposes, primary ion mobilities can be determined correctly from the slope of a plot of the mean drift time, $\bar{t}$, versus drift distance, z.

Solution of the transport equation (Snuggs et al., 1971) for secondary ions leads to the following expression for the number density of secondary ions sampled on the axis of the drift tube as a function of drift distance, z, and drift time, t:

$$n_B(z,t) = s\alpha_A \int_o^t \pi b^{-1/2} \exp\left[-d-\frac{(z-c)^2}{b}\right]\left[1-\exp\left(\frac{-r_o^2}{a}\right)\right] du \qquad (3.4)$$

The quantities a, b, c, and d are defined by the equations

$$a = 4D_{TA}t - 4(D_{TA} - D_{TB})\,u \qquad (3.5a)$$

$$b = 4D_{LA}t - 4(D_{LA} - D_{LB})\,u \qquad (3.5b)$$

$$c = v_{dA}t - (v_{dA} - v_{dB})\,u \qquad (3.5c)$$

$$d = \alpha_A t - (\alpha_A - \alpha_B)\,u \qquad (3.5d)$$

where D_{TA}, D_{LA}, and v_{dA} are the values of D_T, D_L, and v_d for the primary ion. Similar definitions apply for the secondary ion parameters. The primary and secondary ion depleting reaction frequencies are given by α_A and α_B respectively. All the other symbols are defined as for Equation 3.3.

Chapter 4.

Computer Program Development.

4.1 Two-Temperature Theory Program - TT.F77

The two-temperature theory described in Chapter 2 has been incorporated into a computer program. A listing of the sub-programs for the interaction potential fitting, and testing as well as the first and second approximation calculations, are given, with comments, in Appendix B.

4.1.1 Collision Integral Calculation

The main computational task in programming the two-temperature theory is the evaluation of the sometimes badly behaved collision integrals, $\Omega^{(l,s)}(T_{eff})$. A computer program, ACQN, to evaluate the closely related reduced collision integrals, $\Omega^{(l,s)*}(T^*)$ (O'Hara and Smith, 1970, 1971), was obtained from the authors and implemented on a PR1ME 750 computer. The adaptations suggested by Neufeld and Aziz (1971) were applied to the program. The main feature of these changes is the conversion from single to double precision variables to improve the accuracy of the collision integral calculation. I had written a similar program to solve the simpler case of collision integrals arising from a purely repulsive interaction potential; this class of interaction potentials is a subset of the interaction potentials that the O'Hara-Smith program can accommodate. The reduced collision integrals are multiplied by the quantity πr_m^2 to convert them to the required collision integrals:

$$\Omega^{(l,s)}(T_{eff}) = \pi r_m^2 \, \Omega^{(l,s)*}(T^*) \tag{4.1}$$

The reduced temperature, T^*, is related to the effective temperature by another simple relation:

$$T^* = \frac{1}{\varepsilon} k_B T_{eff} \tag{4.2}$$

The quantities r_m and ε have units of distance and energy respectively. It can be shown that the collision integrals, $\Omega^{(l,s)}(T_{eff})$, are independent of the values taken by these scale factors. The

triple integral expression for the reduced collision integrals is very similar to the equations given in Chapter 2 for the unreduced collision integrals. However, the interaction potential is replaced by a dimensionless interaction potential, V*(r*), defined by Equations 4.3 and 4.4:

$$V^*(r^*) = \frac{1}{\epsilon} V(r) \tag{4.3}$$

$$r^* = \frac{r}{r_m} \tag{4.4}$$

The limits on the interaction potential, V*(r*), required by the program, are that

(i) V(r) is continuous and differentiable on the interval $0 < r < \infty$

(ii) V(r) has at most one smooth minimum

(iii) $\lim_{r \to 0} V(r) = \infty$; repulsive at short range

(iv) $\lim_{r \to \infty} r^2 V(r) = 0$; V(r) tends to zero faster than $\frac{1}{r^2}$ as r is increased.

The original version of the program ACQN required the interaction potential to be supplied as an algebraic function, for example a Lennard-Jones potential. In this form the program was tested against a number of tabulations of reduced collision integrals for a variety of interaction potentials. The interaction potentials used were

(i) $$V^*(r^*) = \left[\left(\frac{1}{r^*}\right)^{12} - 2\left(\frac{1}{r^*}\right)^{6}\right] \tag{4.5}$$

Lennard-Jones potential (O'Hara and Smith ,1971)

(ii) $$V^*(r^*) = \frac{n}{n(3+\gamma)-12(1+\gamma)}\left[\frac{12}{n}(1+\gamma)\left(\frac{1}{r^*}\right)^{n} - 4\gamma\left(\frac{1}{r^*}\right)^{6} - 3(1-\gamma)\left(\frac{1}{r^*}\right)^{4}\right] \tag{4.6}$$

(n,6,4) potential (Viehland et al., 1975)

(iii) $$V^*(r^*) = \{\exp[-2\,(c/\sigma)\,(r^*-1)] - 2\exp[-(c/\sigma)\,(r^*-1)]\} \tag{4.7}$$

where c is given by

$$c = \frac{\sigma}{1-\sigma}\ln(2)$$

Morse potential (Smith and Munn, 1964)

The references given after Equations 4.5, 4.6, and 4.7 refer to the tabulations of reduced collision integrals against which our results were compared. In all cases the tabulated values were reproduced within the error limits of the two calculations.

4.1.2 Interaction Potential Interpolation

The first main modification to the collision-integral program was to allow a tabulated interaction potential to be used in place of the algebraic model interaction potentials. Cubic spline interpolation (Conte and de Boor, 1980) of the tabulated points was the chosen method of interpolation for several reasons:

(i) the requirements of continuity and differentiability are satisfactorily met

(ii) the interpolating function could be determined before the collision integral evaluation took place, enabling a fast calculation

(iii) the data does not have to be equally spaced on the x axis

(iv) the cubic spline provides a very 'stiff' interpolation function (minimum curvature)

(v) no information about the first or higher derivatives of V(r) is required

(vi) exact expressions for the derivatives are available.

A cubic spline is a piecewise cubic interpolating function. If a function V(r) is only known at n points, $\{(r_i,V_i), i=1,n\}$ where $V_i=V(r_i)$, then a cubic spline through these points consists of n-1 cubic polynomials, $P_1,P_2,\ldots,P_{n-1}$, defined for each sub-interval $[r_i,r_{i+1}]$ as

$$P_i(r) = a_i(r-r_i)^3+b_i(r-r_i)^2+c_i(r-r_i)+d_i \; ; \qquad r_i \le r \le r_{i+1} \tag{4.8}$$

The coefficients a_i, b_i, c_i, and d_i, in each of the n-1 sub-intervals (4n-4 unknowns), are determined by the following conditions:

$$\begin{aligned}
&\text{(i)} && P_i(r_i) &&= V_i && i = 1,\ldots,n-1 \\
&\text{(ii)} && P_i(r_{i+1}) &&= V_{i+1} && i = 1,\ldots,n-1 \\
&\text{(iii)} && P_i'(r_{i+1}) &&= P_{i+1}'(r_{i+1}) && i = 1,\ldots,n-2 \\
&\text{(iv)} && P_i''(r_{i+1}) &&= P_{i+1}''(r_{i+1}) && i = 1,\ldots,n-2
\end{aligned} \tag{4.9}$$

Conditions (i) and (ii) ensure the spline interpolates the tabulated function values. The other two conditions, (iii) and (iv), guarantee a continuous first and second derivative for the cubic spline. There are 4n-6 equations given in 4.9 to solve for 4n-4 variables, thus two variables can be chosen arbitrarily. The procedure adopted here was to assume that the second derivatives of the cubic spline at r_1 and r_n were linear extrapolations from the second derivatives at r_3, r_2 and r_{n-2}, r_{n-1} respectively.

Extrapolation of the cubic spline to give an interaction potential with the correct behaviour at large and small internuclear separation was achieved by fitting inverse power functions to the two terminal points at each end of the spline:

$$V_{low}(r) = \frac{a}{r^p} + b \qquad 0 < r \leq r_1 \qquad (4.10)$$

$$V_{high}(r) = \frac{c}{(r-d)^q} \qquad r_n \leq r < \infty \qquad (4.11)$$

The values of a, b, c, and d were determined by

$$\begin{aligned} V_{low}(r_1) &= V_1 \\ V_{low}(r_2) &= V_2 \\ V_{high}(r_{n-1}) &= V_{n-1} \\ V_{high}(r_n) &= V_n \end{aligned} \qquad (4.12)$$

The exponents p and q appearing in Equations 4.10 and 4.11 were chosen arbitrarily. Usually p was set to 6 and q to 4 or 5. Collision integrals were calculated to check the effect of varying these values. Less than 0.1% variation in the magnitude of the collision integrals was found for q taking values 4, 5, or 6. One explanation of this result is that the interaction potential used was calculated over a sufficiently wide range of internuclear separation to account for the collision integrals without requiring a contribution from Equations 4.10 or 4.11 (based on the understanding that at any given electric field, ion scattering is largely dominated by the ion-neutral interaction potential over a small range of internuclear separation). The other possible explanation for the independence of the collision integral calculation on the value of q is that if the energies in the extrapolated region, $r > r_n$, are sufficiently small there will be no significant contribution from this region to the integral calculation.

4.1.3 Solving the Two-Temperature Theory Equations

The procedure adopted to solve the two-temperature theory equations (see Chapter 2, Equations 2.20 to 2.25) was as follows:

(i) Define the experimental temperature, T, and the ion and neutral masses, m and M respectively. Choose values for p and q and the scale factors r_m and ε.

(ii) Obtain a tabulated interaction potential $\{(r_i,V_i), i=1,n\}$ where r_i is in ångströms and V_i is in electron volts. Convert this interaction potential to the reduced form $\{(r_i^*,V_i^*), i=1,n\}$ then fit by the cubic spline procedure given above.

(iii) Starting with a set of effective temperatures, $\{T_{eff,j}, j=1,k\}$, use Equation 4.2 to generate the reduced temperatures, $\{T_j^*, j=1,k\}$.

(iv) Calculate the corresponding reduced collision integrals, $\{\Omega^{(l,s)*}(T_j^*), j=1,k\}$, which can then be converted to the required collision integrals, $\{\Omega^{(l,s)}(T_{eff,j}), j=1,k\}$ (Equation 4.1).

(v) First approximation: Set β to zero in Equation 2.20 and solve for the drift velocities, $\{v_{d,j}, j=1,k\}$ corresponding to the effective temperatures, $\{T_{eff,j}, j=1,k\}$. Set α to zero in Equation 2.21. Then using Equation 2.1, the drift velocities, $\{v_{d,j}, j=1,k\}$, and the collision integrals, $\{\Omega^{(l,s)}(T_{eff,j}), j=1,k\}$, solve for the values of the parameter E/N; $\{E/N_j, j=1,k\}$.

(vi) Combining Equations 2.1 and 2.2 an expression is obtained for the reduced mobility (in $cm^2V^{-1}s^{-1}$) in terms of the ion drift velocity (in ms^{-1}) and E/N (in Td):

$$K_0 = 0.3722\frac{v_d}{(E/N)} = \frac{v_d}{N_0}\frac{1}{(E/N)} \qquad (4.13)$$

This relationship is used to convert our drift velocity as a function of E/N results $\{(E/N_j,v_{d,j}), j=1,k\}$ to reduced mobilities as a function of E/N $\{(E/N_j,K_{0,j}), j=1,k\}$

(vii) Second Approximation: Calculate values for α and β, for each effective temperature, using Equations 2.22, 2.23, 2.24, and 2.25. Use steps (iv) and (v) above, but with α and β known, to find the dependence of the drift velocity and hence the reduced mobility on E/N.

The method above was used in our two-temperature theory program, TT.F77. The program has several features in addition to the procedures described above. These options are controlled by the setting (or resetting) of 'flags' in the input file. This allows considerable flexibility in the form of the input file and the way the program behaves. The options available are as follows:

(i) The interaction potential can optionally be entered in atomic units (bohr and hartrees) instead of ångströms and electron volts, and the interaction energy can also tend to a non-zero value at large internuclear separation.

(ii) A suitable sequence of effective temperatures can be internally generated or explicitly defined in the input file.

(iii) After the tabulated interaction potential has been fitted with a cubic spline, all of the local critical points (maxima, minima, and inflection points) occurring in the cubic spline, as well as any axis crossings, are found. Ideally, only find one minimum, one inflection point, and one axis crossing should be found. The presence of more critical points than these can indicate an interaction potential which is not sufficiently smooth to allow a successful collision integral calculation.

(iv) The spline may be used only between (r_2,V_2) and (r_{n-1},V_{n-1}) instead of the full range from (r_1,V_1) to (r_n,V_n); the extrapolation functions can be used outside either of these ranges (see Equation 4.12).

(v) The program also has the facility to interpolate the reduced mobility results, again using a cubic spline, at a set of E/N values corresponding to results from an experiment or another calculation. If required, it will compare the calculated reduced mobility values, for both the first and second approximations of the two-temperature theory, with experimental mobilities.

4.2 Three-Temperature Theory Calculations

A three-temperature theory program, MOBDIF, (Viehland, 1982) was obtained from the author. This program performs a three-temperature theory calculation of both ion mobility and diffusion coefficients. It requires a file containing cross sections, $Q^{(l)}(E')$, determined over a

suitable range of energies, E'. In a similar manner to ACQN, the final integration (to obtain the collision integrals) is carried out using cross sections taken from an interpolated set of previously calculated values. Slight modifications were made to the collision integral program, ACQN, incorporated within TT.F77, to enable the $Q^{(l)}(E')$ values and the required Tschebycheff interpolating coefficients, all suitably scaled into atomic units, to be written to an unformatted file of the type required by MOBDIF.

The consequences of these modifications were that after any two-temperature theory calculation a three-temperature theory calculation on the same system could be performed without recalculating the cross sections. Consequently, since both the two- and three-temperature theory calculations used the same cross sections, calculated from the same interaction potential, the effect of changing the level of theory in these transport coefficient calculations could be evaluated directly.

The three-temperature theory program was tested by comparing results with literature data (Viehland, 1983) for a calculation of the mobility of Li^+ ions in helium using an interaction potential directly determined by inverting the experimental mobility data. The results of this test are given in Table 4.1. Our three-temperature theory reduced mobility calculations converged to within 1%. The collision cross sections, $Q^{(l)}(E')$, required were calculated to 0.5% accuracy.

E/N (Td)	K_0 ($cm^2V^{-1}s^{-1}$) (Viehland, 1983)	K_0 ($cm^2V^{-1}s^{-1}$) (this work)	Δ (%)
2.0	23.3	22.9	-1.7
3.0	23.3	22.9	-1.7
5.0	23.3	23.1	-0.9
8.0	23.7	23.5	-0.8
10.0	24.1	24.0	-0.4
12.0	24.8	24.6	-0.8
15.0	25.9	26.0	0.4
20.0	27.9	27.7	-0.7
25.0	30.5	30.2	-1.0
30.0	32.2	31.8	-1.2
40.0	33.6	33.5	-0.3
50.0	33.4	33.5	0.3
60.0	32.8	32.9	0.3
80.0	31.4	31.5	0.3
100.0	30.0	30.2	0.7
120.0	29.0	29.0	0.0
200.0	26.9	26.9	0.0

Table 4.1 Calculation of the reduced mobility of Li^+ in helium.

As can be seen in Table 4.1, the agreement between these calculations is very good. The slight differences are due to the different interaction potential interpolation methods used and the finite accuracy of the calculations.

Thus the programs `TT.F77` (based on ACQN) and `MOBDIF` form a powerful tool for calculating the transport properties of atomic ions in atomic buffer gases. The 'black-box' nature of these programs allows sophisticated accurate calculations to be performed easily.

4.3 Collecting Experimental Arrival Time Distributions
The Programs ATD and PULSEMC

The drift tube mass spectrometer used in this work has been described in Chapter 3. Control of the instrument to enable the collection of arrival time distributions and the subsequent data acquisition is performed by an APPLE II+ microcomputer running the program ATD listed in Appendix B. This program has been constructed in a modular style to facilitate any future modifications. The program was written in Applesoft II: Extended Floating-Point BASIC (© 1978, 1981, APPLE COMPUTER INC.) using the APPLE II Disk Operating System (© 1980, 1981, APPLE COMPUTER INC.) together with an EPSON RX-80 printer (© 1983, Epson America, Inc.).

The program is based on a subroutine calling sequence, each subroutine performing a specific task. The first routine initialises the parallel interface adapters (PIAs) which provide a means of communication between the computer and the drift tube mass spectrometer. The functions, arrays, and constants to be used are defined after the PIAs have been set up. The program requires the experimental conditions to be supplied before starting the data collection routine. The data collection routine, the primary task of the program ATD, is complex and involves loading a machine language program, PULSEMC, which generates two pulses separated by a time delay. A disassembled listing of the program PULSEMC is given in Appendix B. This section of code is modified by the BASIC program in lines 112 to 138 to give the correct delay between the pulses which are generated by PULSEMC and directed to the ion source and to the drift tube exit plate. The program ATD also sets up the required data acquisition time by modifying PULSEMC. The data collection occurs during a sequence of time delays between the two pulses. For each delay the ion signal is collected for a pre-determined period of time. In this way an arrival time distribution, of the ion being studied, is measured. After each scan through the time delays required, the program can be terminated by pressing 'ESC', otherwise the program repeats the procedure and accumulates the ion signals. The scanning is normally ended when the statistical 'noise' in the arrival time distribution is negligible compared with the accumulated ion signal.

Once an arrival time distribution has been collected the experimental results are smoothed by the application of a five point smoothing polynomial:

$$y_i^{(1)} = \frac{1}{35}\left(-3y_{i-2}^{(0)} + 12y_{i-1}^{(0)} + 17y_i^{(0)} + 12y_{i+1}^{(0)} - 3y_{i+2}^{(0)}\right) \qquad (4.14)$$

During application of Equation 4.14, $y^{(1)}$ corresponds to a smoothed point on the arrival time distribution and $y^{(0)}$ corresponds to an experimental result. The data point corresponding to the largest signal is then located and a five point Lagrange interpolating function fitted about this point to enable the maximum in the arrival time distribution to be found accurately. The time corresponding to this maximum can be used to obtain ion mobilities by including it in a graph of drift distance versus mean arrival time. The slope of such a graph gives the drift velocity of the ion. The Lagrange interpolating function expressions used were

$$p(t) = \sum_{k=0}^{4} y_k^{(1)} l_k(t) \qquad (4.15)$$

$$l_k(t) = \prod_{\substack{i=0 \\ i \neq k}}^{4} \frac{t-t_i}{t_k-t_i} \qquad (4.16)$$

The $y_k^{(1)}$ are smoothed data points at times t_k.

After this analysis the experimental conditions and results are printed, including a graph of both smoothed and raw experimental ion arrival time distributions. The experimental conditions and data are saved to a disk file for subsequent examination and/or modelling. The drift distance, the time corresponding to the maximum signal, the electric field strength, the pressure and temperature, the minimum and maximum delay times (in clock cycles) and increment time, the title, and the raw experimental ion signals is the data saved. This information completely describes the experiment.

4.4 Modelling Experimental Arrival Time Distributions

The Program ATD.F77

In Chapter 3 it was mentioned that the most accurate way to extract mobility information from arrival time distributions was by fitting them with a model arrival time distribution. The

calculation of such a distribution requires estimates of the rate constants for any reactions occurring during the experiment. If a secondary ion distribution is being modelled, then the primary ion mobility is also required. The mobility of the ion being studied is a variable which is changed until there is close agreement between the calculated and measured arrival time distributions.

The program ATD.F77 was written to enable arrival time distributions to be calculated and compared to experimental measurements quickly and efficiently. A listing, with comments, is given in Appendix B. The subroutines SMOOFT, REALFT, FOUR1, QSIMP, and TRAPZD were taken from *Numerical Recipes* (Press et al., 1986). Experimental data, for any number of arrival time distribution measurements, is collected into a file called ATD.DATA. The first line of each set of data contained in this file is a unique title usually including the date and a number, for example 'ATD.031187.1'. For each modelling calculation to be performed the file ATD.INPUT contains the title of the corresponding experimental data, the ion and neutral masses, estimates of all the ion mobilities, rate constants and reaction orders. The proportion of reactant in the gas, and a flag indicating whether the calculation is for the primary or the secondary ion is also required. The input file does not contain any of the experimental conditions (such as the temperature or pressure) because these are contained in the experimental data file. The current version of the program has been configured to allow the secondary ion mobility, and the rate of loss of the primary ion, to be repeatedly varied until the agreement between the calculation and experiment result is good.

The procedure for the calculation is outlined as follows:

(i) Find and read the experimental conditions and arrival time data in file ATD.DATA. From ATD.INPUT read the ion and neutral masses, estimates of the ion mobilities, rate constants, reaction orders, the proportion of reactant , and the primary or secondary ion calculation flag.

(ii) Use the Equations 2.6, 2.13 and 2.14 to calculate the longitudinal and transverse diffusion coefficients for both the primary and secondary ions.

(iii) Calculate an arrival time distribution at the same drift times as the experiment.

(iv) Smooth the raw experimental arrival time distribution. Use a Fourier transform to convert the data into the signal versus frequency domain, filter the high frequency noise then inverse transform back into the signal versus time domain.

(v) Find the times corresponding to the maximum ion signal for both the calculated and experimental arrival time distributions.

(vi) Shift the calculated distribution along the time axis so the corresponding maxima coincide and recalculate the model distribution.

(vii) Scale both distributions so the minimum ion signal is 0 and the maximum is 100.

(viii) Compare the results of the calculation and with the experimental arrival time distribution.

(ix) Repeat steps (i) to (viii) for each experimental arrival time distribution.

The program was compared against a similar, but less sophisticated program (McIntosh, 1984) with excellent agreement. An internal check of the program's performance was also made by calculating a secondary ion arrival time distribution for an ion formed by a very fast reaction, with the arrival time distribution for the same ion being formed as a primary ion. The results were identical as required.

Chapter 5

The Effect of Ion Structure on Gas-Phase Ion Transport Properties.

5.1 Introduction

As shown in Chapter 2, there exist theoretical treatments of the mobility of spherically symmetric charged particles undergoing elastic collisions with neutral particles (in the presence of an applied electric field). These theories show that the observed macroscopic behaviour of ions drifting in a neutral buffer gas may be understood in terms of the microscopic behaviour of individual ions undergoing collisions with buffer gas atoms. The scattering processes which occur are a direct result of the interaction potential existing between the ion and neutral particles. For molecular systems, the intimate relationship between the ion mobility and the ion-buffer gas interaction potential still exists. Although quantitative application of molecular ion drift theory to the general case of a polyatomic ion drifting in a polyatomic buffer gas, or even to the simpler case of a polyatomic ion drifting in an atomic buffer gas, has not yet been achieved, we can make some qualitative observations based on atomic ion-atomic buffer gas systems using a model interaction potential.

At a fixed gas temperature, there are a number of system properties which influence the shape of the interaction potential and consequently the magnitude of the mobility calculated using such an interaction potential. The buffer gas polarisability, α_p, the dipole moment of the ion, μ, the effective size and shape of the ion, and the ion and neutral masses will all play a factor in influencing the calculated mobility. Preliminary calculations have been carried out to assess the relative effect of these properties on the ion mobility in helium using the two-temperature theory of ion mobility. This has been done by varying the parameters in a model interaction potential, which includes terms appropriate for an ion having a dipole moment interacting with a polarisable buffer gas atom, and assessing the effect that these changes have

on the calculated ion mobility. The observed differences in ion mobilities may be explained in terms of differences in the interaction potentials between the ion and the buffer gas atom.

In Section 5.2 the empirical intermolecular potential function used in this work is described. Values for the various parameters occurring in this function are determined. This leads to several intermolecular potential functions, in which the parameters have been systematically varied from a set of default values. Section 5.3 uses the intermolecular potential functions described in Section 5.2 to investigate the effect varying the parameters has on the mobility calculated from these interaction potentials. Differences in ion mobilities in helium, using data from the literature, are qualitatively explained in Section 5.4 in terms of the results from the model calculations given in Section 5.3. Also in Section 5.4 are the results of mobility measurements for some isomeric ions having the formula $C_2H_xO^+$ where x has the value 3, 4 or 5. The differences in ion mobilities for these isomeric ions are explained in terms of differences in the ion-neutral interaction potentials.

5.2 Empirical Intermolecular Functions

Empirical intermolecular potential functions have been used to calculate transport properties of gases as well as second and third virial coefficients. For a comprehensive discussion of empirical intermolecular potential functions as well as the results of some calculations see Hirschfelder et al. (1964).

One function which has been widely used to approximate the interaction between molecules is the Lennard-Jones (6-12) potential:

$$V^{(L-J)}(r) = \varepsilon \left[\left(\frac{r_m}{r}\right)^{12} - 2 \left(\frac{r_m}{r}\right)^{6} \right] \qquad (5.1)$$

The Lennard-Jones potential function has a maximum energy of attraction of ε when the molecular separation, r, is equal to r_m. The inverse sixth power attraction term can represent the induced-dipole - induced-dipole interaction energy. This is the force felt between two neutral non-polar molecules when an instantaneous dipole in one induces a dipole in the other. For polar and/or charged molecules there are other forces felt when they interact with a non-polar neutral molecule. When a molecule carrying charge, q, interacts with a non-polar neutral

molecule or atom, which has a polarisability α_p, it induces a dipole moment in the neutral particle. The energy due to the interaction of the charge with the charge-induced-dipole is given by

$$V^{(q,q\text{-ind }\mu)}(r) = \frac{-\alpha_p q^2}{8\pi\varepsilon_o r^4} \tag{5.2}$$

The quantity ε_o is the permittivity of free space. Similarly, a dipole moment, μ, in one molecule can induce a dipole moment in another molecule (or atom). The magnitude of the induced dipole depends on the orientation of the dipole. The interaction energy due to this effect can be averaged over all possible dipole orientations to obtain the following result:

$$\bar{V}^{(\mu,\mu\text{-ind }\mu)}(r) = \frac{-\alpha_p \mu^2}{4\pi\varepsilon_o r^6} \tag{5.3}$$

There is an interaction between the charge on the ion, with a dipole moment on the neutral particle, where the dipole moment has been induced by the ions dipole moment:

$$\bar{V}^{(q,\mu\text{-ind }\mu)}(r) = \frac{-\alpha_p \mu q}{8\pi\varepsilon_o r^5} \tag{5.4}$$

We can construct an empirical intermolecular potential function which includes the terms required to describe the interaction energy when a charged polar molecule approaches a non-polar neutral target:

$$V(r) = \varepsilon\left[\left(\frac{r_m}{r}\right)^{12} - 2\left(\frac{r_m}{r}\right)^{6}\right] - \frac{\alpha_p \mu q}{8\pi\varepsilon_o r^5} - \frac{\alpha_p q^2}{8\pi\varepsilon_o r^4} \tag{5.5}$$

This generalised potential function, based on the intermolecular forces discussed above, was used to determine the effect of individually varying the well depth, ε', the ion-atom separation corresponding to the minimum in the potential, r'_m, the polarisability of the neutral target, α_p, and the dipole moment, μ, of the ion. If the last two terms are omitted from Equation 5.5 the generalised potential reduces to a Lennard-Jones (6-12) interaction potential and the quantities ε and r_m become identical with ε' and r'_m respectively. The terms in Equation 5.5 corresponding to Equations 5.2 and 5.4 cause a shift away from the Lennard-Jones well depth, ε, and

minimum position, r_m, to give a potential having a well depth of ε' and minimum position, r'_m. The effect of the force given by Equation 5.3 is contained in Equation 5.5 as the term $-\frac{2\varepsilon r_m^6}{r^6}$.

Using Equation 5.5, an interaction potential can be defined by choosing values for the parameters α_p, μ, ε and r_m. However, ε and r_m are not the true interaction potential well depth, ε', and position, r'_m. For the purposes of this work, we required the values of ε' and r'_m to be either kept constant (while α_p and μ are varied) or else varied systematically, while α_p and μ are held constant. Thus, to obtain an interaction potential with the desired characteristics, the parameters ε', r'_m, α_p, and μ are fixed and the unknown parameters, ε and r_m found by solving the equations

$$V(r'_m) = -\varepsilon'$$
$$V'(r'_m) = 0 \qquad (5.6)$$

where

$$V'(r) = \frac{dV}{dr} = -12\frac{\varepsilon}{r}\left[\left(\frac{r_m}{r}\right)^{12} - \left(\frac{r_m}{r}\right)^{6}\right] + 5\frac{\alpha_p \mu q}{8\pi\varepsilon_o r^6} + 4\frac{\alpha_p q^2}{8\pi\varepsilon_o r^5} \qquad (5.7)$$

Using this procedure, values of r_m and ε were found for several interaction potentials which had the required values for the parameters α_p, μ, r'_m and ε. These interaction potentials were constructed so that the effect of independently varying each of the parameters (α_p, μ, r'_m and ε) on the calculated mobility could be determined. Details of the interaction potentials used in this work are given in Table 5.1.

Interaction potential I contains the defaults values for the model interaction potential parameters. The other interaction potentials were generated by systematically changing the parameter values from the default values. A comparison of the interaction potentials in Table 5.1 shows that the values of the parameters of potentials II to XI differ from the values in potential I. Interaction potentials II, III and IV differ by the value of the dipole moment, μ; V and VI have different well depths; VII and VIII have a different position of the minimum in the interaction potential; IX and X have different neutral polarisabilities; and XI has a different mass.

	I	II	III	IV	V	VI	VII	VIII	IX	X	XI
r'_m (Å)	2.000						1.900	2.100			
ε' (eV)	0.200				0.190	0.210					
α_P (Å^3)	0.205								0.103	0.308	
μ (D)	1.080	0.540	2.000	3.920							
r_m (Å)	2.080	2.074	2.096	2.115	2.086	2.075	2.003	2.164	2.034	2.148	
ε (eV)	0.105	0.109	0.098	0.083	0.095	0.114	0.085	0.121	0.150	0.064	
m (gmol^{-1})	30.0										40.0

Table 5.1 Interaction potential parameters used in model calculations. r'_m and ε' are the actual position and depth of the interaction potential well; α_p, μ, r_m and ε are parameters appearing in Equation 5.1, and m is the ion mass.

5.3 Ion Mobility Calculations

The theoretical dependence of the drift velocity and the ion mobility on E/N were calculated for the model interaction potentials I to XI in Table 5.1 assuming a neutral mass of 4.0 gmol^{-1}, and a buffer gas temperature of 300 K. The results of these two-temperature theory calculations, at the second approximation, are given in Tables 5.2a and 5.2b.

These calculations suggest that increasing the dipole moment of the ion from 1.08 D, dipole moment of HCl, to 3.92 D will decrease the reduced mobility, K_0, or equivalently the drift velocity, v_d, by only 1.1±0.3%. This effect is only present below 80 Td. Decreasing the well depth by 0.1 eV leads to an increase in K_0 of 2.0±0.7%. There is a corresponding decrease in K_0 if the well depth is increased by 0.1 eV. Changing the position of the minimum in the ion-neutral potential by 0.1 Å leads to a more significant change in K_0. Increasing in the minimum from 2.0 Å to 2.1 Å gives rise to a 7.7±1.2% decrease in K_0. Decreasing in the minimum from 2.0 Å to 1.9 Å gives a 8.4±1.7% increase in K_0. The effect of changing the polarisability of the neutral particle, like changing the dipole moment of the ion, is only felt significantly at low values of E/N.

E/N	I	II	III	IV	V	VI	VII	VIII	IX	X	XI
4	143.1	143.5	142.1	141.1	144.9	140.9	152.9	133.3	153.8	132.7	141.0
8	285.6	286.3	283.6	281.6	289.4	281.3	305.2	266.2	306.9	265.2	281.4
10	356.4	357.3	353.9	351.5	361.4	351.2	381.0	332.2	383.0	331.5	351.2
15	532.1	533.5	528.5	525.1	540.3	524.8	569.5	496.0	570.8	496.8	524.4
20	706.5	708.2	701.8	697.5	717.4	696.2	756.6	658.0	754.4	661.1	696.4
30	1049.	1051.	1043.	1037.	1067.	1033.	1127.	975.8	1112.	988.0	1034.
40	1388.	1391.	1380.	1374.	1415.	1364.	1498.	1288.	1460.	1316.	1368.
60	2092.	2095.	2081.	2074.	2149.	2042.	2295.	1919.	2171.	2006.	2055.
80	2909.	2912.	2898.	2895.	3011.	2809.	3253.	2614.	2966.	2822.	2850.
100	3788.	3790.	3779.	3786.	3905.	3673.	4219.	3400.	3816.	3754.	3724.
120	4578.	4578.	4563.	4578.	4684.	4474.	5035.	4161.	4581.	4580.	4518.
140	5265.	5264.	5250.	5269.	5356.	5172.	5733.	4827.	5251.	5275.	5208.
180	6409.	6408.	6392.	6416.	6485.	6334.	6919.	5950.	6384.	6438.	6352.
r'_m	2.00 Å						1.90 Å	2.10 Å			
ε'	0.20 eV				0.19 eV	0.21 eV					
α_p	0.205 Å^3								0.103 Å^3	0.308 Å^3	
μ	1.080 D	0.54 D	2.00 D	3.92 D							
m	30 gmol^{-1}										40 gmol^{-1}

Table 5.2a Calculation of the drift velocity (m/s) as a function of E/N (Td) using a model interaction potential. The bottom section of the Table lists the parameters which have been changed from the values listed for potential (i).

E/N	I	II	III	IV	V	VI	VII	VIII	IX	X	XI
4	13.32	13.35	13.22	13.13	13.48	13.11	14.23	12.40	14.31	12.35	13.12
8	13.29	13.32	13.19	13.10	13.46	13.09	14.20	12.38	14.28	12.34	13.09
10	13.27	13.30	13.17	13.08	13.45	13.07	14.18	12.36	14.26	12.34	13.07
15	13.20	13.24	13.11	13.03	13.41	13.02	14.13	12.13	14.16	12.33	13.01
20	13.15	13.18	13.06	12.98	13.35	12.96	14.08	12.25	14.04	12.30	12.96
30	13.01	13.04.	12.94	12.87	13.24	12.82	13.98	12.11	13.80	12.26	12.83
40	12.92	12.94	12.84	12.79	13.17	12.69	13.94	11.98	13.59	12.25	12.73
60	12.98	13.00	12.91	12.87	13.33	12.67	14.24	11.90	13.47	12.44	12.75
80	13.53	13.55	13.48	13.47	14.01	13.07	15.13	12.16	13.80	13.13	13.26
100	14.10	14.11	14.07	14.09	14.53	13.67	15.70	12.65	14.20	13.97	13.86
120	14.20	14.20	14.15	14.20	14.53	13.88	15.62	12.91	14.21	14.21	14.01
140	14.00	13.99	13.96	14.01	14.24	13.75.	15.24	12.88	13.96	14.02	13.85
180	13.25	13.25	13.22	13.27	13.41	13.10	14.31	12.30	13.20.	13.31	13.13
r_m'	2.00Å						1.90Å	2.10Å			
ε'	0.20eV				0.19eV	0.21eV					
α_P	0.205Å^3								0.103Å^3	0.308Å^3	
μ	1.080D	0.54D	2.00D	3.92D							
m	30gmol^{-1}										40gmol^{-1}

Table 5.2b Calculation of the reduced mobility ($cm^2V^{-1}s^{-1}$) as a function of E/N (Td) using a model interaction potential. The bottom section of the Table lists the parameters which have been changed from the values listed for potential (i).

An increase in α_p from the helium value of 0.205 Å^3 to 0.308 Å^3 causes a 6.5±0.8% decrease in K_0 below 60 Td. The last change considered in the present study was the effect of changing the ion mass from 30 gmol^{-1} to 40 gmol^{-1}. This had the effect of lowering K_0 by 1.5±0.3% over the range of E/N considered.

5.4 Ion Mobility Measurements

The influence of ion structure on the reduced mobilities for ions of dissimilar composition is shown in Figure 5.1 for positive ions of mass (in gmol^{-1}) to charge (in units of the elementary charge) ratio, m/z, having the values 16, 18, 28, and 41.

The information in Figure 5.1 was taken from the literature (Ellis et al., 1976 and 1978; Barrasin et al., 1983; Harland and McIntosh, 1983 and 1984). When reporting mass-to-charge ratios it is usual to use the symbols m for mass and z for charge, thus m/z. The drift tube used in this work was able to reproduce the drift velocity at several values of E/N for all of the ions in Figure 5.1 within 3% with the exception of NH_2^+ and ArH^+ which present considerable experimental difficulties (NH_2^+ is rapidly removed by reaction, and ArH^+ requires gas mixtures containing substantial partial pressures of hydrogen), with the relative values of the mobilities for each pair of ions, of the same m/z ratio, being in the direction shown in Figure 5.1, that is H_2O^+ more mobile than NH_4^+ etc.

The model calculations, using an assumed form for the interaction potential, together with two-temperature drift theory, provide a means for qualitative prediction of the expected effect of ion dipole moment and dimension which agree with the differences observed in the mobilities of ions of dissimilar composition. The figures quoted for the relative magnitude of these effects are reliable within the constraints of the chosen form for the interaction potential and considering the assumptions inherent in the two-temperature theory. In the absence of realistic interaction potentials for the ion studied it is not feasible to unfold the individual contributions of these parameters on the experimentally observed mobilities. However, it is possible to rationalise the results in terms of the theoretical calculations given above.

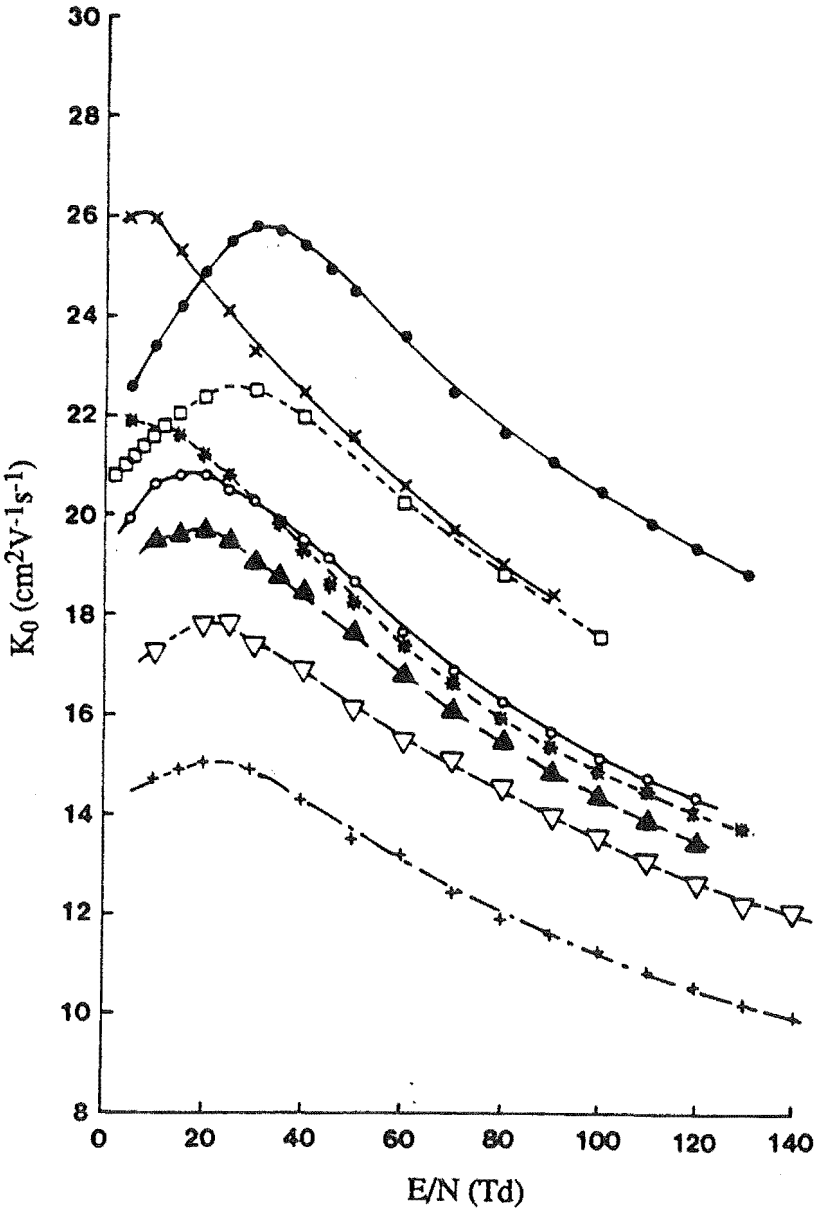

Figure 5.1 Reduced mobilities as a function of E/N for pairs of chemically dissimilar positive ions of m/z = 16, 18, 28 and 41, in helium at or close to 300 K. •, O^+ (16); x, NH_2^+ (16); □, H_2O^+ (18); o, CO^+ (28); *, NH_4^+ (18); ▲, ArH^+ (41); ▽, H_2CN^+ (28); +, $C_2H_3N^+$ (41).

The ions of m/z=16 (NH_2^+ and O^+) and m/z=41 (ArH^+ and $C_2H_3N^+$) provide the most graphical illustration of the effect of ionic spatial volume on the mobility of these ions as a function of E/N.

For ions of m/z=41, a difference of 0.4 Å in the effective diameter of the ions would be sufficient to account for these observations which is in agreement with a previous study on the

effect of ionic size on ion mobility (Lin et al., 1974). However, the same effect could be caused by a change of 0.2 eV in the well depth at a fixed separation.

For ions of m/z=16, NH_2^+ is less mobile than O^+ as expected for a larger ion. A difference of 0.2 Å in the effective ion diameter would be sufficient to account for the observed difference in accordance with covalent radii considerations.

The literature values for the reduced mobilities of N_2^+ and CO^+ (Ellis et al., 1976), m/z=28, are in close agreement as might be anticipated for ions of the same shape (N_2^+ is not included in Figure 5.1 for clarity), the small dipole moment of 0.117 D for CO exerts only a minor influence on the He-CO^+ interaction potential. The H_2CN^+ ion, of the same nominal mass as N_2^+ and CO^+, is a larger ion which would exhibit a higher collision cross-section and therefore a lower mobility. The dipole moment of the H_2CN species will be about 1D and would not be a significant influence on the interaction potential. The observed differences between the mobilities of the CO^+ and H_2CN^+ ions may be attributed directly to the effect of the ion structure on the interaction potential, that is ε and r_m. A change in effective ion size of 0.2 Å could account for the difference observed here between CO^+ and H_2CN^+.

According to the calculations the dipole moment of H_2O, 1.85 D, would tend to slightly decrease the mobility of the H_2O^+ ion, m/z=18, relative to a non-polar, but otherwise equivalent ion. This effect is strongest at low values of E/N. The non-polar ion, NH_4^+, is larger than H_2O^+ which would lead to a significant decrease in the observed mobility. The experimental result, shown in Figure 5.1, is a mobility difference of 11% at E/N=30 Td and 18% at E/N=100 Td, relative to the mobility of the NH_4^+ ion in accord with the expected effect of ion size. The curves of reduced mobility versus E/N cross at low E/N, the H_2O^+ curve exhibiting a maximum in mobility at about 25 Td. The shape of the curves are quite different reflecting differences in the interaction potentials of these ions with helium (Gatland et al., 1977b). This difference is at least partially due to the presence of the previously mentioned dipole moment in H_2O.

The mobilities of several structural isomers of the $C_2H_xO^+$ series, where x takes the value 3, 4, or 5, were determined in order to investigate the effect of more subtle structural differences on the transport properties of ions. The choice of isomers was restricted by the requirements for ions formed with a high dissociative charge transfer cross-section from He^+

and high isomerisation barriers to interconversion. The recombination energy of helium is 24.6 eV, and the appearance energies for the $C_2H_xO^+$ ions from the precursor molecules, acetaldehyde, ethylene oxide, dimethyl ether and ethanol, all lie within the energy range from 10.2 to 14.5 eV (Franklin et al., 1969; Rosenstock et al., 1977). The neutral products of the ionisation process are helium with either or both hydrogen atoms and hydrogen molecules. These light fragmentation products will carry away a substantial fraction of the excess energy released in the dissociative charge-transfer process in the form of recoil energy with any internal ion energy being thermalised in collisions with the helium buffer gas. The structural isomers studied have been shown to exist as non-interconverting species in kinetic and collisional dissociation studies, and both experimental and theoretical values for the enthalpies of formation are available (Tables 5.3 and 5.4). The drift tube mass spectrometer and reagents used have been described in Chapter 3. The drift velocities and ion mobilities were determined from the slopes of the best fit line through mean arrival time versus drift distance graphs. Typically, measurements were made at eight to ten drift distances for each value of E/N.

5.4.1 $C_2H_5O^+$ (m/z=45)

Four stable structures for the $C_2H_5O^+$ ion are shown in Table 5.3 with experimental (Corderman et al., 1976; Harrison et al., 1971; Staley et al., 1974; and Refeay and Chupka, 1968) and theoretical (Lischka and Kohler, 1979) relative enthalpies of formation. The absolute enthalpy of formation for the protonated acetaldehyde molecular ion, structure (A), was reported to be 598 kJ mol^{-1} (Corderman et al., 1976).

Drift velocities were determined for the $C_2H_5O^+$ fragmentation ion from dilute mixtures (0.2%) of ethanol and dimethyl ether in helium and for the protonated molecular ion of acetaldehyde for mixtures <0.5% of acetaldehyde in helium. Plots of reduced mobility versus E/N are shown in Figure 5.2.

	structure	relative ab-initio energy (kJmol-1)	relative experimental energy (kJmol-1)
(A)	$CH_3\overset{+}{C}HOH$	0	0
(B)	$CH_3\overset{+}{O}CH_2$	–	63
(C)	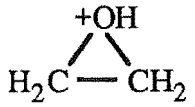	132	109
(D)	$\overset{+}{C}H_2CH_2OH$	182	–

Table 5.3 Isomers of $C_2H_5O^+$.

The mobility of the $C_2H_5O^+$ ion produced from dimethyl ether, which has a C-O-C skeletal structure, is between 3 and 6% lower than the mobility determined for the same ion produced from ethanol or protonated acetaldehyde, which both have a C-C-O skeletal framework. The actual structures for the ions can only be inferred from the information in Table 5.3; the ion produced from dimethyl ether is assumed to be the C-O-C isomer (B) and the species formed from ethanol and acetaldehyde, which have the same ion transport properties, is assumed to be isomer (A). This being the case, then the C-O-C isomer exhibits a higher momentum transfer collision integral, and therefore a lower mobility, than the C-C-O isomer. This may be rationalised in terms of the structures shown in Table 5.3. Terminal carbon atoms carry at least two hydrogen atoms projecting away from the carbon-oxygen skeleton, whereas a terminal oxygen carries only one hydrogen atom. The oxygen atom in structure (A) also carried the charge which further constrains the spacial volume at the oxygen end of the ion. The magnitude of $\Omega^{(1,1)}(T)$ reflects the spacial volume, and hence the collision cross-section of the ions on helium, in the same way as discussed above for chemically dissimilar ions of the same nominal mass (Figure 5.1). The two observed structural isomers of $C_2H_5O^+$ observed in this study are given in Figure 5.3.

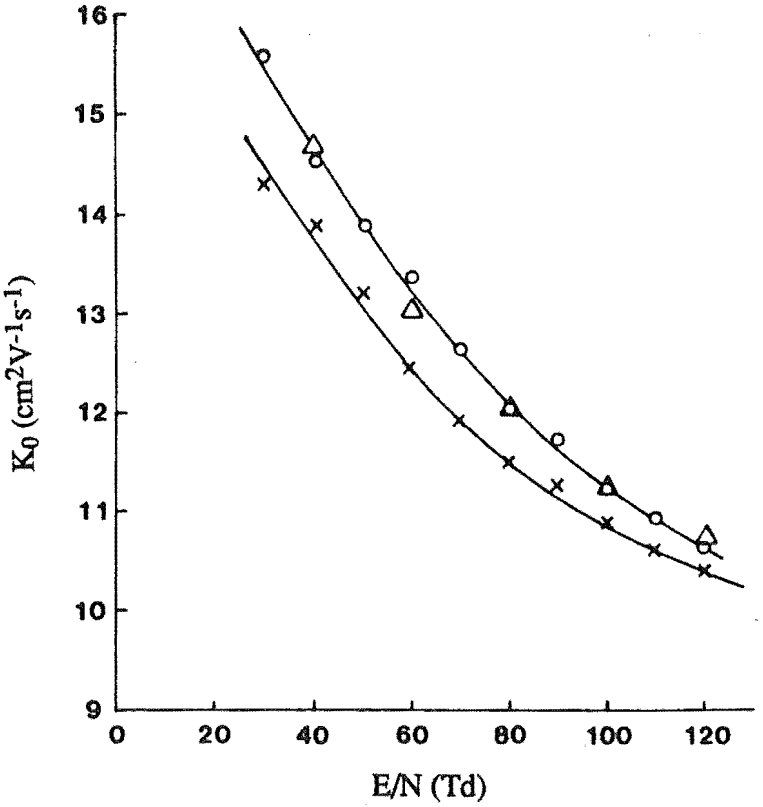

Figure 5.2 Reduced mobilities as a function of E/N for the $C_2H_5O^+$ ion produced from three different precursor molecules in helium at 293K.
x, CH_3OCH_3; o, C_2H_5OH; Δ, CH_3CHO.

The effect of the number of terminal hydrogen atoms on mobility is well illustrated by a comparison of the mobilities of the CN^+, HCN^+ and H_2CN^+ ions, where the difference in mobility are far greater than would be anticipated on the basis of their unit-mass changes (Harland and McIntosh, 1985).

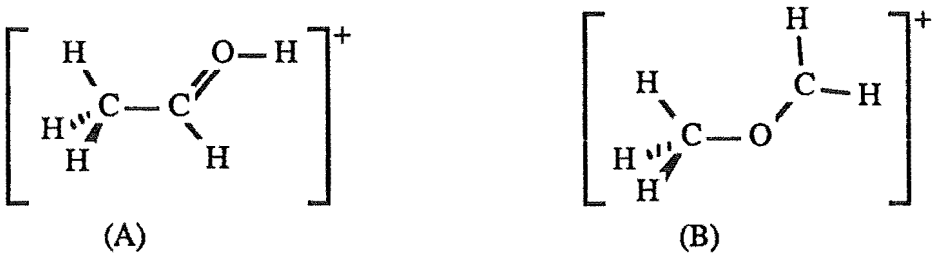

(A) (B)

Figure 5.3 Observed structural isomers of $C_2H_5O^+$.

5.4.2 $C_2H_4O^+$ (m/z=44)

The structures, relative ab-initio (Bouma et al.,1979) and experimental (Corderman et al., 1976; Van de Sande and McLafferty, 1975; Bouma et al.,1978; and Holmes et al., 1976) energies for the $C_2H_4O^+$ isomers are shown in Table 5.4. The four structural isomers shown correspond to the molecular ions of vinyl alcohol (A), acetaldehyde (B) and ethylene oxide (D). Structure (C) corresponds to a ring-opened ethylene oxide or a fragmentation product of dimethyl ether. The relative enthalpies of formation shown in Table 5.4 are referenced to an absolute value of 757 kJ mol^{-1} for isomer (A), which was determined by 'monochromatic' electron impact (Holmes et al., 1976).

	structure	relative ab-initio energy (kJmol-1)	relative experimental energy (kJmol-1)
(A)	$CH_2CH\overset{+}{O}H$	0	0
(B)	$CH_3CH=\overset{+}{O}$	52.3	63
(C)	$CH_2\overset{+}{O}CH_2$	124.9	101
(D)	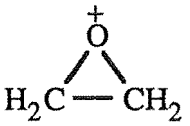	182.6	209

Table 5.4 Isomers of $C_2H_4O^+$.

Mobility data for $C_2H_4O^+$ ions from dilute (<0.2%) mixtures of ethanol and ethylene oxide are shown with data for CO_2^+ (m/z=44) in Figure 5.3.

The electron-impact study identified the $C_2H_4O^+$ ion from ethanol as the vinyl alcohol structure (A) and two ion cyclotron resonance studies (Harrison et al., 1971; Van de Sande and McLafferty, 1975) both proposed that the $C_2H_4O^+$ isomer from ethylene oxide is the ring-opened structure (C). The isomerisation barrier for conversion of the closed ethylene oxide structure (D) to the more stable ring-opened structure (C) has been estimated to be 105-120 kJ mol^{-1} (Bouma et al.,1979). The exothermicity of the charge-transfer reaction of He^+ on

$(CH_2)_2O$ is 1.45 MJ mol^{-1}. This would certainly provide enough internal energy to drive isomerisation. The mobility curves shown in Figure 5.4 have been labelled according to these considerations. The difference in mobilities between the two isomers, (A) and (C), is about 10%, the C-O-C isomer, (C), exhibiting a lower mobility (higher collision cross-section) than the C-C-O isomer, (A), in accord with the $C_2H_5O^+$ results. Data for the mobility of CO_2^+ in helium were taken from the literature (Ellis et al., 1978).

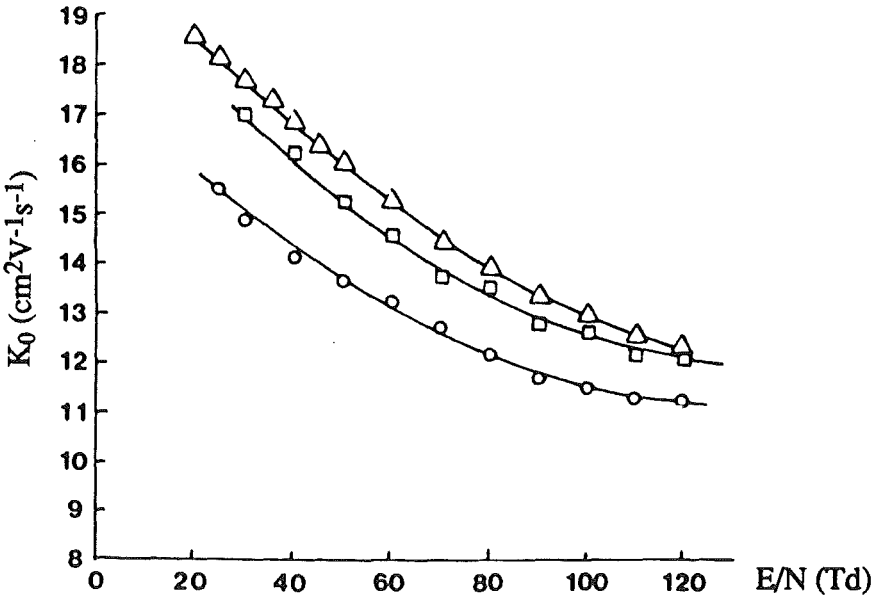

Figure 5.4 Reduced mobilities as a function of E/N for the $C_2H_4O^+$ ion produced from two different precursor molecules and for CO_2^+ produced from CO_2 in helium at 293 K. Δ, CO_2^+ / CO_2; □, $C_2H_4O^+ / C_2H_5OH$ (A); o, $C_2H_4O^+ / (CH_2)_2O$ (C).

The two observed structural isomers of $C_2H_4O^+$ observed in this study are given in Figure 5.5. Isomer (C) was found to have a lower mobility than isomer (A).

Figure 5.5 Observed structural isomers of $C_2H_4O^+$.

5.4.3 $C_2H_3O^+$ (m/z=43)

The $C_2H_3O^+$ ion is a minor product (about 1%) of total He^+ dissociative charge transfer ionisation of dimethyl ether and (about 9%) from ethanol. The ion density in the drift tube must be maintained low enough (about 10^{-4} cm^{-3}) to preclude Coulombic repulsion and the distortion of the arrival-time profiles. This seriously limited the $C_2H_3O^+$ ion signal and the reliability of the measurements. Nevertheless, the mobility of the $C_2H_3O^+$ ion produced from ethanol and dimethyl ether were measured over the range 80-140 Td, the values for the C-O-C isomer from dimethyl ether being consistently about 3% lower than the C-C-O isomer from ethanol.

5.5 Summary

The effects of ion structure on ion transport properties in helium have been qualitatively predicted from drift theory and confirmed experimentally. Significant differences between the mobilities of chemically dissimilar ions of the same mass-to-charge ratio, m/z, have been rationalised in terms of dipole moment, ion size (shape) and structure in accord with predictions of model potential calculations. Smaller differences in mobility have been found for the structural isomers of $C_2H_xO^+$ (x is 3,4 or 5).

Chapter 6

Determination of the Mobility of N^+ in Helium

6.1 Introduction

As a result of some preliminary calculations of the mobility of N^+ in helium, which are discussed in Chapter 10, an unexpected kink was found in the theoretical reduced mobility curve. This feature occurred at about 70 Td. A comparison with previously reported experimental data (Johnsen et al., 1970; McFarland et al., 1973; Kaneko et al., 1978; Fahey et al., 1981; Fhadil et al., 1985) showed a significant degree of uncertainty in the measurements, especially in the medium field region. It was decided to perform an experimental measurement of the mobility of N^+ in helium for two reasons. Firstly, to resolve some of the uncertainty in the measured value, and secondly, to see if we could observe anything unusual in the shape of the mobility versus E/N curve.

Most positive ions, like N^+, are formed in the drift tube primarily by the chemical ionisation of a trace additive by buffer gas ions. Only a very small proportion result from direct electron impact ionisation. The principal process occurring in the ion source is the electron impact ionisation of helium to form He^+ (the primary ion) because helium is the main component of the buffer gas. The He^+ ions drift down the electric field gradient inside the drift tube and can react with any N_2 encountered to form the secondary ions N_2^+ and N^+. The $He^+ + N_2$ reaction is a thermal energy charge transfer (Laudenslager et al., 1974) which proceeds to give an excited state of N_2^+ as shown:

$$He^+ (^2S) + N_2 (X\ ^1\Sigma_g^+) \rightarrow He\ (^1S) + N_2^+ (C\ ^2\Sigma_u^+, \upsilon=4) \qquad (6.1)$$

Consequently, the N_2^+ ($C\ ^2\Sigma_u^+$) may then either radiate, to give ground state N_2^+, or predissociate to give atomic nitrogen and its corresponding positive ion:

$$N_2^+ (C\ ^2\Sigma_u^+) \rightarrow N_2^+ (X\ ^2\Sigma_g^+) + h\upsilon$$
$$\rightarrow N^+ (^3P) + N (^4S) \qquad (6.2)$$

We have performed our own independent measurements of the reduced mobility of N^+ in helium from 35 Td to 140 Td. In this study a 1% mixture of N_2 in helium was admitted to the drift tube. As has been explained in Chapter 2, the arrival time distributions obtained during these experiments need to be modelled to obtain an accurate result, especially for the case of a secondary ion . During these modelling calculations, to get an accurate fit to the trailing edge of the arrival time distribution, it was necessary to use a rate coefficient for the loss of the primary ion which increased with increasing electric field strength. This was contrary to what had been expected on the basis of an earlier experimental measurement of the rate constant as a function of centre of mass collision energy, and consequently an independent measurement of the rate coefficient was made for the charge transfer reaction of He^+ to nitrogen. The results of that experiment confirmed the behaviour found during the modelling calculations.

6.2 Experimental Details

The mobility and kinetic measurements were made using the drift tube described in Chapter 3. Prior to these experiments the particle multiplier, a Channeltron Electron Multiplier type 4816 (Galileo optics), was replaced, also several ion source filament materials were tested before choosing 0.007" rhenium wire. The filament was coated with a layer of barium zirconate (McNair, 1967) to improve its emission characteristics. The filament was typically operated at approximately 3.2 A from a 12 V DC power supply. Under continual pumping, the drift tube and mass spectrometer vacuum chambers obtained pressures of 1.8×10^{-8} Torr and 4×10^{-7} Torr respectively. The nitrogen in helium mixtures were prepared on the gas handling line, described in Chapter 3, after passing the scientific grade (>99.995% purity) gases through liquid nitrogen traps.

6.3 Mobility Measurements

Prior to, and regularly during the mobility measurements, mass spectra were recorded to check on the composition of the buffer gas and to detect the presence of any impurities. Figures 6.1 and 6.2 show two mass spectra; the first for pure helium, and the second for a 1.0% nitrogen in helium mixture.

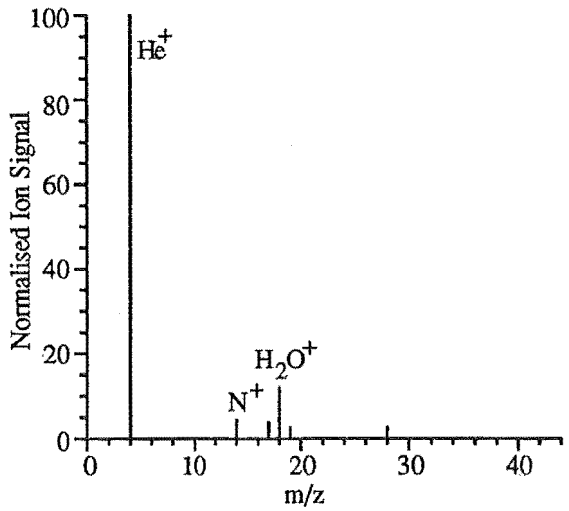

Figure 6.1 Mass spectrum of pure helium.

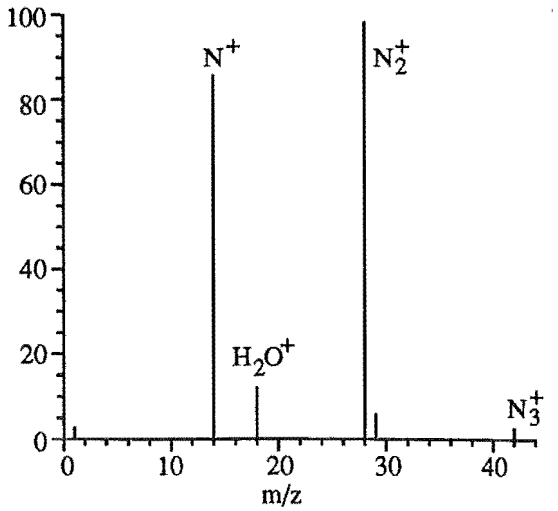

Figure 6.2 Mass spectrum of 1% N_2 in helium

To determine the mobility of N^+ or He^+ ions in helium, arrival time distributions were collected at six to twelve drift distances in the range 3 cm to 9 cm for each value of E/N. The mobility of helium was measured to ensure the satisfactory operation of the drift-tube after maintenance. The reduced mobility was obtained after modelling the He^+ arrival time distributions using the program ATD.F77. The experimental reduced mobility of He^+ in helium as a function of E/N is given in Table 6.1.

E/N (Td)	A ($cm^2V^{-1}s^{-1}$)	B ($cm^2V^{-1}s^{-1}$)	difference (%)
40	9.84	9.28	6.0
60	8.79	8.67	1.4
80	8.06	8.12	-0.74
100	7.73	7.67	0.78
120	7.12	7.25	-1.8

Table 6.1 Experimentally determined reduced mobility of He^+ in helium. A, this study; B, Ellis et al., (1976).

The mobility of N^+ was measured from 35 Td to 140 Td in steps of 5 Td. Two typical experimental arrival time distributions obtained for N^+ are shown in Figure 6.3. Both of the arrival time distributions given in Figure 6.3 were recorded at 70 Td under identical conditions except that the drift distance, z, was changed between measurements. The change in drift distance affects the mean arrival time and the width of the distribution.

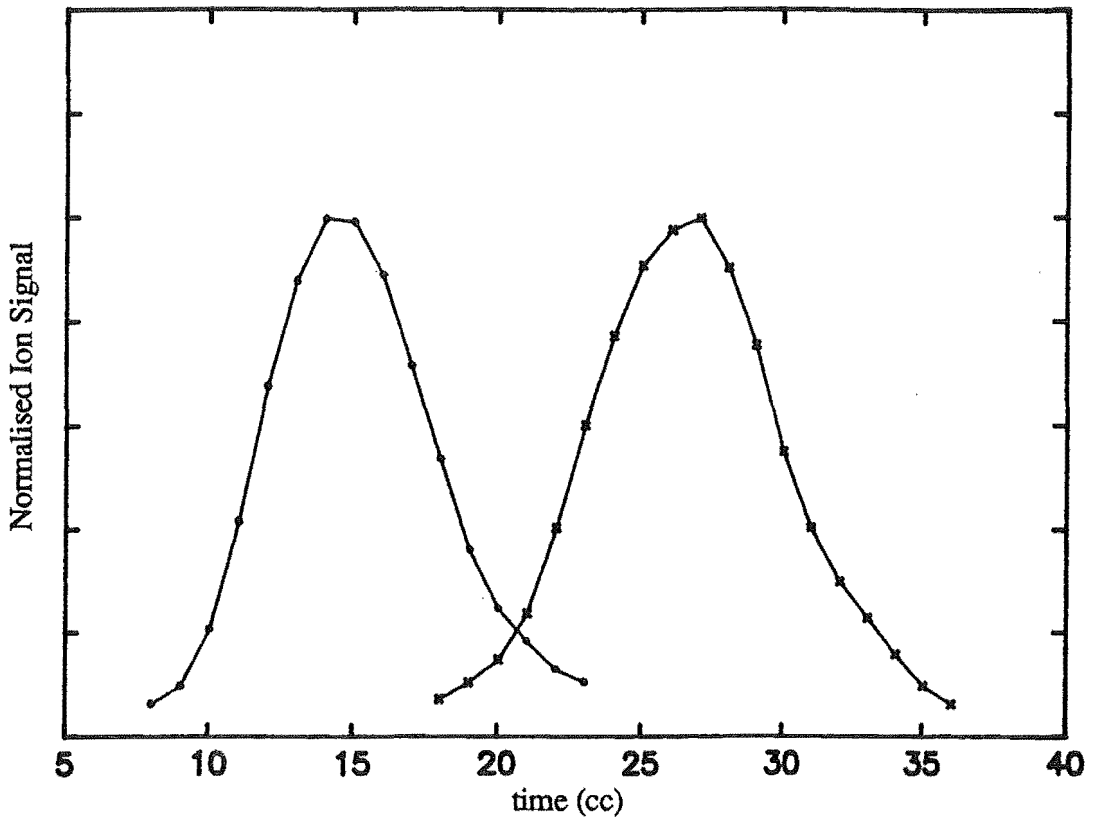

Figure 6.3 Experimental arrival time distributions for N^+ in helium. •, z=4.67 cm; x, z=8.67. The time is given in clock cycles (cc) where 1 cc = 0.97752 μs.

The arrival time distributions obtained for N^+ in helium were modelled to obtain the mobility. During this procedure, estimates are required for the mobilities and depletion rate constants for the primary and secondary ions. The mobility of the primary ion, He^+, was taken from the literature (Ellis et al., 1976). The rate coefficient for the loss of N^+, by reaction with N_2, was set to $1.8 \times 10^{-10} cm^3 s^{-1}$ (Fehsenfeld et al., 1974). The other two parameters needed before the arrival times could be modelled were the mobility of the secondary ion (N^+) and the rate constant for the loss of the primary ion. These were treated as variables during the fitting procedure. Variation of the secondary ion mobility shifted the position of the arrival time along the time axis and enabled the leading edge and the maximum value of the calculated distribution to be matched with the experimental results. Changing the rate constant for the loss of the primary ion enabled the trailing edges of the arrival time distributions to be closely fitted. The results of fitting one arrival time is shown in Figure 6.4. This arrival time distribution was

recorded at an E/N value of 85 Td, a drift distance of 7.24 cm, and a gas temperature of 300 K. For the calculation the reduced mobility of N^+ was 19.7 $cm^2V^{-1}s^{-1}$ and the rate constant for the loss of N^+ was $4.2x10^{-9}$ cm^3s^{-1}.

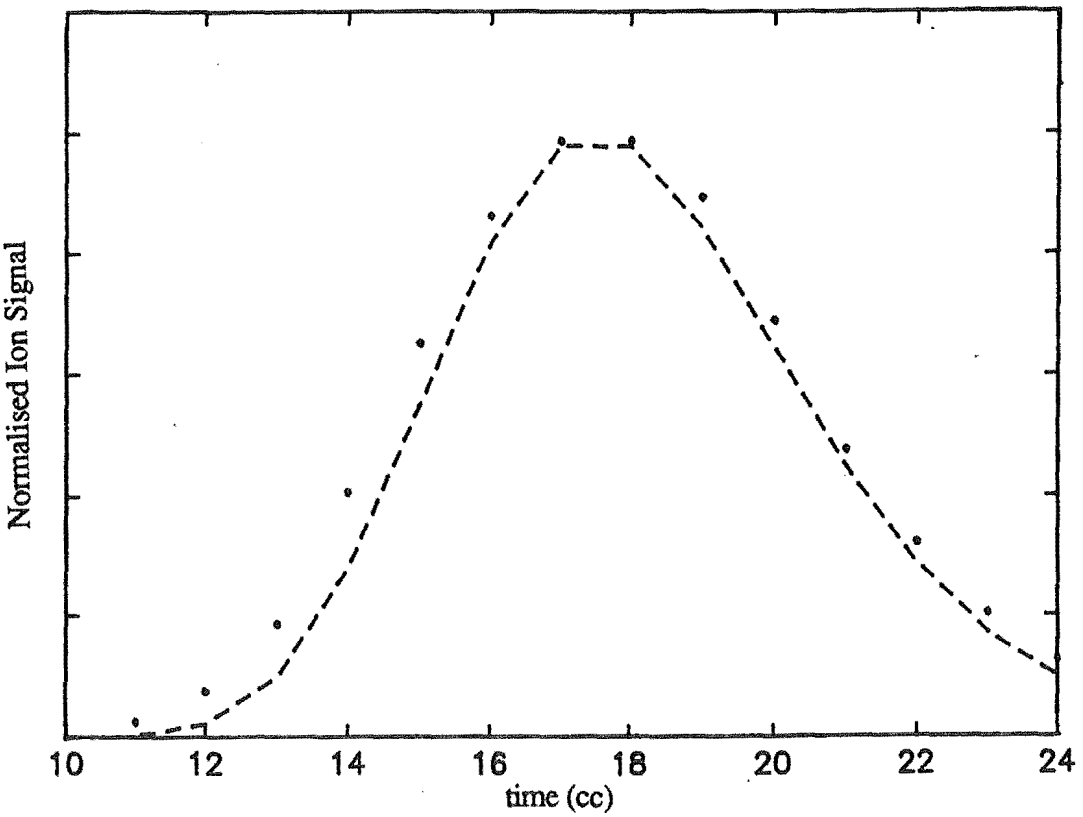

Figure 6.4 Experimental and calculated arrival time distributions for N^+ in helium. •, experimental measurements; – – –, calculated distribution. The time is given in clock cycles (cc) where 1 cc = 0.97752 μs.

The results of the mobility measurements for N^+ in helium are given in Table 6.2 and compared graphically to previous measurements in Figure 6.5.

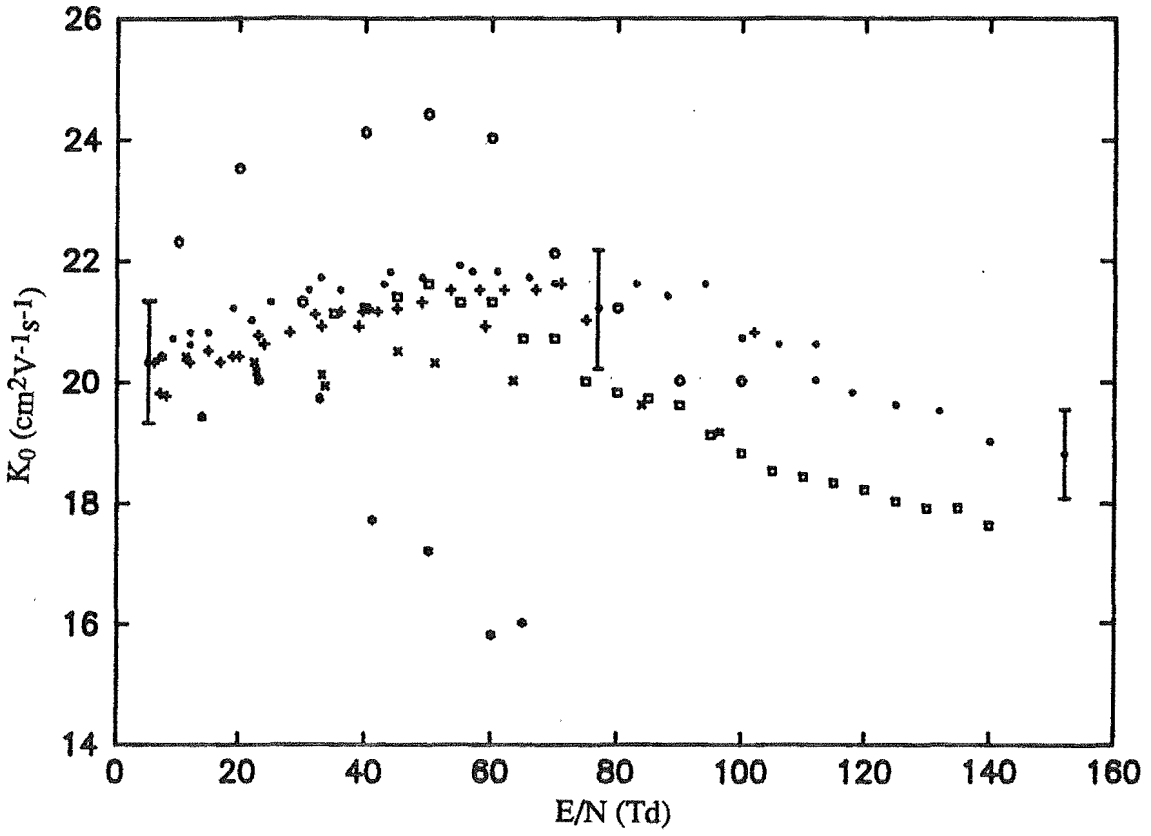

Figure 6.5 Experimental measurements of the mobility of N^+ in helium. □, this work; *, Johnsen et al. (1970); +, McFarland et al., (1973); x, Kaneko et al., (1978); ●, Fahey et al., (1981); o, Fhadil et al., (1985).

E/N (Td)	K_0 ($cm^2V^{-1}s^{-1}$)	k (10^{-9} cm^3s^{-1})
35	21.1	2.8
40	21.2	2.9
45	21.4	3.1
50	21.6	3.1
55	21.3	3.5
60	21.3	3.4
65	20.7	3.8
70	20.7	3.9
75	20.0	4.0
80	19.8	4.1
85	19.7	4.2
90	19.6	4.4
95	19.1	4.4
100	18.8	4.6
105	18.5	4.4
110	18.4	4.5
115	18.3	4.5
120	18.2	4.8
125	18.0	4.9
130	17.9	5.0
135	17.9	5.1
140	17.6	5.7

Table 6.2 Experimentally determined reduced mobility, K_0, of N^+ in helium and rate coefficient, k, for the loss of He^+ required to model the arrival time distributions.

6.4 Rate Coefficient Measurement

Drift tubes can be used to measure ion-molecule rate coefficients for an ion-molecule process by determining the attenuation of the reactant ion signal as a function of the partial pressure of added neutral reactant gas. This process is an exponential type decay of the ion signal as shown:

$$I^+ = I_0^+ \exp(-\sigma N_r z) \tag{6.3}$$

In Equation 6.3 σ is the reaction cross section, z is the drift distance, and N_r is the particle density of reactant molecules. Thus a plot of $\ln(I^+)$ versus N_r has slope $-\sigma z$. The rate coefficient depends upon the ion velocity distribution, the reaction cross section, and the parameter E/N (Russ et al., 1975):

$$k(E/N) = \int_{v_r^*}^{\infty} v_r \, g'(v_r,E/N) \, \sigma(v_r) \, dv_r \tag{6.4}$$

where v_r^* is the threshold speed, $g'(v_r,E/N)$ is the joint ion-neutral speed distribution, and $\sigma(v_r)$ is the velocity dependent cross section. If we assume the velocity distribution is a delta function, $\delta(v_r-v_d)$ (Williams, 1980), then Equation 6.4 reduces to

$$k(E/N) = \sigma(v_d) \, v_d \tag{6.5}$$

The gas density, N_r, can be written in terms of the standard gas density, N_0, the pressure of the reactant in Torr, p_r, and the gas temperature, T, in K:

$$N_r = N_0 \frac{p_r}{760} \frac{273.15}{T} \tag{6.6}$$

An expression for the rate constant can be derived using the above equations:

$$k = \frac{T}{273.15} \frac{760}{p_r} \frac{v_d}{N_0} \ln\left(\frac{I_0^+}{I^+}\right) \tag{6.7}$$

The rate coefficient for a bimolecular reaction, k, is normally expressed in cm^3s^{-1} units.

The rate coefficient for the charge transfer reaction of He^+ with nitrogen was measured by observing the attenuation of the He^+ signal with increasing partial pressures of nitrogen in

the helium buffer gas. Measurements were made over the E/N range from 20 Td to 140 Td. The results are plotted in Figure 6.6 together with the rate constants derived during the arrival time distribution measurements.

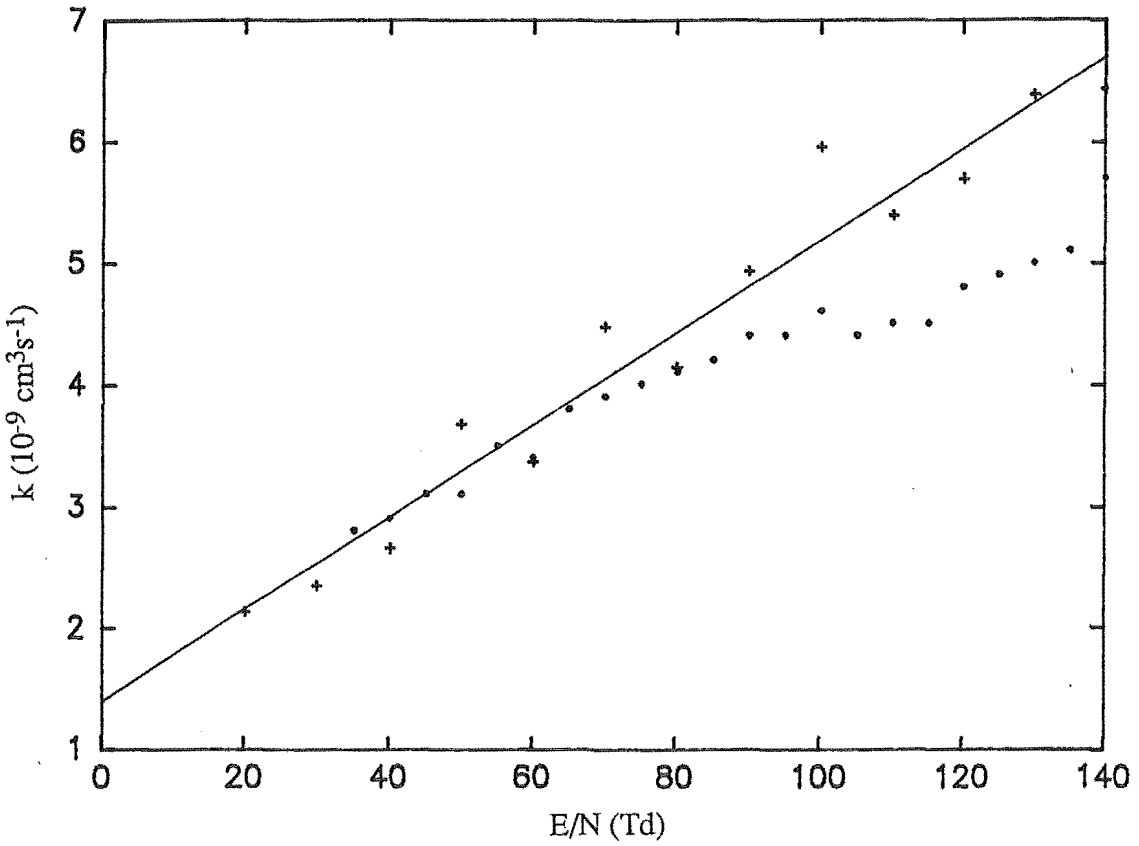

Figure 6.6 Reaction rate coefficient for the charge transfer reaction of He^+ with nitrogen. +, experimental measurements; o, derived from arrival time distribution calculations; ——, least squares line through the experimental measurements.

At 0 Td the intercept of the least squares line through the data is at 1.37×10^{-9} cm^3s^{-1}. This corresponds to a rate coefficient measurement at 300 K and is acceptably close to previous values which lie in the range $1.2\text{-}1.8 \times 10^{-9}$ cm^3s^{-1} (Anicich and Huntress, 1986; Lindinger et al., 1979).

6.5 Discussion

The measurement of an increasing rate coefficient with increasing E/N, while agreeing with our findings from our arrival time modelling (during the analysis of mobility data), disagrees with a previous study of the dependence of the rate coefficient on the centre of mass collision energy (Lindinger et al., 1979) which found that the rate coefficient is essentially independent of collision energy. However, the corroboration of our two independent estimates of the rate coefficient on E/N gives us confidence that our measurements are reasonable.

The mobility measurements of N^+ in helium, reported in this chapter, while providing accurate information, did not show any unusual behaviour of the dependence of the reduced mobility on E/N which could not be explained in terms of the experimental uncertainties.

Chapter 7

Calculation of the Mobility of F^- in Helium

7.1 Introduction

The mobility of F^- in helium has been calculated using the two-temperature theory of ion transport. The interaction potential required for this calculation is the $^1\Sigma$ state of HeF^-. The theory and program used have been described in Chapters 2 and 4. This ion-helium system has previously been studied experimentally. The results of this work are compared to the experimental measurements. The mobility of F^- in helium has not been studied by purely ab-initio methods because of the lack of suitable interaction potentials

7.2 Molecular Orbital Theory

The large majority of ab-initio calculations performed to date use molecular orbital theory to describe the molecular wave function. This is due to the relative ease of implementation and consequently, efficient programs are available to perform these calculations. A comprehensive review of ab-initio molecular orbital theory is available (Hehre et al.,1986). Molecular orbital models require the assignment of single electrons to one electron functions called spin orbitals. Spin orbitals are the product of a spin function, α or β, designating the two spin states available to an electron, and a spatial molecular orbital function, ψ_i. These spin orbitals are collected together to form a many electron wave function Ψ, usually a Slater determinant (or a sum of several Slater determinants), as this has the correct symmetry and permutation properties.

7.2.1 Hartree-Fock Model

The simplest molecular orbital approximation to the Schrödinger equation assumes the true wave function is described by a single Slater determinant; this is the Hartree-Fock

approximation. In practice the molecular orbitals, ψ_i, must be constructed from a linear combination of one electron basis functions, ϕ_μ , corresponding to atomic orbitals:

$$\psi_i = \sum_{\mu=1}^{N} c_{\mu i}\, \phi_\mu \qquad (7.1)$$

The coefficients of the atomic orbital basis set functions, $c_{\mu i}$, are variationally determined to self consistency to minimise the energy of the many electron wave function, Ψ, this is sometimes termed the LCAO-SCF (linear combinations of atomic orbitals self consistent field) procedure. The SCF procedure gives the best wave function possible within the Hartree-Fock (HF) approximations of a finite basis set and only a single many electron wave function. As the basis set is improved, the energy calculated is lowered towards the Hartree-Fock limit. The HF limit for the variational energy lies above the true energy because the single determinant description of the wave function does not describe the correlated motion of the electrons. Instead the electrons are assumed to be moving in the average field created by the other electrons. This limitation is a consequence of the form of the wave function chosen. To go beyond the HF limit, several Slater determinants are required to describe the wave function. The two main ways of obtaining multiple determinant molecular orbital wave functions are the method of Configuration Interaction (CI) and Møller-Plesset (MP) perturbation theory. Both these methods require an initial HF calculation to determine the molecular orbitals.

7.2.2 Configuration Interaction

We can construct a wave function of the form

$$\Psi = a_0\Psi_0 + a_1\Psi_1 + a_2\Psi_2 + \ldots \qquad (7.2)$$

where Ψ_0 is the HF wave function. Here Ψ_1, Ψ_2, ... are wave functions (usually Slater determinants) for other configurations. This forms the basis of the configuration interaction (CI) procedure. The coefficients of the atomic orbitals used to construct the molecular orbitals in Ψ_0, and the coefficients, a_j, in Equation 7.2 are variationally determined. If all possible Ψ_i are used, for a particular basis, the resulting CI calculation is termed full CI and is the best calculation possible with that particular basis set.

7.2.3 Møller-Plesset Perturbation Theory

The other common method of going beyond the HF limit is to use perturbation theory. This is similar to the CI procedure described above, as it starts with an initial SCF calculation, but it differs in the way the other configurations are chosen. One particular perturbation theory known as Rayleigh-Schrödinger Many-Body Perturbation Theory, RSMBPT (see Levine, 1985) was applied to molecules by Møller and Plesset (1934) and is incorporated into the program GAUSSIAN82. This method assumes that the exact wave function can be expressed as a perturbation from the HF wave function; this is an expansion in powers of the degree of perturbation, λ:

$$\Psi_\lambda=\Psi^{(0)} + \lambda\Psi^{(1)} + \lambda^2\Psi^{(2)} + \ldots \tag{7.3}$$

$$E_\lambda=E^{(0)} + \lambda E^{(1)} + \lambda^2 E^{(2)} + \ldots \tag{7.4}$$

Equations 7.3 and 7.4 are terminated at the required point to give second (MP2), third (MP3), or fourth order (MP4) expressions for the wave function and its associated energy. For MP theory to be successful, the virtual orbitals in the HF wave function need to be accurately described. Expressions for the terms $\Psi^{(1)}$, $E^{(1)}$, ..., as well as a detailed account of Møller-Plesset perturbation theory, are available (Hehre et al., 1986, and Pople et al., 1976). The Møller-Plesset perturbation theory satisfies most of the requirements for theoretical chemical models (Pople et al., 1976), including size consistency (extensivity). This property is very important when studying potential energy surfaces for molecular dissociation. It ensures that 'super-molecule' energies (molecules consisting of essentially isolated fragments) are equal to the sum of the energies calculated for each fragment separately.

7.3 Basis Sets

As has been mentioned briefly, a basis set of atomic orbital functions is required before an ab-initio calculation is performed. There is a large range of possible sets, but the one chosen should suit the type of calculation and the accuracy required. The initial choice is whether to

use Slater type orbitals (STOs) or Gaussian type orbitals (GTOs). Some normalised Slater type orbitals are shown in Equation 7.5.

$$\phi_{1s}=\left(\frac{\zeta_1^3}{\pi}\right)^{1/2} \exp(-\zeta_1 r)$$

$$\phi_{2s}=\left(\frac{\zeta_2^5}{96\pi}\right)^{1/2} r \exp(-\zeta_2 r)$$

$$\phi_{2p_x}=\left(\frac{\zeta_2^5}{32\pi}\right)^{1/2} x \exp(-\zeta_2 r) \qquad (7.5)$$

The orbital exponents, ζ_1 and ζ_2, are constants which determine the size of the orbitals. The STOs are based upon the solutions of the Schrödinger equation for the hydrogen atom and are thought to be similar to the orbital functions in other atoms. However, STO functions lead to difficulties in evaluating the integrals required for the solution of the SCF equations. Gaussian type orbitals do not suffer this problem, the integrals required can be solved explicitly without recourse to numerical integration, but are less satisfactory as representations of atomic orbitals because they do not have a cusp at the origin. Some normalised GTOs are given in Equation 7.6:

$$g_s(\alpha,r)=\left(\frac{2\alpha}{\pi}\right)^{3/4} \exp(-\alpha r^2)$$

$$g_x(\alpha,r)=\left(\frac{128\alpha^5}{\pi^3}\right)^{1/4} x \exp(-\alpha r^2)$$

$$g_y(\alpha,r)=\left(\frac{128\alpha^5}{\pi^3}\right)^{1/4} y \exp(-\alpha r^2)$$

$$g_z(\alpha,r)=\left(\frac{128\alpha^5}{\pi^3}\right)^{1/4} z \exp(-\alpha r^2) \qquad (7.6)$$

For the calculations described in this Chapter, Gaussian orbital functions were used exclusively, principally because large Gaussian basis sets are built into the GAUSSIAN82 program. There are a number of standard Gaussian basis sets which have become widely used

and their strengths and weaknesses are well known (Hehre et al., 1986). The least sophisticated of these are the STO-nG basis sets, for example STO-3G, which simulate Slater type orbitals by a number of Gaussian type orbitals; in this case three. This is a minimal basis set; only enough orbitals are included to accommodate the electrons. This basis has been largely superseded by split valence basis sets. In a split valence basis each valence atomic orbital is split into two (or sometimes three) parts; a compact inner orbital and a larger, more diffuse outer orbital. The advantage of a split valence basis set is that the coefficients, determined during MO formation, allow the orbitals to vary in size. One such basis is named 4-31G. This basis set has four Gaussian orbitals combined for each core orbital, and three and one Gaussian orbitals combined for the inner and outer parts of the valence orbitals respectively. The next step in improving a basis set is to add polarization functions. For heavy (non-hydrogen) atoms these are usually d-orbitals. Hydrogen polarisation functions are p-orbitals. These functions do not usually behave like orbitals in the normal bonding sense, but mix with p- or s-orbitals to produce 'polarised' orbitals. These are orbitals whose centres are shifted away from the atomic nucleus. The 6-31G* basis has polarisation functions on heavy atoms, whereas the 6-31G** basis has polarisation functions on hydrogen atoms as well. One other basis set deficiency is lessened by the inclusion of diffuse functions. These are necessary to improve the description of long range interactions. A single '+' in the basis set description (6-31+G*) shows that very diffuse s- and p-orbitals have been added to each heavy atom; a 6-31++G* basis has diffuse s-orbitals on each hydrogen as well. The number of basis set functions rises rapidly with increasing sophistication and consequently the computer time and storage space required increases dramatically. As a result of this, complex computations like geometry optimisations are performed with small basis sets, and are followed by large basis single point calculations.

7.4 The GAUSSIAN82 Program

The GAUSSIAN82 program is the latest version of one of the most widely used computer programs publicly available for ab-initio molecular orbital type calculations. A general overview of the program, giving examples of the input required and the output from several

different problems, is available (Clark, 1985). This program requires only minimal user input and functions very much as a 'black-box'. Typical input required for a calculation would be a z-matrix giving the details of the molecular geometry, and the charge and the spin multiplicity. The type of calculation would also be stated; for example one could specify an energy calculation at a fixed geometry, or an energy minimisation could be performed to find preferred geometries of stable molecules or transition states. The user is also required to choose the type of basis set, the program includes several Gaussian basis sets, or to furnish details of the particular basis set required. Finally, the last piece of information needed before the program will execute, is the highest level of theory required. The program initially calculates a Hartree-Fock (HF) self consistent field wave function, then uses this as the zero-order wave function in a Møller-Plesset perturbation theory expansion. The orbitals selected for occupation in the HF wave function can be altered if required. The highest level of perturbation the program will allow is a fourth order calculation involving all single, double, and quadruple excitations from the zero order wave function. When the number of electrons becomes large and a complex basis set is used this is a major computational effort taking many hours of processor time. When post Hartree-Fock methods are used, inner shell (core) electrons can be excluded from the correlation energy calculation. One of the main limitations of the perturbation theory being used, is that often the single reference wave function description is not capable, in the general case, of describing molecular dissociation. Multiconfiguration methods are possible which overcome this limitation but they have not yet been widely distributed. The HeF^- dissociation can be described by a single Slater determinant. The notation used in describing a calculation carried out using the GAUSSIAN82 program gives the level of theory and the basis set used. For example, MP4SDQ/6-311+G(3df,3pd) describes a calculation using Møller-Plesset (MP) perturbation theory taken to fourth order (4) including all single, double and quadruple excitations (SDQ) from the reference HF function. The '/' separates details of the level of theory from the information about the basis set. The core atomic orbitals are described by 6 Gaussian functions. The valence atomic orbitals are split into three parts; the inner most part is described by 3 Gaussian functions, the two outer parts are described by 1 Gaussian function each. This basis set al.so has diffuse functions on non-hydrogen atoms, signified by the '+', and polarisation functions on each atom, d- and f-orbitals on fluorine and p- and d-orbitals on

helium.

7.5 The HeF^- Interaction Potential

At the time this work was undertaken there were no accurate ab-initio calculations on the ground state of the HeF^- molecule ion. One interaction potential that had been reported (Kirkpatrick and Viehland, 1985) was derived by inverting the available experimental data and consequently was of minor interest to us, as our aim was to calculate the mobility of the F^- ion in helium without using the experimental measurements. However, this potential was submitted to both two- and three-temperature theory calculations and the results discussed in Section 7.7. Before any mobility calculations could be performed, an accurate ab-initio interaction potential had to be obtained. The ground-state interaction potential of HeF^-, separating at infinity to He ^1S and F^- ^1S, was calculated using the GAUSSIAN82 program. Initially, calculations were performed using a 6-311+G** basis set but this basis was superseded by an even larger basis set when it was realised that there was a long range van der Waals attraction present in this molecule ion. Consequently, calculations were performed at the MP4SDQ/6-311+G(3df,3pd) level of theory, excluding core contributions to the correlation energy. At this level of theory the electron affinity of fluorine was calculated to be 3.157eV, as compared with the experimental value of 3.399eV. The error in the calculation of the energy of the He ^1S atom is 0.13eV. The results of the HeF^- calculation at the HF, MP2, and MP4SDQ levels of theory are shown in Table 7.1.

r (Å)	E (hartree)		
	HF	MP2	MP4SDQ
0.875	-101.735086	-102.081608	-102.083380
1.000	-101.905339	-102.250593	-102.251498
1.125	-102.045273	-102.379418	-102.382096
1.250	-102.141120	-102.468781	-102.472140
1.375	-102.202732	-102.526809	-102.530412
1.500	-102.241556	-102.563573	-102.567240
1.625	-102.265880	-102.586701	-102.590348
1.750	-102.281073	-102.601225	-102.604807
1.875	-102.290532	-102.610340	-102.613838
2.000	-102.296412	-102.616072	-102.619482
2.250	-102.302361	-102.621997	-102.625253
2.500	-102.304661	-102.624385	-102.627529
2.750	-102.305525	-102.625332	-102.628402
3.000	-102.305827	-102.625683	-102.628708
3.125	-102.305880	-102.625749	-102.628759
3.250	-102.305897	-102.625773	-102.628772
3.375	-102.305893	-102.625771	-102.628761
3.500	-102.305875	-102.625751	-102.628736
4.000	-102.305771	-102.625620	-102.628595
4.500	-102.305687	-102.625510	-102.628480
5.000	-102.305637	-102.625443	-102.628411
5.500	-102.305608	-102.625407	-102.628374
∞	-102.305551	-102.625345	-102.628311

Table 7.1 Hartree-Fock, HF, second order Møller-Plesset, MP2, and fourth order Møller-Plesset (including all single, double and quadruple excitations), MP4SDQ, total energies as a function of internuclear separation for HeF^-.

As described in Chapter 4, a cubic spline was used to transform the calculated potential points into the continuous function required by the collision integral calculation. Analytic functions were fitted to both ends of the cubic spline to ensure that the interaction potential function, and its first derivative, were defined for all internuclear separations, $0 < r < \infty$. Outside the range of internuclear separation spanned by the cubic spline ($r_{min} < r \leq r_{max}$) the extrapolating functions, 7.7 and 7.8, were of the same form as previously described in Chapter 4:

$$V(r) = \frac{a}{r^m} + b \qquad 0 < r \leq r_{min} \qquad (7.7)$$

$$V(r) = \frac{c}{(r-d)^n} \qquad r_{max} \leq r < \infty \qquad (7.8)$$

The constants a, b, c, and d were determined slightly differently in the version of the two-temperature theory program used in this work. For given values of m and n, a and b were chosen so that Equation 7.7 matched the spline and its first derivative at $r = r_{min}$. Coefficients c and d were determined by requiring that Equation 7.8 match the two interaction potential points at the large-r end of the spline. The values of the collision integrals obtained were relatively insensitive to the values of m and n chosen as discussed in Chapter 4. The mobility calculations performed in this Chapter were calculated with $m = n = 5$. The collision integrals were insensitive to the variation of n and m, changing by less than 0.1% over the range from 4 to 7. For internuclear separations important in determining the values of the collision integrals at low E/N, the dispersion r^{-6} term appears to have a significant contribution as well as the ion-induced dipole r^{-4} term. The calculated points are shown in Figure 7.1. The ground state of the HeF^- molecule ion is essentially a repulsive interaction except for the presence of a small, but important, van der Waals type attraction at large distance.

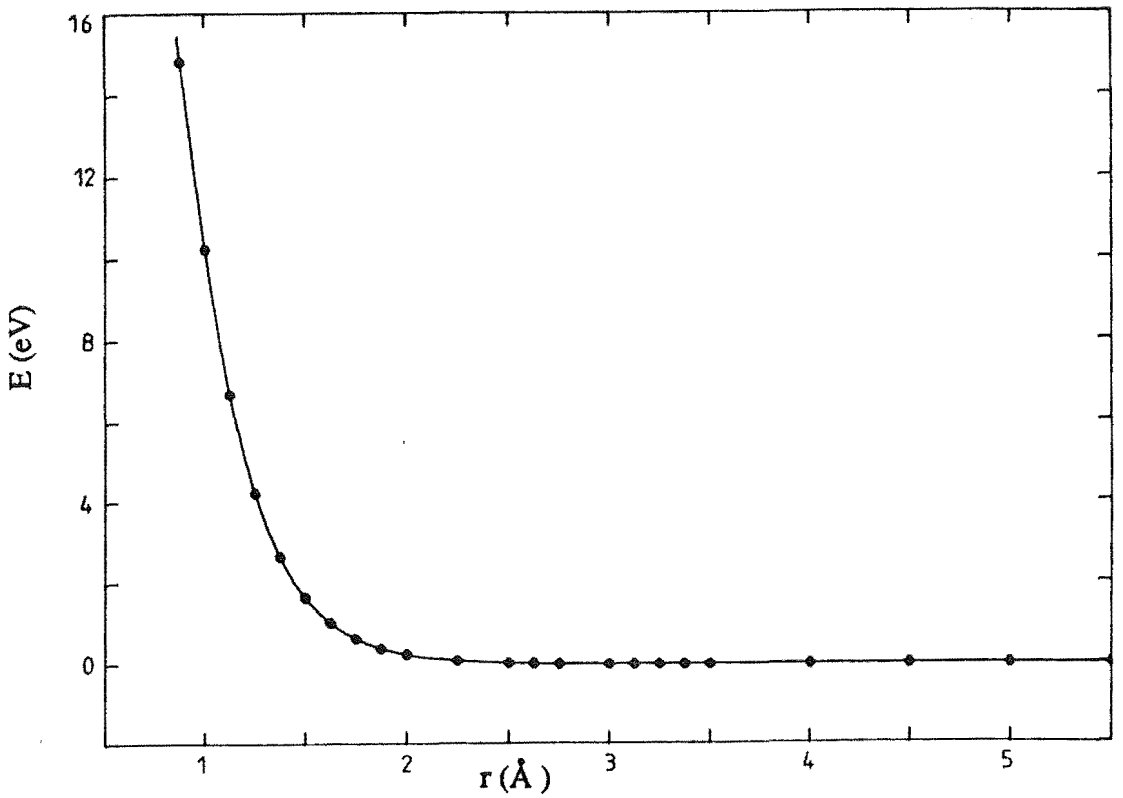

Figure 7.1 Interaction potential of $^1\Sigma$ HeF^-. ●, MP4SDQ/6-311+G(3df,3pd) values.

7.6 Two-Temperature Theory Calculations

The reduced mobility of F^- in helium as a function of E/N has been reported by Dotan et al. (1977,1979) and subsequently included in a compilation of mobility data (Ellis et al., 1978). These values have been used as the basis for the comparison of theory and experiment. The two-temperature theory has been applied, calculating α and β to first order at the second approximation of the theory, to several related HeF^- interaction potentials, thus determining the theoretical dependence of both the reduced mobility, K_0, and drift velocity, v_d, of F^- in helium on the parameter E/N. The following interaction potentials were used in the two-temperature theory calculations:

(i) MP4SDQ/6-311+G(3df,3pd)

(ii) HF/6-311+G(3df,3pd)

(iii) same as (i) except only the points on a purely repulsive curve were used

(iv) same as (i) except the well depth was halved, that is, the interaction potential $\{r,E'(r)\}$ is used where $E'(r)=\frac{E(r)}{2}$ if $E(r) < E(r=\infty)$ otherwise $E'(r)=E(r)$.

Interaction potential (ii) was the Hartree-Fock result using a large basis set. Interaction potential (i) was the highest level of theory used (fourth order Møller-Plesset perturbation theory) with the same basis set as (i). A comparison of the results of the mobility calculations for these two interaction potentials showed that the potential (i) was not as good at calculating the low field mobility of F^- in helium as potential (ii). The principal difference between these interaction potentials lay in the depth of a small attractive well at ~3.3 Å. The well depth was 0.0125 eV in potential (i) but only 0.0094 eV in potential (ii). Although the difference in well depths was small, it was investigated as a possible cause of the difference in calculated low field mobilities. Potential (iii), a purely repulsive curve, was constructed to completely ignore this well . It was formed by truncating the calculated points in potential (i) at 2.25 Å, before the attractive part of that curve. The extrapolating function (Equation 7.8) then approached V(r)=0 as r was increased, but never became negatively valued. Potential (iv) halved the depth of the well in (i) by forming a new interaction potential where the energies were the same as in (i) with the exception of those which were less than the infinite separation energy; these were halved.

In Table 7.2 are listed the results from the two-temperature calculation using potential (i); the effective temperature values, T_{eff}, used were determined by setting β to zero and using the Equation 7.9 to convert the experimental drift velocities to approximate effective temperatures. This was done to ensure that the collision integrals obtained from these calculations could be used to calculate the mobility of F^- in helium over a similar range of E/N as the experiment results:

$$T_{eff} \approx T + \frac{1}{3k_B} M v_d^2 \qquad (7.9)$$

Table 7.3 compares the reduced mobilities from all the calculations and the drift velocity from the calculation using potential (i) with the corresponding experimental quantities; the raw calculated reduced mobilities and drift velocities were interpolated using a cubic spline to provide values at the experimental values of E/N in this tabulation.

T_{eff} (K)	$\Omega^{(1,1)}(T_{eff})$ (Å^2)	α	β	v_d (ms^{-1})	E/N (Td)	K_0 (cm^{2}V^{-1}s^{-1})
298.0	23.51	0.000	-0.000	78.94	1.171	25.09
310.0	23.07	0.000	-0.000	284.6	4.226	25.07
360.0	21.56	0.003	-0.002	627.2	9.356	25.95
450.0	19.65	0.008	-0.006	979.4	14.81	24.62
534.	18.42	0.013	-0.010	1221.	18.75	24.24
590.	17.77	0.016	-0.012	1359.	21.12	24.96
770.	16.25	0.022	-0.016	1731.	27.92	23.07
870.	15.63	0.024	-0.018	1907.	31.39	22.62
990.	15.02	0.026	-0.019	2098.	35.32	22.11
1277.	13.92	0.030	-0.021	2497.	44.09	21.08
1750.	12.69	0.032	-0.023	3044.	57.24	19.76
2321.	11.69	0.033	-0.023	3593.	71.58	18.69
3170.	10.66	0.034	-0.023	4281.	90.86	17.54
4600.	9.517	0.033	-0.023	5238.	119.6	16.30
5500.	8.999	0.033	-0.022	5758.	136.1	15.75
6400.	8.573	0.032	-0.023	6235.	151.5	15.32
7400.	8.176	0.031	-0.021	6724.	167.7	14.93
8600.	7.777	0.030	-0.020	7267.	186.0	14.55
10700.	7.215	0.029	-0.019	8130.	215.6	14.04
12200.	6.888	0.028	-0.018	8692.	235.2	13.75

Table 7.2 Calculated momentum-transfer collision integrals, drift velocities, reduced mobilities and related quantities for He + F^-.

	K_0 ($cm^2V^{-1}s^{-1}$)					v_d (10^2ms^{-1})	
E/N (Td)	MP4SDQ	HF	Half well	Repulsive	Experiment	MP4SDQ	Experiment
2.0	25.1	27.1	29.7	33.6	29.2	1.35	1.57
4.0	25.1	27.0	29.5	33.2	28.9	2.69	3.10
6.0	25.0	26.9	29.2	32.5	28.5	4.04	4.60
8.0	25.0	26.7	28.8	31.8	28.2	5.37	6.06
10.0	24.9	26.5	28.4	30.9	27.8	6.70	7.47
12.0	24.8	26.2	27.9	30.1	27.5	8.00	8.86
15.0	24.6	25.8	27.2	28.9	27.0	9.92	10.9
20.0	24.1	24.9	25.9	27.2	26.1	13.0	14.0
30.0	22.8	23.2	23.8	24.5	24.6	18.4	19.8
40.0	21.5	21.8	22.2	22.6	23.2	23.2	24.9
60.0	19.6	19.6	19.9	20.1	20.9	31.5	33.7
80.0	18.1	18.1	18.3	18.5	19.3	39.0	41.5
100.	17.1	17.0	17.2	17.3	18.0	45.9	48.4
120.	16.3	16.2	16.4	16.4	17.0	52.5	54.8
140.	15.6	15.5	15.7	15.7	16.3	58.8	61.3
160.	15.1	15.0	15.2	15.2	15.7	64.9	67.4
180.	14.7	14.5	14.7	14.7	15.1	70.9	73.0
200.	14.3	14.2	14.3	14.3	14.6	76.8	78.5
220.	14.0	13.8	14.0	14.0	14.2	82.6	83.9

Table 7.3 Theoretical and experimental values for the reduced mobility and the drift velocity of F^- in helium.

The theoretical calculated and measured experimental values of the reduced mobility, K_0, as a function of E/N are compared graphically in Figure 7.2.

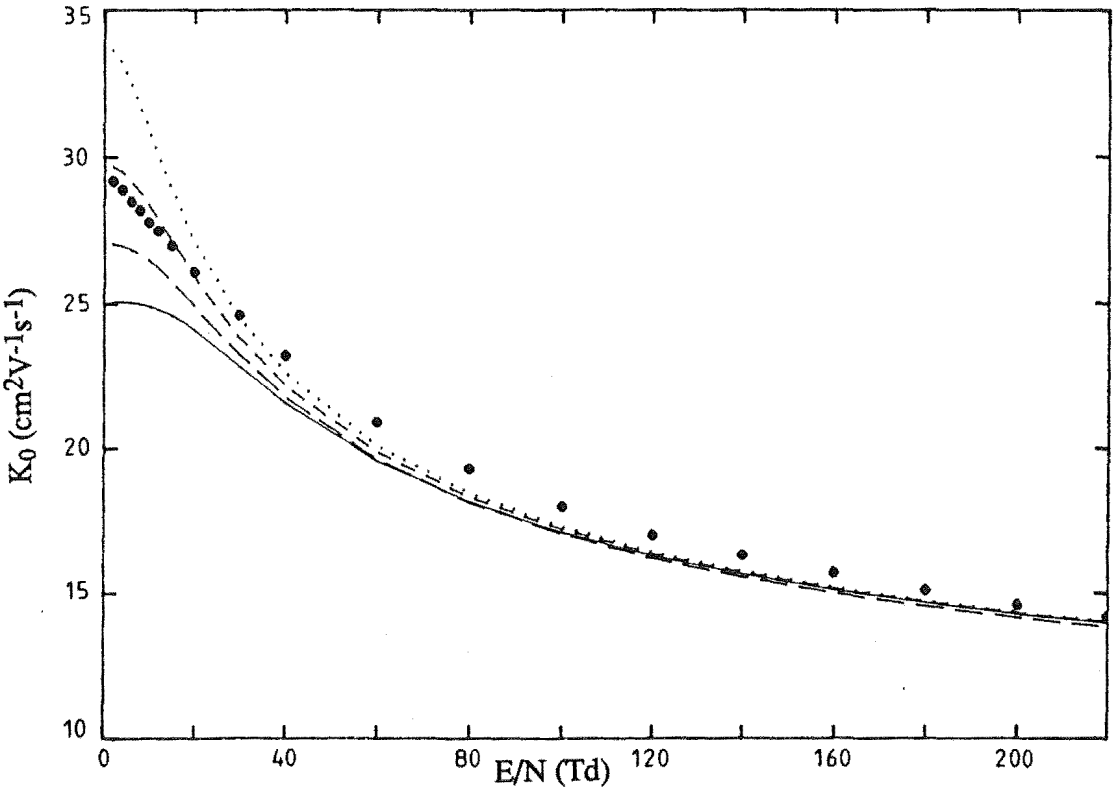

Figure 7.2 Calculated and experimental reduced mobilities of F^- in helium. ●, experiment; ——, MP4SDQ; — —, HF; - - -, half well; · · · · ·, repulsive curve.

The graphical comparison of the theoretical calculated and measured experimental drift velocities as a function of E/N is shown in Figure 7.3.

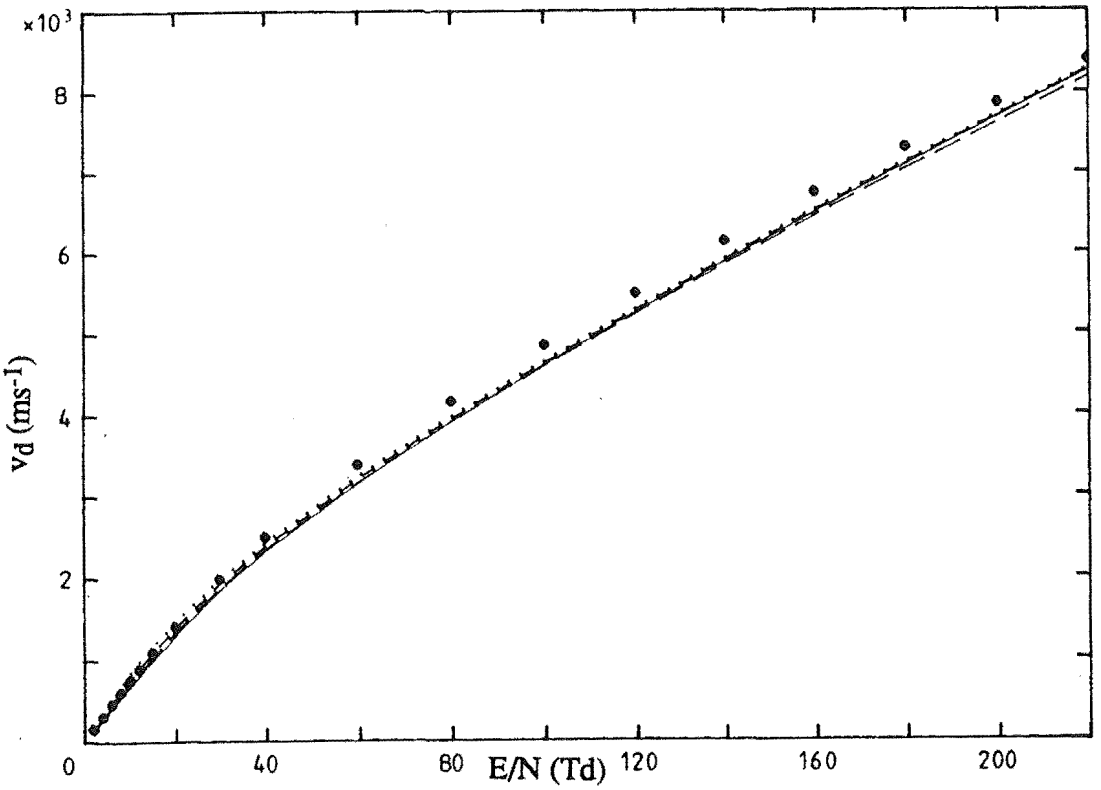

Figure 7.3 Calculated and drift velocities of F^- in helium. ●, experiment; ——, MP4SDQ; — —, HF; - - -, half well; · · · · ·, repulsive curve.

The MP4SDQ potential (i) provided good agreement with the experimental reduced mobility at large E/N but was poorer than the Hartree-Fock potential (ii) at very low values of E/N. The reason for this is explained by the results from potential curves (iii) and (iv) as shown in Figure 7.2 and Table 7.3. The difference in the calculated mobilities from the MP4SDQ and HF interaction potentials, (i) and (ii), can be rationalised in terms of the difference in the well depth. The half well potential (iii) accurately reproduces the mobility of F^- in helium over the range of E/N covered by experimental measurements and on the basis of this it appears that our MP4SDQ interaction potential has overestimated the depth of the attractive well by approximately 0.006 eV.

Thus, although correlation energy makes an important contribution to the interaction energy, it must be determined consistently over a wide range of internuclear distance for the interaction potential to be useful in mobility calculations. Comparison of the mobilities at large E/N, above 100 Td, calculated using the MP4SDQ and HF potentials with the experimental values, shows the MP4SDQ potential to be slightly better in this region. At high field the

mobility is dominated by scattering off the repulsive wall of the interaction potential. A comparison of the HF and MP4SDQ curves, at short range, suggests that at small internuclear separation the calculated interaction potentials may not be steep enough.

The drift-velocity comparisons, as shown in Figure 7.3, do not show the effect of changing the potential well depth and it appears that the agreement with experiment is good for v_d values at low E/N but not as good at high E/N. However, at a given value of E/N, the percentage errors between the calculated drift velocities and the experimental measurements are the same as the percentage errors between the calculated reduced mobilities and the corresponding experimental values.

7.7 Three-Temperature Theory Calculations

In order to check the reliability of our two-temperature theory calculations, using our interaction potential calculated at the MP4SDQ/6-311+G(3df,3pd) level of theory, three-temperature theory calculations were performed on this interaction potential. Also, three-temperature theory calculations were performed on a recently available high level (fourth order) many-body perturbation theory, MBPT(4), interaction potential (Dierckson and Sadlej, 1986). The MBPT(4) interaction potential had been calculated using a very large polarised basis set of Gaussian type orbitals. For helium the basis included four contracted s-orbitals to which were added a diffuse s-orbital and p- and d-orbital functions. A similar contracted basis was used for fluorine and extended by diffuse s- and p- functions as well as d- and f-polarisation functions. The resulting interaction potential has a well depth of 0.008 eV at 3.45 Å.

For the three-temperature theory calculations the collision cross sections, $Q^{(l)}(E')$, required were calculated to 0.1% accuracy and the reduced mobility converged to an accuracy of 0.75%. In a comparison of computer processor usage it was found that a three-temperature theory calculation is at least an order of magnitude slower than the corresponding two-temperature theory calculation, taking more than 2000 s for each of the calculations reported here. The results of these calculations are summarised in Table 7.4.

E/N (Td)	Exp.	MP4SDQ		MBPT(4)	
		3-T	2-T	3-T	2-T
2	29.2	25.13	25.09	27.88	27.92
4	28.9	25.12	25.08	27.82	27.85
6	28.5	25.09	25.05	27.72	27.85
8	28.2	25.04	25.00	27.57	27.57
10	27.8	24.97	24.93	27.37	27.36
12	27.5	24.86	24.82	27.12	27.10
15	27.0	24.66	24.61	26.69	26.60
20	26.1	24.19	24.09	25.84	25.62
30	24.6	23.04	22.80	24.07	23.68
40	23.2	21.87	21.55	22.50	22.03
60	20.9	19.87	19.56	20.10	19.64
80	19.3	18.45	18.14	18.45	18.07
100	18.0	17.42	17.09	17.28	16.97
120	17.0	16.57	16.28	16.41	16.16
140	16.3	15.91	15.64	15.75	15.56
160	15.7	15.36	15.11	15.23	15.09

Table 7.4 Two- and three-temperature calculations of the reduced mobility of F^- in helium using two different $^1\Sigma$ HeF^- interaction potentials. All reduced mobilities are in $cm^2V^{-1}s^{-1}$ units.

It can be seen that the three-temperature theory is slightly better than the two-temperature theory at estimating the mobility at high values of E/N, for both interaction potentials, but the improvement is not dramatic. The results still lie below the experimental values in this region but are easily within experimental error (±7%). Adjustment of the repulsive wall of these interaction potentials would bring the calculated high field results into alignment with the experimental results but there is unnecessary. The low field results, for the two- and three-

temperature theory calculations, are almost identical which is to be expected since the three-temperature theory is only an improvement over the two-temperature theory at high field strengths where the ion swarm becomes significantly anisotropic. A comparison of the results obtained for both interaction potentials, with the experimentally determined mobility, shows that the MBPT(4) potential is better at calculating the mobility at low values of E/N than the MP4SDQ potential but the results are very similar at high field. This supports our earlier findings that the value for low field mobilities was dominated by the depth of the van der Waals well in the interaction potential. It may have been noted that the position of the minimum in these interaction potentials is slightly different (3.25 Å and 3.45 Å for the MP4SDQ and the MBPT(4) potentials respectively) and this may be responsible for the observed difference in calculated mobilities at low field. However, this is not the case as the attractive part of the potential has a significant depth over a large region of internuclear separation and it is the magnitude of this depth, and not the position of the minimum in a low curvature region of the potential, that exerts the major influence over the calculated transport coefficients. Similar two- and three-temperature theory calculations were performed on the interaction potential obtained by inverting mobility data (Kirkpatrick and Viehland, 1985). This potential does not exhibit a minimum in the interaction potential as it is only tabulated up to 2.43 Å, less than the position of the minimum in the ab-initio calculations. These calculations accurately recover the mobility above 30 Td, but like our repulsive curve calculations produced mobility values significantly higher than the experimental mobility at low values of E/N. This may indicate that insufficient low field mobility data was used in the inversion process that was used to obtain the interaction potential. An interaction potential obtained from inverting mobility data retains the experimental errors so ideally the mobility data needs to be extremely accurate over a large range of E/N if the interaction potential obtained is to be meaningful.

7.8 The Temperature Dependence of the Mobility of F^- in Helium

Once an accurate interaction potential has been obtained for an ion-neutral system and tested for accuracy by comparing the calculated transport properties, using such an interaction potential, with the corresponding experimental measurements, predictions may be made for the

mobility of the ion at other temperatures. An attempt has been made (Parent and Bowers, 1981) to compare calculated mobilities with experimental measurements made over a range of temperatures but this had little success. It appears that this was due to shortcomings with the interaction potentials used. The accuracy of the low-temperature experiments was also questionable.

In the first approximation of the two-temperature theory, as mentioned in Chapter 2, the calculated reduced mobility depends only on the effective temperature, T_{eff}. In the first approximation T_{eff} depends only on the experimental temperature, T, and the parameter E/N. To prove this Equations 2.2 and 2.21 are combined to obtain

$$K_0 = \frac{3q}{8N_0}\left(\frac{\pi}{2\mu k_B T_{eff}}\right)^{1/2}\frac{1+\alpha}{\Omega^{(1,1)}(T_{eff})} \tag{7.10}$$

Equation 7.9 is rewritten using Equation 4.13 to give Equation 7.11:

$$T_{eff} \approx T + \frac{N_0^2}{3k_B} M K_0^2 (E/N)^2 \tag{7.11}$$

Thus, T_{eff} and correspondingly K_0, depend only on T and E/N as required. When T is significant compared to T_{eff}, variation in T requires a large change in E/N to give the same T_{eff}. In the case of $T_{eff} >> T$, the same variation of T requires only a small change in E/N.

These findings are illustrated by first order two-temperature theory calculations of the mobility of F^- in helium using our MP4SDQ/6-311+G(3df,3pd) interaction potential for HeF^- with the well depth halved. This interaction potential gave the closest fit to the experimental measurements at 297 K and was expected to give good results at 100 K and 500 K. The results are summarised in Table 7.5.

Accurate fourth order three-temperature theory calculations at the same temperatures and using the same interaction potential as the two-temperature theory calculations above have been performed. The collision cross sections, $Q^{(l)}(E')$, required were calculated to 0.1% accuracy and the reduced mobility converged to an accuracy of 1.0%. The results are presented in Table 7.6.

T_{eff} (K)	K_0 ($cm^2V^{-1}s^{-1}$)	E/N (Td)		
		A	B	C
511.	26.4	22.6	16.3	3.71
573.	25.6	24.9	19.0	9.79
646.	24.9	27.6	22.1	14.3
734.	24.1	30.6	25.4	18.6
837.	23.4	34.1	29.2	23.1
960.	22.6	38.1	33.5	27.9
1105.	21.8	42.7	38.3	33.1
1278.	21.1	47.9	43.7	38.9
1483.	20.3	53.7	49.8	45.3
1726.	19.6	60.4	56.6	52.4
2014.	18.9	67.9	64.3	60.4
2356.	18.3	76.4	73.0	69.3
2761.	17.6	85.9	82.7	79.2
3243.	17.0	96.7	93.6	90.3
3814.	16.5	109.	106.	103.
4491.	15.9	122.	119.	116.
5294.	15.4	137.	135.	132.
6248.	15.0	154.	151.	148.
7378.	14.5	173.	170.	168.
8720.	14.1	193.	191.	189.

Table 7.5 The temperature dependence of the mobility of F^- in helium using the first approximation of the two-temperature theory. Calculations were performed at the following gas temperatures; A, 100 K; B, 297 K; C, 500 K.

E/N	K_0 ($cm^2V^{-1}s^{-1}$)		
(Td)	A	B	C
2.	33.09	29.72	26.53
3.	33.14	29.65	26.49
5.	33.12	29.42	26.37
8.	32.70	28.92	26.11
10.	32.16	28.51	25.88
12.	31.49	28.18	25.63
15.	30.36	27.44	25.25
20.	28.53	26.25	24.48
25.	26.89	25.19	23.74
30.	25.49	24.22	23.04
35.	24.43	23.36	22.42
40.	23.52	22.59	21.80
50.	21.94	21.28	20.72
60.	20.72	20.25	19.81
80.	18.98	18.69	18.39
100.	17.62	17.54	17.25
120.	16.75	16.65	16.50
140.	16.06	16.03	15.85
160.	15.44	15.47	15.45

Table 7.6 Three-temperature theory calculations of the mobility of F^- in helium at three different neutral gas temperatures. Calculations were performed at the following gas temperatures; A, 100 K; B, 297 K; C, 500 K

7.9 The Dependence of Zero-Field Ion-Mobilities on Well Depth, ε, and Minimum Position, r_m, in the Ion-Neutral Interaction Potential

The results of our calculation of the mobility of F^- in helium showed that very small changes to the depth of the attractive well in this interaction potential led to significant changes in the values calculated for low field reduced mobilities. The size of these changes are of the same order of magnitude as the accuracy of the best ab-initio calculations available. The sensitivity of the zero field reduced ion mobility, at fixed temperature, on the well depth, ε, and minimum position, r_m, was investigated for a range of hypothetical ion-neutral interaction potentials. From these calculations it was found that for certain values of the ε and r_m, the interaction potential need only be changed slightly to effect large changes on the calculated mobility. This sensitivity varies significantly over the range of r_m and ε considered.

The interaction of an atomic ion and a neutral atom at short-medium range is either attractive or repulsive. If the interaction is attractive, there will be a definite minimum in the potential energy curve, V(r). At long range, the interaction energy is dominated by the attractive ion-induced dipole term, $-\frac{1}{2}\alpha^2 q^2/4\pi\varepsilon_o r_m^4$. At very short range the potential is always repulsive. Thus, there will always be a minimum in the potential energy curve. It has been shown (Gatland et al., 1977b) that the ion mobility at large E/N is principally determined by V(r) at low r, while the ion mobility at small values of E/N is determined principally by V(r) at large internuclear separation. Therefore, it might be expected that the reduced mobility at zero field strength, $K_0(0)$, would be given by the Langevin model where the potential is just the ion-induced dipole term. This would mean that at zero field strength, the effect of other short range terms is negligible. We find this is not the case.

To explore the effect of the position and depth of the potential energy minimum on the zero field mobility an (n,6,4) potential of the following form was used:

$$V(r)=\frac{n\varepsilon}{n(3+\gamma)-12(1+\gamma)}\left[\frac{12}{n}(1+\gamma)\left(\frac{r_m}{r}\right)^n-4\gamma\left(\frac{r_m}{r}\right)^6-3(1-\gamma)\left(\frac{r_m}{r}\right)^4\right] \qquad (7.12)$$

where ε and r_m are the depth and position of the potential energy minimum respectively. The value of the dimensionless parameter, γ, has been constrained so that the r^{-4} term corresponds to the value appropriate to an ion interacting with helium (polarisability, α=0.204 $Å^3$), that is,

$3\varepsilon(1-\gamma)\, r_m^4=\alpha q^2/4\pi\varepsilon_o$ where ε_o is the vacuum permittivity. This form for a model interaction potential has been previously used to calculate reduced collision integrals (Viehland et al., 1975). In the two-temperature theory calculations, an ion mass corresponding to F^+ or F^- was used. The results were extrapolated back to 0 Td to obtain the zero-field reduced mobility value, $K_0(0)$. In presenting the results of the calculations of zero field ion mobilities, it was found useful to scale the well depth, ε, by a factor of $\varepsilon'=\frac{1}{2}\alpha q^2/4\pi\varepsilon_o r_m^4$; the value of the ion-induced dipole term at the minimum. In Figure 7.4 a contour plot of $K_0(0)$ as a function of ε/ε' and r_m is presented, assuming a gas temperature value of 300 K. Where the minimum in the potential, r_m, is at small r, a very large change in ε is required to vary $K_0(0)$ by a large amount from the Langevin value for the F^+/F^- ion of 16.90 $cm^2V^{-1}s^{-1}$. At r_m=1.2 Å, ε'= 0.708 eV (68.3 $kJmol^{-1}$), but at 3.2 Å, ε'=0.0140 eV=1.35 $kJmol^{-1}$. At large r_m, a very small change in ε has a very large effect on $K_0(0)$. For the (12-6-4) potential, at r_m=3.2 Å, doubling ε from $\varepsilon=\varepsilon'$ to $\varepsilon=2\varepsilon'$, a difference of 0.014 eV, to give a slightly more attractive potential, decreases $K_0(0)$ from 21.1 $cm^2V^{-1}s^{-1}$ to 15.2 $cm^2V^{-1}s^{-1}$. Halving ε from $\varepsilon=\varepsilon'$ to $\varepsilon=\varepsilon'/2$, to give a slightly more repulsive short range potential, a difference of only 0.007 eV, increases $K_0(0)$ from 21.1 $cm^2V^{-1}s^{-1}$ to 27.9 $cm^2V^{-1}s^{-1}$. At r_m=1.2 Å, the values of $K_0(0)$ at $\varepsilon'/2$, ε' and $2\varepsilon'$ are 18.5, 17.5 and 16.0 $cm^2V^{-1}s^{-1}$ respectively. If an (8-6-4) potential is used, essentially the same contour diagram is obtained with the mobilities at small r_m being slightly smaller.

These observations have an important consequence when ab-initio methods are used to calculate V(r) for use in ion mobility calculations. To obtain accurate estimates of $K_0(0)$, the values of V(r) at about 3 Å need to be very accurate (to within better than 0.001 eV) to obtain $K_0(0)$ correct to two significant figures. A basis set that is adequate to describe a bond of 1-2 Å length may not be adequate at a separation of 3 Å. The dependence of the correlation energy on internuclear separation must be correct.

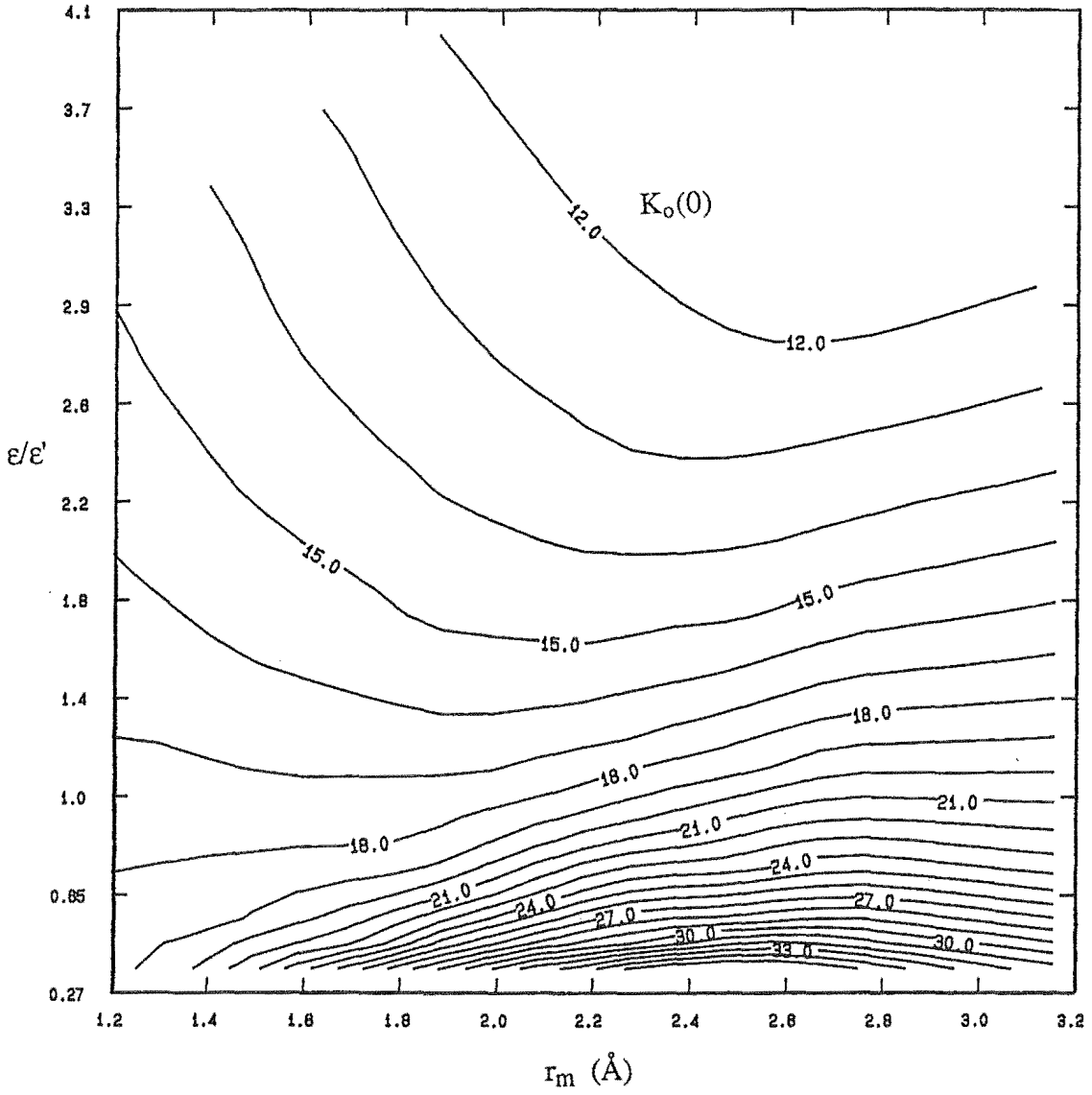

Figure 7.4 Zero field reduced ion mobility ($cm^2V^{-1}s^{-1}$) as a function of reduced well depth (ε/ε') and minimum position.

7.10 Discussion

This study on the mobility of F^- in helium has shown that very small fluctuations in an interaction potential, especially at large distance, can have a major effect on the calculated mobility. Thus, a comparison of calculated transport coefficients with experimental measurements can indicate deficiencies in the interaction potential used. As the level of theory is increased, or the basis set improved, in the calculation of the interaction potential, one would expect the calculated transport properties, using successive improvements to the potential to monotonically approach the experimental values but this is not necessarily the case. Using a standard large basis set (6-311+G(3df,3pd)), improving the level of theory from close to the Hartree-Fock limit to a level which recovers a large part of the correlation energy (MP4SDQ), actually made the agreement between calculated and experimental mobility at low field worse. Improving the basis set, but calculating the interaction energy at a similar level of perturbation theory (MBPT(4)), reversed this trend. Such oscillatory behaviour is not uncommon in ab-initio calculations, especially of potential surfaces, and reflects the localised improvements made to various parts of the surface as a result of basis set or theory changes. However, once an accurate interaction potential has been obtained, it can then be used to calculate the dependence of the reduced mobility, K_0, or the drift velocity, v_d, as a function of E/N, possibly at temperatures outside the range accessible to experimentalists.

Chapter 8.

Valence-Bond Calculations on N_2 and Isoelectronic Species

8.1 Introduction

There are two basic approximate approaches to the description of the electronic structure of molecules; the molecular-orbital method, which leads to configuration interaction and perturbation techniques, and the valence-bond method. Although both methods start with alternative descriptions of the molecular electronic wave function and provide different information, they become equivalent when all the possible valence-bond structures and all the possible molecular-orbital electron configurations are considered (McWeeny, 1979). In the molecular-orbital approach, one starts with the bare nuclei in fixed positions. The molecular orbitals are formed from atomic orbitals and are then filled with the available electrons begining with the lowest in energy. The basic idea of the valence-bond method is also very simple. In the valence-bond method the wave function for the electrons in a molecule is constructed directly from the atomic wave functions by starting with the atoms at infinity and allowing them to come together to form the equilibrium configuration of the molecule. As the atoms approach each other, the wave function involves terms which may be interpreted physically as charge-transfer, spin-pairing, promotion into a valence state etc. The ionic or charge-transfer structures may also be interpreted as accounting for atomic orbital deformation occurring as the internuclear separation is decreased. The molecular-orbital method has been used far more extensively than the valence-bond method. The reason for this, historically, is because of the computational complexity of the valence-bond method. Primarily this is caused by the non-orthogonal nature of atomic orbitals on different centres , as compared with the relative ease with which the molecular-orbital method may be implemented. This problem has been largely overcome and now the choice of which method to use largely depends on which is more suitable, given the type of information required. In the molecular-orbital self consistent field (SCF) method the one- and two-electron integrals over atomic basis functions are calculated.

Then, in an iterative cycle (after an initial guess at the molecular-orbital coefficient matrix, C), the Fock, F, and overlap, S, matricies are set up and the eigenvalue problem $(F-\varepsilon S)C=0$ is solved to obtain a new coefficient matrix and molecular orbital energies ε. This cycle is carried out to "self consistency", that is, when there is no improvement in the molecular-orbital coefficients possible that will lower the electronic energy. It can be shown that this energy is a rigorous upper bound to the true energy. In the valence-bond method the same one- and two-electron integrals over atomic basis functions are used but molecular orbitals are never formed. Instead, all the significant Slater determinant wave functions involving atomic orbitals are used to construct the Hamiltonian, H, and overlap, S, matricies. The spin-free Born-Oppenheimer Hamiltonian operator, H, can be written explicitly, in atomic units, as

$$H = \sum_{i=1}^{N} \left(-\frac{1}{2}\nabla_i^2 - \sum_{\alpha=1}^{N} \frac{z_\alpha}{r_{\alpha i}} \right) + \sum_{i<j}^{N} \frac{1}{r_{ij}} + \sum_{\alpha<\beta} \frac{z_\alpha z_\beta}{r_{\alpha\beta}} \qquad (8.1)$$

where $r_{\alpha i}$ is the distance between electron i and nucleus α and z_α is the charge on nucleus α. The eigenvalue problem $(H-ES)C=0$ is solved only once to give the energy eigenvalues, E, of the several lowest molecular states. The coefficient matrix C contains information on the importance each determinant played in forming the various molecular states. In the valence-bond method, far fewer eigenvalues and eigenfunctions are needed, than for the molecular orbital method, usually only the lowest ones. Also the eigenvalues, E, correspond to spectroscopic states, unlike the molecular orbital energies, ε. At present the valence-bond method is defined as a configuration interaction which allows for complete flexibility for the overlap between single particle orbitals, where there is no requirement for the orbitals to be orthogonal (Gallup et al., 1982). Historically, the first valence-bond type of calculation was on H_2 by Heitler and London (1927) who used a two-electron wave function of the form

$$\Psi_\pm = \frac{1}{\sqrt{2(1-S^2)}} [\phi_A(1)\,\phi_B(2) \pm \phi_B(1)\,\phi_A(2)] \qquad (8.2)$$

where $\phi_A(1)$ denotes electron 1 in an orbital on centre A. Ψ_+ is symmetric and Ψ_- is antisymmetric under electron exchange and neither wave function takes electron spin into account. Ψ_+ gave a fairly good description of the ground state of H_2. The two main improvements made to the valence-bond method since 1927 have been the explicit inclusion of

spin-functions, and the determination of the configuration coefficients. Despite a recent renewed interest in the use of the valence-bond approach (Raimondi et al., 1985; Gallup et al., 1982; Gerrat, 1974; Jans and Maclagan, 1984; Skrezenek and Harcourt, 1984), ab-initio valence-bond calculations have been restricted almost entirely to hydrides. Contrary to this trend, calculations were performed on the N_2 isoelectronic series: N_2, CO, BF, NO^+ and CN^-. This series of molecules has been used for generations as examples in teaching bonding theory, especially in connection with molecular orbital theory. The only other ab-initio valence-bond calculations on these molecules are by Hurley (1960) who reported for CO a minimal basis calculation to which was added his intra-atomic correlation correction. Other ab-initio valence-bond calculations on non-hydride molecules include those of Balint-Kurti and Yardley (1977) on LiF and Maclagan (1981) on BeO and MgO.

In these calculations we were interested to see which structures were most important according to various criteria including structure energy, structure population, wave function coefficient and position in build-up study (Maclagan and Schnuelle, 1971), to make a comparison with the energy calculated by the molecular orbital (Hartree-Fock) method and also to observe the relative importance of σ-bonding and π-bonding in different ionic structures. A build-up study is a series of valence bond calculations, each one including one more structure than the last. The information obtained from such a study includes the minimum number of structures needed to go beyond the Hartree-Fock limit (by comparison with a molecular orbital calculation using the same basis set) and the relative importance of each structure in terms of the total wave function energy.

8.2 Method

In these calculations, the experimental or best theoretical estimate bond lengths, r_e, were used. These were N_2, r_e=2.074 bohr; CO, r_e=2.132 bohr; BF, r_e=2.385 bohr; NO^+, r_e=2.0067 bohr and CN^-, r_e=2.20 bohr. The atomic unit of distance, the bohr, is defined as being equal to 0.529177Å. The valence-bond program used in this work has been described previously (Maclagan and Schnuelle, 1971). Briefly, the calculation can be summarised as follows. The first step involves defining the molecular geometry in cartesian coordinates and

also the nuclear charge for each atomic centre. The basis set to be used is read in next. The current version of the program always works with Slater-type orbitals (STOs) which have radial factors of the form:

$$f_n(r)=r^{(n-1)} \exp\left(-\frac{z_{eff}r}{n}\right) \qquad (8.3)$$

where n is the principle quantum number, r is the distance in atomic units (bohr) and $\frac{z_{eff}}{n}$ is the orbital exponent which is usually given the symbol ζ; a small value indicates a diffuse orbital whereas a large value indicates a more compact electron distribution. z_{eff} is the effective nuclear charge. The angular part of the STO depends on the quantum number *l*. A double-zeta (DZ) basis of the type used in this work has two orbitals for each n,*l* pair differing only by the orbital exponent ζ. The double-zeta best atom sp Slater-type basis set of Huzinaga and Arnau (1970) was used for the diatomic molecule calculations. The one- and two-electron integrals required were calculated using Steven's integral package (Stevens, 1971). Following the integral calculation the basis was contracted to a 2s1p basis set using the atomic wave function coefficients (Huzinaga and Arnau, 1970). The DZ contraction used transformations of the form:

$$\begin{aligned} 1s &\leftarrow a_{1s}1s + b_{1s}1s' + c_{1s}2s + d_{1s}2s' \\ 2s &\leftarrow a_{2s}1s + b_{2s}1s' + c_{2s}2s + d_{1s}2s' \\ 2p &\leftarrow a_{2p}2p + b_{2p}2p' \end{aligned} \qquad (8.4)$$

Although the effect of this contraction is significant, it is not large and should not affect the qualitative results obtained from this study. During the next stage of the calculation hybridisation of the orbitals can be performed if required; in our case it was sp hybridisation using the p orbital lying along the internuclear axis.The hybrid orbitals designated s and σ on the two atoms A and B are defined as

$$\begin{aligned}
\sigma_A &\leftarrow \sqrt{1-\alpha^2}\ 2\sigma_A - \alpha\ 2\pi_{\sigma A} \\
\sigma_A &\leftarrow \alpha\ 2\sigma_A + \sqrt{1-\alpha^2}\ 2\pi_{\sigma A} \\
\sigma_B &\leftarrow \sqrt{1-\beta^2}\ 2\sigma_A - \beta\ 2\pi_{\sigma B} \\
\sigma_B &\leftarrow \beta\ 2\sigma_B + \sqrt{1-\beta^2}\ 2\pi_{\sigma B}
\end{aligned} \qquad (8.5)$$

where α and β are the degrees of sp hybridisation on centres A and B respectively. A large value indicates more orbital mixing.

Both the orbital contraction and hybridisation involve determining a new list of integrals over the latest orbital functions constructed from combinations of the last list of integrals using the relevant transformation functions. The integral calculation is summarised in Figure 8.1.

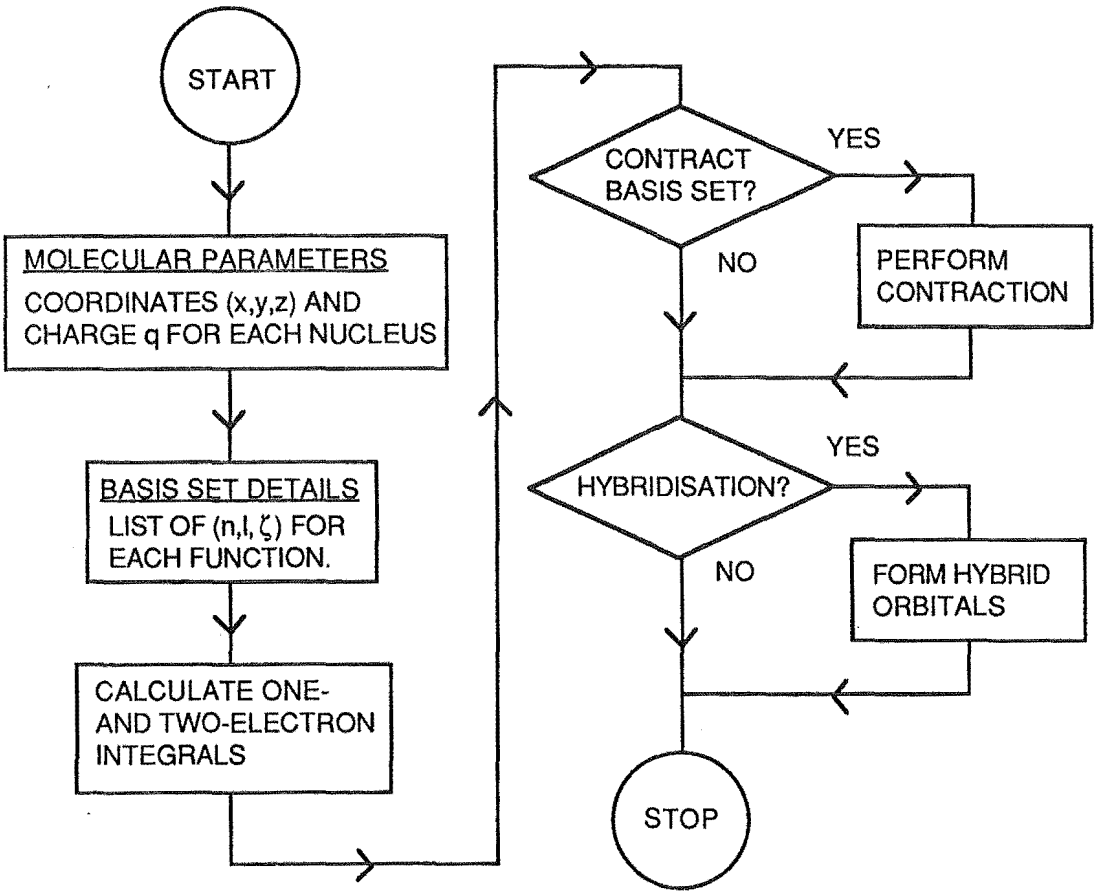

Figure 8.1. Flow diagram for integral calculation.

In the valence-bond part of the calculation a list of Slater determinants is read; the number of spin-orbital functions per determinant defines the overall molecular charge, and the number of spin-orbital functions per atomic centre defines the charge carried by that atom. The

Hamiltonian, H, and overlap, S, matrix elements between all determinants are evaluated next. For a given number of cycles the program solves the eigenvalue equation (H-ES)C=0 for the required subset of input determinants and prints out the results including coefficients, structure population and energy for the lowest states required. Typically a calculation could calculate the valence-bond wave function for a set of configurations and also calculate the energy for each configuration separately. The computational scheme followed by the valence-bond program is shown in Figure 8.2.

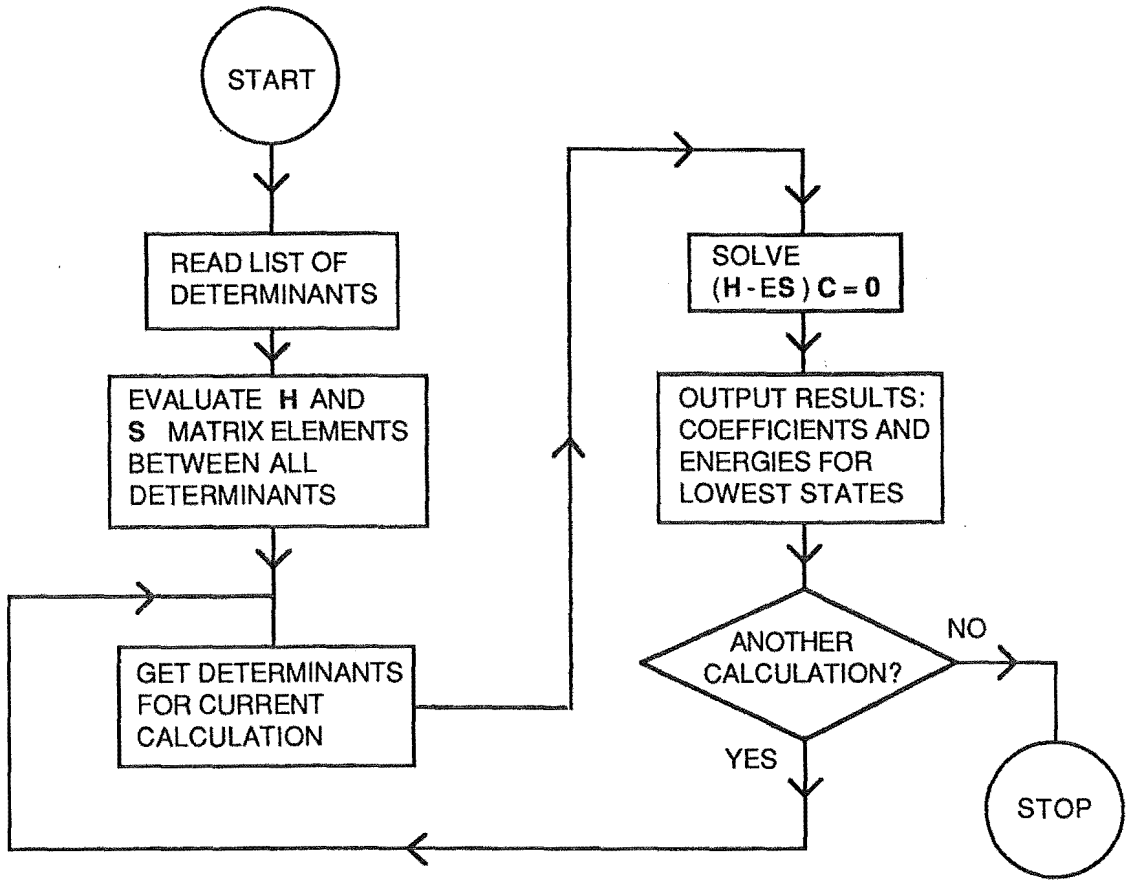

Figure 8.2 Flow diagram for the valence-bond program.

The structure population has recently been added to the program and is defined as:

$$P_i = \sum_j c_i \, c_j \, S_{ij} \qquad (8.6)$$

where c_i are the coefficients of the structure wave functions in the total valence-bond wave function and S_{ij} is the overlap integral between structure wave functions. Because the atomic

orbitals on different centres are not orthogonal, the magnitude of S_{ij} can be large. The molecular orbital (Hartree-Fock) results quoted used the same contracted basis set.

For N_2 the covalent structure configuration is

$$1s_A^2 2s_A^2 \sigma_A \pi_A \pi_A' \; 1s_B^2 2s_B^2 \sigma_B \pi_B \pi_B' \qquad (8.7)$$

and the orbital hybridisation parameters α and β are equal due to molecular symmetry. Initially calculations were performed with the hybrid orbitals s_A and s_B doubly occupied. For the results quoted in Tables 8.1-8.5 some configurations in which either s_A or s_B is singly occupied with a structure population greater than 0.001 or a large wave function coefficient were added to the initial set of structures.

8.3 Results and Discussion

The results of the valence-bond calculations are summarised in Tables 8.1-8.5. The first two columns list the configurations, ignoring the $1s_A$ and $1s_B$ orbitals, and also the hybrid s orbitals on each centre if all of these are doubly occupied. The third column contains the charge carried by one of the atoms in each structure. The energy of each configuration, in hartrees, is given in the fourth column. The structure population and wave function coefficient determined in a calculation involving all the configurations are also tabulated. The column headed χ lists the degeneracy of the particular configurations.

Table 8.1 contains the results of the calculations for the N_2 molecule. The most important structure is the triple-bond covalent structure involving the spin-pairing of a pair of σ-orbitals and two pairs of π-orbitals. The next most important configuration on the basis of the structure populations or wave function coefficients is a double-bond ionic structure involving the spin pairing of a pair of σ-orbitals and a pair of π-orbitals. However, a build-up study gives greater importance to the non-ionic structure which might be described as involving σ donation and π back-donation. This structure together with the covalent triple-bond structure gives an energy of -108.8051 hartree which is lower than the molecular orbital energy. Only two structures are required to get below the molecular orbital (Hartree-Fock) energy. When the ionic double-bond structure is added as a third structure the energy is lowered to -108.8279

hartree. The addition of the ionic structure involving two π-bonds lowers the energy to -108.8321 hartree. Hybridisation is important. The valence-bond energy with $\alpha = 0$ is -108.7975 hartree. The value of α goes to zero as the internuclear separation is increased. The energy with both s_A and s_B orbitals always doubly occupied is -108.8713 hartree, a very small rise in energy compared to the full valence-bond wave function. The total population for all non-ionic (covalent) structures is 0.615. For singly ionised structures it is 0.417. The total populations for $N^{2+}N^{2-}$ and $N^{3+}N^{3-}$ structures are negative with values of -0.028 and -0.002, respectively. Although a negative population generally means a very small contribution to the energy, some structures with negative populations can have an important contribution to the total energy.

As can be seen from the data in Table 8.2, the most important structure for CO is a covalent structure involving a σ-bond and a π-bond. On the basis of orbital populations the next most important structure is a C^+O^- structure with a single π-bond. However, a build-up study and the wave function coefficient criterion gives a covalent structure with two π-bonds as the next most important structure. The two covalent structures with a σ-bond and a π-bond give an energy of -112.4611 hartree. With the two π-bonds structure the energy is lowered to -112.5883 hartree. Again only two sets of structures are required to give an energy lower than the molecular orbital energy with the same basis set. The addition of the C^+O^- structure with a single π-bond lowers the energy to -112.6174 hartree. On the basis of orbital populations the next most important structure is a C^-O^+ structure with a single σ-bond and two π-bonds. Such a structure is presumably important in giving the CO molecule a dipole moment with C^-O^+ polarity. Not included in Table 8.2 and subsequent tables are those structures or configurations which were included in the calculations but gave a population whose magnitude was less than 0.001. The total populations for covalent structures is 0.605, which is quite close to the value of 0.615 for N_2. The C^+O^- structures have a total population of 0.269, the $C^{2+}O^{2-}$ structure a population of 0.006, the C^-O^+ structures a total population of 0.144 and the $C^{2-}O^{2+}$ structures a total population of -0.029. One structure with a singly occupied s-orbital on the C atom has the significant population of 0.024. This is not related to the most important covalent structure, but to the C^+O^- structure with a π-bond. There appears to be a general trend that the most important structures with a singly occupied s-orbital are not derived

from the most important structures with doubly occupied s-orbitals. These figures are very different to Pauling's estimates (Pauling, 1960) of 0.1 for C^+O^-, 0.4 for C=O and 0.5 for $C^-\equiv O^+$. The energy obtained with structures containing only doubly occupied s-orbitals has an energy of -112.6635 hartree, but the optimum hybrid orbital parameters were α=0.364 and β=0.317, a greater difference than the difference in energies might suggest. The optimum orbital parameters are sensitive to the set of structures included in the calculation. With α=0 and β=0 the energy is -112.6344 which is not as great a difference as obtained with N_2. The importance of allowing hybridisation of the 2s and 2p orbitals has been noted by McWeeny (1979). For CO it can be seen that there exists a tendency, when ionic structures are included, for the less electronegative element (C in the case of CO) to lose a σ-orbital and gain a π-orbital. This is a general phenomenon. The same phenomenon is mirrored in the importance of the covalent structure with two π-bonds which might be regarded as having been formed from the most important structure by a process of σ donation and π back-donation. In valence-bond studies on BeO and MgO (Maclagan, 1981) π-bond formation was again found to be favoured.

In Table 8.3 it is shown that for BF two structures are of similar importance: a covalent structure with a single π-bond and the B^+F^- structure. The only other structures of importance are the covalent structure with a σ-bond, the B^-F^+ structures, one with a σ-bond and a π-bond and the other with two π-bonds. The greater importance of the covalent structure with a π-bond was also found in BeO (Maclagan, 1981), where the most important structure was found to be the Be^+O^- structure with a single π-bond which has a very similar electronic structure to the BF covalent structure. The sum of the overlap populations for the covalent structure is 0.588, for the B^+F^- structure it is 0.336, for the B^-F^+ structure it is 0.074 and for the $B^{2+}F^{2-}$ structure it is -0.015. As might be expected from the smaller number of valence electrons, the molecular orbital result is closer to the valence-bond result for BF.

The result for NO^+ are contained in Table 8.4. The most important structure for NO^+ is the N^+O structure with a σ-bond and a π-bond isoelectronic with the most important CO structure. Of almost equal importance is the NO^+ structure isoelectronic with the covalent triple-bond structure for N_2. The NO^+ structure actually has a lower energy than a single N^+O structure, but the existence of the second degenerate structure gives the CO-like structure the greater importance. As in CO, the N^+O structure with two π-bonds is important. For the NO^+

structure there appears to be a tendency to either lose a π-orbital or gain a π-orbital, while for the N^+O structure the tendency is to lose a σ-orbital and gain a π-orbital in forming ionic structures. The sums of structure populations were 0.397 for NO^+, 0.530 for N^+O, 0.084 for $N^{2+}O^-$ and 0.010 for N^-O^{2+}. In choosing which of the structures in which s-orbitals were singly occupied to include, it was found that some structures with relatively large negative populations gave a significant contribution to the energy.

Although the hybrid orbital parameters for all the other species have values about 0.3, the hybrid orbital parameters for CN^- were found to be significantly larger. Thus there is significant p_σ character in the s-orbital. The most important structure is a C^-N structure with the same configuration as the N_2 covalent triple-bond structure. Then, in order, follows two CN^- structures, the structure with a σ and a π-bond as in the C=O structure and then the structure with two π-bonds. The sum of orbital populations is 0.565 for the C^-N structures, 0.477 for the CN^- structures, 0.017 for the $C^{2-}N^+$ structures and 0.010 for the C^+N^{2-} structures.

Comparison of the orbital populations in Tables 8.1 and 8.2 with Tables 8.4 and 8.5 provides some insight into the bonding in the neutral molecules N_2 and CO with the ions NO^+ and CN^-. NO^+ appears to resemble CO more closely than N_2. The triple-bond structure population of 0.213 is lower than the N_2 value of 0.326 and approaches the CO value of 0.082. The double ($\sigma+\pi$)-bond structure is higher than the N_2 value of 0.224 and approaches the CO value of 0.367. CN^- appears to resemble N_2 more closely. The triple-bond population of 0.319 is almost as high as the N_2 value and the double-bond population of 0.250 is almost as low as the N_2 value of 0.224.

In Figure 8.3 the principle valence-bond structures for each of the diatomic molecules studied are shown in pictorial form with the most important structures on the left side of the diagram. Traditional bonding theory would predict the molecular bonding found in the dominant valence structures for N_2, NO^+, CO, BF and CN^-. However, the other valence structures that this study found to play a significant part in describing the bonding in these molecules would normally not be considered important.

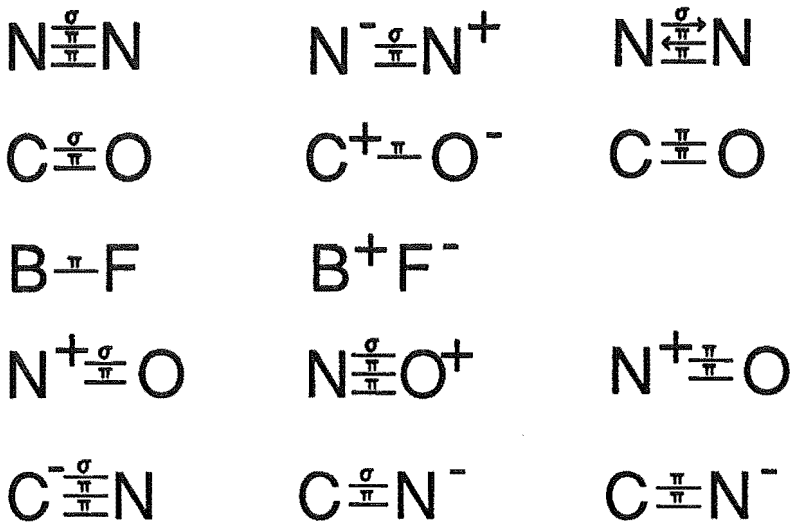

Figure 8.3 Principal valence structures found in the 14 electron diatomic molecules studied.

8.4 Summary

In this series of molecules and ions with ten valence electrons, it has been shown that there are two alternatives for the most important structure: one with a single σ-bond and a pair of π-bonds, as found for N_2 and CN^- and one with a σ-bond and a π-bond as found for CO and NO^+. BF, in which only one B orbital effectively participates in bonding, does not fit into this pattern. Generally, π-bonding often tends to be favoured over σ-bonding. The importance of the structures with two π-bonds formed by σ donation and π back-donation reflects this phenomenon. Only a few structures are required to get below the molecular orbital energy for these molecules. Except for the case of CN^-, only 10-15% of the σ-bonding hybrid orbital is 2s in character. However, this small degree of hybridisation is important energetically. The most important valence structure found for each molecule studied agrees with the usual theories of molecular bonding.

Table 8.1 Valence-Bond Calculations on N_2; $\alpha = 0.350$.

Configuration						Wavefn.
N	N	Q_N	E /hartrees	Pop	χ	Coeff.
$\sigma\pi\pi'$	$\sigma\pi\pi'$	0	-108.6527	0.326	1	0.367
			-108.1476	0.002	1	0.041
			-107.0958	0.004	1	0.060
$\sigma^2\pi$	$\pi\pi'^2$	0	-108.1144	0.186	4	0.089
$\sigma\pi^2$	$\sigma\pi'^2$	0	-108.3057	0.097	2	0.111
$\pi\pi'$	$\sigma^2\pi\pi'$	+1	-108.2189	0.134	2	0.087
			-107.7672	0.0004	2	0.006
$\sigma\pi$	$\sigma\pi\pi'^2$	+1	-108.2515	0.224	4	0.097
			-107.7659	-0.0000	4	0.001
σ^2	$\pi^2\pi'^2$	+1	-107.5531	0.013	2	0.021
π^2	$\sigma^2\pi'^2$	+1	-107.8724	0.039	4	0.025
σ	$\sigma\pi^2\pi'^2$	+2	-107.3935	-0.006	2	0.009
π	$\sigma^2\pi\pi'^2$	+2	-107.5215	-0.022	4	0.012
	$\sigma^2\pi^2\pi'^2$	+3	-106.3673	-0.002	2	0.004
$s\sigma^2\pi$	$s^2\sigma\pi\pi'^2$	+1	-107.6065	0.007	4	0.004
	$E_{V.B.}$		-108.8714			
	$E_{M.O.}$		-108.7419			

Table 8.2 Valence-Bond Calculations on CO; $\alpha = 0.315$, $\beta = 0.402$.

Configuration						Wavefn.
C	O	Q_C	E /hartrees	Pop	χ	Coeff.
$\sigma\pi$	$\sigma\pi\pi'^2$	0	-112.3164	0.367	2	0.257
σ^2	$\pi^2\pi'^2$	0	-111.6695	0.024	1	0.049
$\pi\pi'$	$\sigma^2\pi\pi'$	0	-112.2402	0.164	1	0.233
π^2	$\sigma^2\pi'^2$	0	-111.9205	0.050	2	0.076
σ	$\sigma\pi\pi'^2$	+1	-112.1024	0.076	1	0.126
π	$\sigma^2\pi\pi'^2$	+1	-112.1787	0.193	2	0.142
	$\sigma^2\pi^2\pi'^2$	+2	-111.6400	0.006	1	0.011
$\sigma\pi\pi'$	$\sigma\pi\pi'$	-1	-112.0532	0.082	1	0.119
			-110.7650	0.002	1	0.044
$\sigma^2\pi$	$\pi\pi'^2$	-1	-111.5772	0.025	2	0.023
$\pi\pi'^2$	$\sigma^2\pi$	-1	-111.5143	0.014	2	0.022
$\sigma\pi^2$	$\sigma\pi'^2$	-1	-111.7378	0.020	2	0.029
$\sigma\pi\pi'^2$	$\sigma\pi$	-2	-111.0069	-0.011	2	0.019
$\pi^2\pi'^2$	σ^2	-2	-110.3276	-0.001	1	0.006
$\sigma^2\pi\pi'$	$\pi\pi'$	-2	-111.0076	-0.012	1	0.025
$\sigma^2\pi^2$	π'^2	-2	-110.6975	-0.005	2	0.010
$s\sigma\pi$	$s^2\sigma^2\pi\pi'^2$	+1	-111.6568	0.024	2	0.026
$s\sigma^2$	$s^2\sigma\pi^2\pi'^2$	+1	-111.3842	0.007	1	0.020
$s\sigma$	$s^2\sigma^2\pi^2\pi'^2$	+2	-111.1470	0.002	1	0.005
$s\sigma^2\pi\pi'$	$s^2\sigma\pi\pi'$	-1	-111.3206	-0.003	1	0.008
$s^2\sigma^2\pi$	$s\sigma\pi\pi'^2$	-1	-111.2134	-0.024	2	0.026
	$E_{V.B.}$		-112.6674			
	$E_{M.O.}$		-112.5650			

Table 8.3 Valence-Bond Calculations on BF; $\alpha = 0.294$, $\beta = 0.290$.

Configuration						Wavefn.
B	F	Q_B	E /hartrees	Pop	χ	Coeff.
σ	$\sigma\pi^2\pi'^2$	0	-123.7073	0.232	1	0.308
π	$\sigma^2\pi\pi'^2$	0	-123.7622	0.356	2	0.299
	$\sigma^2\pi^2\pi'^2$	+1	-123.8315	0.336	1	0.396
$\sigma\pi$	$\sigma\pi\pi'^2$	-1	-123.2130	0.059	2	0.063
σ^2	$\pi^2\pi'^2$	-1	-122.7479	0.001	1	0.003
$\pi\pi'$	$\sigma^2\pi\pi'$	-1	-123.1396	0.012	1	0.038
π^2	$\sigma^2\pi'^2$	-1	-122.8916	0.002	2	0.005
$\sigma\pi\pi'$	$\sigma\pi\pi'$	-2	-122.1655	-0.005	1	0.021
$\sigma^2\pi$	$\pi\pi'^2$	-2	-121.8555	-0.006	2	0.014
$\pi\pi'^2$	$\sigma^2\pi$	-2	-121.7260	-0.001	2	0.007
$\sigma\pi^2$	$\sigma\pi'^2$	-2	-121.9246	-0.003	2	0.011
$s\sigma\pi$	$s^2\sigma^2\pi\pi'^2$	0	-123.3212	-0.003	2	0.005
$s\sigma$	$s^2\sigma^2\pi^2\pi'^2$	+1	-123.3079	+0.025	1	0.066
$s^2\sigma^2\pi$	$s\sigma\pi\pi'^2$	-2	-121.5008	-0.007	2	0.013
	$E_{V.B.}$		-124.0798			
	$E_{M.O.}$		-124.0414			

Table 8.4 Valence-Bond Calculations on NO^+; $\alpha = 0.308$; $\beta = 0.270$.

Configuration N	Configuration O	Q_N	E /hartrees	Pop	χ	Wavefn. Coeff.
$\sigma\pi\pi'$	$\sigma\pi\pi'$	0	-128.2980	0.213	1	0.265
			-127.8322	0.002	1	0.036
			-126.8708	0.002	1	0.044
$\sigma^2\pi$	$\pi\pi'^2$	0	-127.7468	0.073	2	0.068
$\pi\pi'^2$	$\sigma^2\pi$	0	-127.7055	0.048	2	0.062
$\sigma\pi^2$	$\sigma\pi'^2$	0	-127.9541	0.060	2	0.077
$\sigma\pi$	$\sigma\pi\pi'^2$	+1	-128.2933	0.297	2	0.220
σ^2	$\pi^2\pi'^2$	+1	-127.5846	0.020	1	0.051
$\pi\pi'$	$\sigma^2\pi\pi'$	+1	-128.1877	0.165	1	0.219
π^2	$\sigma^2\pi'^2$	+1	-127.8410	0.049	2	0.068
σ	$\sigma\pi^2\pi'^2$	+2	-127.7691	0.020	1	0.042
π	$\sigma^2\pi\pi'^2$	+2	-127.8092	0.064	2	0.054
	$\sigma^2\pi^2\pi'^2$	+3	-126.9114	-0.003	1	0.009
$\sigma\pi\pi'^2$	$\sigma\pi$	-1	-127.4449	0.004	2	0.006
$\pi^2\pi'^2$	σ^2	-1	-126.7120	-0.000	1	0.002
$\sigma^2\pi\pi'$	$\pi\pi'$	-1	-127.3896	0.005	1	0.009
$\sigma^2\,\pi^2$	π'^2	-1	-127.0493	0.000	2	0.000
$s^2\sigma\pi\pi'$	$s\sigma^2\pi\pi'$	0	-127.7098	-0.005	1	0.008
$s\sigma^2\pi\pi'$	$s^2\sigma\pi\pi'$	0	-127.4842	-0.009	1	0.020
$s\sigma\pi\pi'^2$	$s^2\sigma^2\pi$	0	-127.0750	-0.005	2	0.010
$s\sigma^2\pi^2$	$s^2\sigma\pi'^2$	0	-127.1368	-0.002	2	0.006
$s\sigma^2\pi$	$s^2\sigma\pi\pi'^2$	+1	-127.5222	0.003	2	0.004
$s\sigma\pi$	$s^2\sigma^2\pi\pi'^2$	+2	-127.3098	0.005	2	0.005
$s\sigma^2$	$s^2\sigma\pi^2\pi'^2$	+2	-127.0408	0.002	1	0.006
	E_{VB}		-128.6915			
	E_{MO}		-128.5550			

Table 8.5 Valence-Bond Calculations on CN^-; $\alpha = 0.467$, $\beta = 0.656$.

Configuration C	Configuration N	Q_C	E /hartrees	Pop	χ	Wavefn. Coeff.
$\sigma\pi$	$\sigma\pi\pi'^2$	0	-91.8719	0.250	2	0.190
σ^2	$\pi^2\pi'^2$	0	-91.2171	0.013	1	0.034
$\pi\pi'$	$\sigma^2\pi\pi'$	0	-91.9084	0.172	1	0.206
π^2	$\sigma^2\pi'^2$	0	-91.5825	0.042	2	0.051
σ	$\sigma\pi^2\pi'^2$	+1	-91.3117	0.006	1	0.014
π	$\sigma\pi\pi'^2$	+1	-91.5404	0.006	2	0.005
	$\sigma^2\pi^2\pi'^2$	+2	-90.7637	-0.005	1	0.012
$\sigma\pi\pi'$	$\sigma\pi\pi'$	-1	-92.0235	0.319	1	0.366
			-91.5291	0.002	1	0.048
			-90.3914	0.009	1	0.098
$\sigma^2\pi$	$\pi\pi'^2$	-1	-91.5656	0.064	2	0.055
$\pi\pi'^2$	$\sigma^2\pi$	-1	-91.5478	0.087	2	0.089
$\sigma\pi^2$	$\sigma\pi'^2$	-1	-91.6983	0.084	2	0.097
$\sigma\pi\pi'^2$	$\sigma\pi$	-2	-91.4470	0.027	2	0.027
$\pi^2\pi'^2$	σ^2	-2	-90.7875	0.001	1	0.005
$\sigma^2\pi\pi'$	$\pi\pi'$	-2	-91.5054	-0.005	1	0.007
$\sigma^2\pi^2$	π'^2	-2	-91.1821	-0.006	2	0.008
$\sigma\pi^2\pi'^2$	σ	-3	-90.4709	-0.004	1	0.015
$\sigma^2\pi\pi'^2$	π	-3	-90.7191	-0.014	2	0.017
$s\sigma^2$	$s^2\sigma\pi^2\pi'^2$	+1	-90.4770	0.001	1	0.005
$s\sigma\pi$	$s^2\sigma^2\pi\pi'^2$	+1	-90.8784	0.002	2	0.003
$s^2\sigma\pi\pi'$	$s\sigma^2\pi\pi'$	-1	-91.0342	-0.030	1	0.080
$s\sigma^2\pi\pi'$	$s^2\sigma\pi\pi'$	-1	-91.1980	-0.012	1	0.027
$s\sigma\pi\pi'^2$	$s^2\sigma^2\pi$	-1	-90.8851	-0.010	2	0.017
	E_{VB}	-92.2763				
	E_{MO}	-92.1621				

Chapter 9

Interaction Potentials and Mobility Calculations for the HeO^+ System

9.1 Introduction

The He-O^+ system has previously been investigated by both experimental techniques (mobility measurements and beam experiments) and using ab-initio calculations. Mobility measurements of O^+ in helium serve as a probe to investigate the HeO^+ interaction potential, and conversely ab-initio or otherwise detemined HeO^+ interaction potentials can be used to calculate the mobility of O^+ in helium.

The O^+ ion is one of the most abundant ions in the ionosphere (Ferguson et al., 1971) where satellite measurements have found 38% of O^+ is in the ^2D state and 20% in the ^2P state (Oppenheimer et al., 1977). Consequently, it has been desirable to determine rate coefficients for reactions involving these electronic states of the O^+ ion. The determination of rate coefficients of ion-neutral reactions using inert gas buffered flow tubes or static drift tubes requires a knowledge of the ion mobility over the experimental range of electric field to particle density ratio E/N.

A number of experimental investigations of the mobility of O^+ in helium have been reported, including several recent studies in which a less mobile ion of m/z=16 was observed and assigned to the excited ^2D state of the O^+ ion. Interaction potentials for the $^4\Sigma$ (^4S), $^2\Delta$ (^2D), $^2\Pi$ (^2D), $^2\Sigma$ (^2P), and $^2\Pi$ (^2P) states of HeO^+, for use in mobility computations, have been calculated. In the notation for the molecular state, the term in parenthesis refers to the electronic state of O^+ formed at the dissociative limit. The two- and three-temperature theories of ion mobility have been used with these interaction potentials to calculate the mobility of the three lowest electronic states of O^+ (^4S, ^2D, and ^2P) in helium. Our results indicate that the

$^4\Sigma$ (^{4}S) ground state of HeO^+ satisfactorily accounts for the mobility of the major ion (m/z=16) observed experimentally, and that the minor ion is the ^{2}P state of O^+.

9.2 Previous Work

The mobility of O^+ in helium has been of continuing interest in experimental gas phase ion chemistry. Mobility measurements are required so that reaction rate data from flow tubes can be analysed to obtain rate coefficients. Heimerl et al. (1969) and Johnsen et al. (1970) reported drift tube mass spectrometer measurements of the mobility of O^+ in helium. Later these were improved by McFarland et al. (1973) and Lindinger and Albritton (1975) to the stage where the mobility of ground state O^+ in helium was well characterised. In 1975, Kosmider and Hasted realised that their ion drift tube could produce an appreciable proportion of excited O^+ ions. Using a test reaction for excited O^+ ions (Ong and Hasted, 1969) they were able to control their ion source conditions to produce exclusively ground state O^+. The resulting mobility measurements agreed well with those of McFarland et al. (1973). It was not until satellite data were analysed (Oppenheimer et al., 1977) that the importance of excited states of O^+ in the ionosphere was realised, and consequently it was desirable to measure rate coefficients for reactions involving both ground and excited states of the O^+ ion. Johnsen and Biondi (1980) reported a difference in ionic mobilities of metastable-state and ground-state ions in helium, the first case in which state specific mobilities have been observed for ions in a chemically different gas. Following this, Rowe et al. (1980) used a selected ion flow tube to measure some reaction rates and the mobility of O^{+*} with an experimental error of 7%. During the mobility measurements slightly skewed O^+ arrival time distributions were observed, consistent with two ions of m/z=16 being present in the flow tube. The major ion appeared to be the ^{4}S ground state and the slower minor ion was assigned as the ^{2}D state of O^+. The mobility of this metastable ion in helium was determined over the electric field to gas density ratio (E/N) range 5Td to 100Td. Johnsen et al. (1982) returned to the problem of measuring the mobility of O^{+*} in helium but they could only observe it over a limited field range, E/N < 40Td. In the most recent study on O^+ and O^{+*} mobility to date, Fhadil et al. (1982) reproduced the data of Lindinger and Albritton (1975) for the ground state O^+ ion, and also extended the data

of Rowe et al. (1980) for O^{+*} up to 150Td, but with reduced errors (less than 5%). They used an injected ion drift tube to make these measurements. The identity of the O^{+*} ion in all these studies is still debated although evidence from a number of different sources suggested that the O^{+*} ions were most likely in the ^2D state. However, this assignment was not unambiguous. In particular satellite data for the reaction of O^+ ^2D ions with N_2 cannot be reconciled with ion flow tube measurements of O^{+*} with N_2 (Rowe et al., 1980) which implies that the O^{+*} ions are largely in the O^+ ^2P state. It should be noted that the experimental observation of excited states of ions in a flow or drift tube is very difficult and the presence or absence of these ions can be strongly dependent upon the ion source conditions during the experiment.(McFarland et al., 1973; Fhadil et al., 1985).

There have been several attempts at calculating interaction potentials for the HeO^+ ion. SCF molecular orbital calculations have been carried out on the $^2\Pi$ and $^2\Sigma$ states using Gaussian orbitals (Leibman and Allen, 1971), and on the $^2\Pi$ state using Slater orbitals (Cooper and Wilson, 1981). The most extensive ab-initio calculation on HeO^+ (Augustin et al., 1973), used a minimal basis set and full CI to calculate potential curves corresponding to all the valence states of HeO^+, as well as an O (6s,4p,1d), He (2s,2p) basis set for more accurate calculations on a few selected states, but did not include enough information on each state for these interaction potentials to be useful in calculating ion mobility.

A Monte Carlo simulation of ion motion (Lin and Bardsley, 1977) has been used to determine a ground state interaction potential for HeO^+ by fitting calculation results to the observed mobility of O^+ in helium.

An empirical (n,6,4) potential has been determined (Viehland and Mason, 1977) which will reproduce the experimental mobility of O^+ in helium when used with the two-temperature theory of ion mobility.

The lack of very accurate mobility data (1-2% error) for O^{+*} in helium over a wide range of E/N precludes the possibility of obtaining an interaction potential by inverting such data (Viehland et al., 1976a).

9.3 Details of Interaction Potential Calculations

9.3.1 Ground State

The ground-state interaction potential of HeO^+, separating at infinity to He ^1S and O^+ ^4S, was calculated using the GAUSSIAN82 program (Binkley et al., 1983) at the MP4SDQ/6-311+G(3df,3pd) level of theory, excluding core contributions to the correlation energy. The results of the calculation are given in Table 9.1.

At 1.191 Å we estimate an energy of -77.25638 hartree which compares well with the MP4SDTQ/6-311G(2df,2pd) calculation by Koch and Frenking (1986) who obtained a single point energy of -77.25858 hartree.

9.3.2 Valence Bond Methods: Application to the Ground State of HeO^+

For ground state O^+ ^4S there is only one molecular ion state formed with He ^1S which is HeO^+ $^4\Sigma$. However, there are three states of HeO^+ which dissociate to give O^+ ^2D + He ^1S. These are the $^2\Pi$ (^2D), $^2\Sigma$ (^2D), and $^2\Delta$ (^2D) states. Similarly, there are two states of HeO^+, $^2\Pi$ (^2P) and $^2\Sigma$ (^2P), which dissociate to give O^+ ^2P and He ^1S.
All of the molecular ion states which dissociate into He ^1S + O^+ ^2P and He ^1S + O^+ ^2D require multiple reference functions to describe this process correctly. The GAUSSIAN82 program is not able to describe interaction potentials which require more than one reference function to correctly describe molecular dissociation so a different theoretical method was required for the doublet states of HeO^+. Valence bond methods do not have this limitation so this approach was used. The valence bond program has been described in Chapter 5. In a preliminary valence bond study, a minimum basis set calculation was carried out to identify the electronic configurations of HeO^+ which dissociate to give doublet O^+ and He ^1S and to assign these to the various molecular ion states available. It was found, as expected (Turner, 1974), that the $^2\Pi$ (^2P) and $^2\Pi$ (^2D) molecular states arise from the $1s^2_{He}1s^2_O2s^2_O\,2p_{x,O}\,2p^2_{y,O}$ and $1s^2_{He}1s^2_O2s^2_O\,2p_{x,O}\,2p^2_{z,O}$ configurations. The $^2\Delta$ (^2D) molecular state arises from the $1s^2_{He}1s^2_O2s^2_O2p^2_{x,O}\,2p_{z,O}$, $1s^2_{He}1s^2_O2s^2_O\,2p^2_{y,O}\,2p_{z,O}$ and $1s^2_{He}1s^2_O2s^2_O2p_{x,O}\,2p_{y,O}\,2p_{z,O}$ configurations. The $^2\Sigma$ (^2P) state arises from the $1s^2_{He}1s^2_O2s^2_O2p^2_{x,O}\,2p_{z,O}$ and $1s^2_{He}1s^2_O2s^2_O\,2p^2_{y,O}\,2p_{z,O}$ configurations. The $^2\Sigma$ (^2D) state arises from the

$1s^2_{He}1s^2_O 2s^2_O 2p_{x,O} 2p_{y,O} 2p_{z,O}$ configuration. This preliminary study provided the necessary base functions from which excitations using a better basis set could yield a large number of configurations to be included in more extensive valence bond calculations of He + O^+ interaction potentials. Valence bond calculations were performed to determine the interaction potential energies of the $^4\Sigma$ (^{4}S), $^2\Pi$ (^{2}D), $^2\Delta$ (^{2}D), $^2\Sigma$ (^{2}P), and $^2\Pi$ (^{2}P) states of HeO^+ using a double-zeta (DZ) basis set with orbital exponents from Huzinaga and Arnau (1970). This basis was contracted to He (1s,2s) and O (1s,2s,3s,2p,3p) using contraction coefficients which had been determined from atomic calculations on He ^{1}S, O^+ ^{4}S, and O^+ ^{2}D using the program of Roos et al. (1968). Table 9.2 lists the contraction coefficients. For the $^2\Pi$ (^{2}P) state and the $^2\Sigma$ (^{2}P) state of HeO^+, the O^+ (^{2}D) contraction coefficients were used. This basis set was augmented with the addition of polarization functions (p on He, d on O) and diffuse functions on each centre (2s on He; 3s and 3p on O). The diffuse functions were based upon the diffuse Gaussian orbitals used in a study on HeO (Staemmler and Jaquet, 1985). The details of these additional functions are also contained in Table 9.2.

For the $^4\Sigma$ (^{4}S) state, 64 configurations were chosen. The majority of these being single excitations from three base configurations; $1s^2_{He}1s^2_O 2s^2_O p_{x,O} p_{y,O} p_{z,O}$, $1s^2_{He}1s^2_O 2s_O p_{x,O} p_{y,O} p^2_{z,O}$ and $1s_{He}1s^2_O 2s^2_O p_{x,O} p_{y,O} p^2_{z,O}$. These included all the p→p, s→s and p→d excitations possible from the base configurations. Also included in the configurations list were a limited number of double excitations of s functions.

A summary of the results of the valence bond calculations for this state is contained in Table 9.3.

r (Å)	E (hartree)	
	HF	MP4SDQ
0.875	-76.7514702	-76.9222716
1.000	-76.9380163	-77.1065691
1.125	-77.0514140	-77.2172854
1.250	-77.1207391	-77.2833816
1.375	-77.1636020	-77.3229667
1.500	-77.1900503	-77.3466523
1.625	-77.2061351	-77.3606862
1.750	-77.2157244	-77.3688549
1.875	-77.2213008	-77.3734764
2.000	-77.2244308	-77.3759696
2.250	-77.2269326	-77.3777564
2.375	-77.2273021	-77.3779278
2.500	-77.2274276	-77.3779150
2.625	-77.2274290	-77.3778187
2.750	-77.2273715	-77.3776911
3.000	-77.2272033	-77.3774311
3.500	-77.2269022	-77.3770453
4.000	-77.2266993	-77.3768044
4.500	-77.2265830	-77.3766713
5.000	-77.2265239	-77.3766051
∞	-77.2264369	-77.3765110

Table 9.1 MP4SDQ and HF energies for HeO^+ $^4\Sigma$ (^4S).

Contraction coefficients

	$O^+ (^4\Sigma)$	$O^+ (^2D)$	He (^1S)	
1s	0.717389		0.717282	0.844778
	0.291325		0.291490	0.179640
	0.00219174		0.00231399	
	-0.00259988		-0.00283206	
2s	-0.326755		-0.327532	1.621280
	0.0275763		0.027710	-1.819329
	0.241122		0.236383	
	0.840833		0.845501	
2p	0.662810		0.673097	
	0.424228		0.412989	
3s	-0.551153		-0.549790	
	0.199934		0.199358	
	-2.14320		-2.14363	
	2.13209		2.13004	
3p	1.18607		1.18026	
	-1.29078		-1.29442	

Additional functions included in basis set.

centre	polarisation functions	diffuse functions
He	2p (ξ = 1.5)	2s (ξ = 0.687)
O	3d (ξ = 1.0)	3s (ξ = 1.342)
		3p (ξ = 0.794)

Table 9.2 Basis set for Valence Bond calculations on HeO^+.

9.3.3 Excited State Calculations for HeO^+

For the doublet states of HeO^+ a procedure similar to that described above for the quartet state was used resulting in a total of 71 configurations. Five base functions were used to describe the $^2\Pi$ (^2D) and $^2\Pi$ (^2P) molecular states; $1s^2_{He}1s^2_O2s^2_O\,p_{x,O}\,p^2_{y,O}$, $1s^2_{He}1s^2_O2s^2_O\,p_{x,O}\,p^2_{z,O}$, $1s_{He}1s^2_O2s^2_O\,p_{x,O}\,p^2_{y,O}\,p_{z,O}$, $1s^2_{He}1s^2_O2s_O\,p_{x,O}\,p^2_{y,O}\,p_{z,O}$ and $1s_{He}1s^2_O2s_O\,p_{x,O}\,p^2_{y,O}\,p^2_{z,O}$. Twenty five configurations were generated by single and double excitation from each of bases 1 and 2, twelve from base 3 and the remainder from bases 4 and 5. Valence bond calculations were performed over the range 1.5 to 10.0 bohr. A similar procedure was used to obtain the $^2\Delta$ (^2D) and $^2\Sigma$ (^2P) molecular state energies based upon the following base functions; $1s^2_{He}1s^2_O2s^2_O\,p_{z,O}\,p^2_{y,O}$, $1s^2_{He}1s^2_O2s^2_O\,p_{z,O}\,p^2_{x,O}$, $1s_{He}1s^2_O2s^2_O\,p_{z,O}\,p^2_{y,O}\,p_{x,O}$, $1s^2_{He}1s^2_O2s_O\,p_{z,O}\,p^2_{y,O}\,p_{x,O}$ and $1s_{He}1s^2_O2s_O\,p_{z,O}\,p^2_{y,O}\,p^2_{x,O}$.

The results of valence bond calculations on these doublet states are contained in Table 9.3.

r (bohr)	E (hartree)				
	$^4\Sigma$ (^{4}S)	$^2\Pi$ (^{2}D)	$^2\Delta$ (^{2}D)	$^2\Pi$ (^{2}P)	$^2\Sigma$ (^{2}P)
1.5	-76.47719577	-76.82769060	-76.02786115	-75.57893059	-75.97154902
2.0	-76.98185993	-77.04540842	-76.72682300	-76.52575887	-76.64767977
2.25	-77.08936567	-77.07638531		-76.74312948	
2.5	-77.15170748	-77.08820785	-76.97576110	-76.87092145	-76.89450107
2.75	-77.18771894	-77.09215716		-76.94390211	
3.0	-77.20830785	-77.09420493	-77.06111525	-76.98342083	-76.97899156
3.25	-77.21988280	-77.09641963		-77.00323826	
3.5	-77.22623741	-77.09862644	-77.08921760	-77.01248325	-77.00670163
4.0	-77.23133304	-77.10135900	-77.09802729	-77.01839797	-77.01534112
4.5	-77.23247341	-77.10216818	-77.10062883	-77.01941597	-77.01786729
5.0	-77.23253795	-77.10224718	-77.10135087	-77.01946756	-77.01855944
5.5	-77.23236316	-77.10215627	-77.10153640	-77.01935558	-77.01873462
6.0	-77.23216384	-77.10205587	-77.10157586	-77.01924441	-77.01877135
6.5	-77.23198506	-77.10197619	-77.10157596	-77.01915977	-77.01877121
7.0	-77.23183213	-77.10191587	-77.10156460	-77.01909784	-77.01876021
7.5	-77.23170518	-77.10187227	-77.10155250	-77.01905447	-77.01874843
8.0	-77.23159969	-77.10184022	-77.10154156	-77.01902334	-77.01873770
10.0	-77.23138643	-77.10177686		-77.01896273	
∞	-77.23123482	-77.10172932	-77.10149522	-77.01891696	-77.01869395

Table 9.3 Valence Bond energies for the doublet molecular states of HeO^+ which dissociate into O^+ ^{2}D and O^+ ^{2}P.

9.4 Results and Discussion

Both the quartet and doublet calculations exhibited the correct separation behaviour:

$$
\begin{aligned}
HeO^+\,{}^4\Sigma &\rightarrow He\,{}^1S + O^+\,{}^4S \\
HeO^+\,{}^2\Sigma\,({}^2D) &\rightarrow He\,{}^1S + O^+\,{}^2D \\
HeO^+\,{}^2\Pi\,({}^2D)) &\rightarrow He\,{}^1S + O^+\,{}^2D \\
HeO^+\,{}^2\Delta\,({}^2D) &\rightarrow He\,{}^1S + O^+\,{}^2D \\
HeO^+\,{}^2\Sigma\,({}^2P) &\rightarrow He\,{}^1S + O^+\,{}^2P \\
HeO^+\,{}^2\Pi\,({}^2P) &\rightarrow He\,{}^1S + O^+\,{}^2P
\end{aligned}
\qquad (9.1)
$$

The two doublet state calculations were performed simultaneously because only one calculation was required to get energies for each state. With the exception of calculations performed at small internuclear separation, the lowest energy and eigenfunction corresponded to the $^2\Pi\,(^2D)$ and the second lowest to the $^2\Pi\,(^2P)$ state. The VB calculated energy separations between the states compare well with the atomic energy levels. The calculated energy for the $O^+\,(^2D)$ state lies 28400 cm^{-1} above, and the $O^+\,(^2P)$ state the $O^+\,(^2D)$ state 46600 cm^{-1} above, the ground state compared with 26819 cm^{-1} and 40468 cm^{-1} observed spectroscopically (Moore, 1971). The differences observed in the separated atom energies for the same oxygen ion state is due to the effect of d-orbitals in the calculations. The calculated interaction potentials were used as input to our two-temperature theory program.

It was necessary to carry out a valence bond calculation on the ground state of $HeO^+\,{}^4\Sigma\,(^4S)$ in order to compare the quality of the mobility calculated from an interaction potential at this level of theory with the mobility calculated from the more accurate MP4SDQ/6-311+G(3df,3pd) $HeO^+\,(^4\Sigma)$ interaction potential. The confidence we have in our results for the doublet state mobilities of O^+ in helium is based on the good agreement between the mobilities calculated for ground state O^+ in helium, by both the valence bond and fourth order Møller-Plesset methods, with the experimental measurements.

The calculated reduced mobility of O^+ in helium as a function of E/N from the MP4SDQ interaction potential of $HeO^+\,(^4\Sigma)$, shown in Figure 9.1, accurately reproduces the

experimental measurements on ground state O^+ in helium (Lindinger and Albritton, 1975; Fhadil et al., 1982). The corresponding VB calculation is 12% too low at 5Td, but above 25Td the agreement is better than 7%. Valence bond calculations with an extended basis set employing a suitably chosen set of configurations should therefore provide an interaction potential which can accurately describe the mobility of an ion above 30Td. The reduced mobility calculated from the HF interaction potential is higher than the experimental measurements at low values of E/N and is less suitable for determining the position of the maximum in the experimental reduced mobility than either of the calculations based on the MP4SDQ or VB interaction potentials. On the basis of our previous mobility calculations for F^- in helium we know that this HF interaction potential well depth is too small resulting in a calculated reduced mobility which is higher than the experiment results at low values of E/N. Table 9.4 lists some parameters derived from the interaction potentials in the present study; r_m is the distance corresponding to the minimum energy, ε the well depth, and σ the internuclear separation at which the energy is zero.

state	method	σ (Å)	r_m (Å)	ε (eV)
$^4\Sigma$	MP4SDQ	2.04	2.42	0.0388
$^4\Sigma$	HF	2.16	2.56	0.0273
$^4\Sigma$	VB	2.11	2.53	0.0363
$^2\Pi$ (^{2}D)	VB	2.19	2.55	0.0145
$^2\Delta$ (^{2}D)	VB	2.81	3.30	0.0023
$^2\Pi$ (^{2}P)	VB	2.20	2.51	0.0162
$^2\Sigma$ (^{2}P)	VB	2.80	3.29	0.0022

Table 9.4 Interaction Potential Parameters for HeO^+. $V(\sigma)=0$ and $V(r_m)=-\varepsilon$.

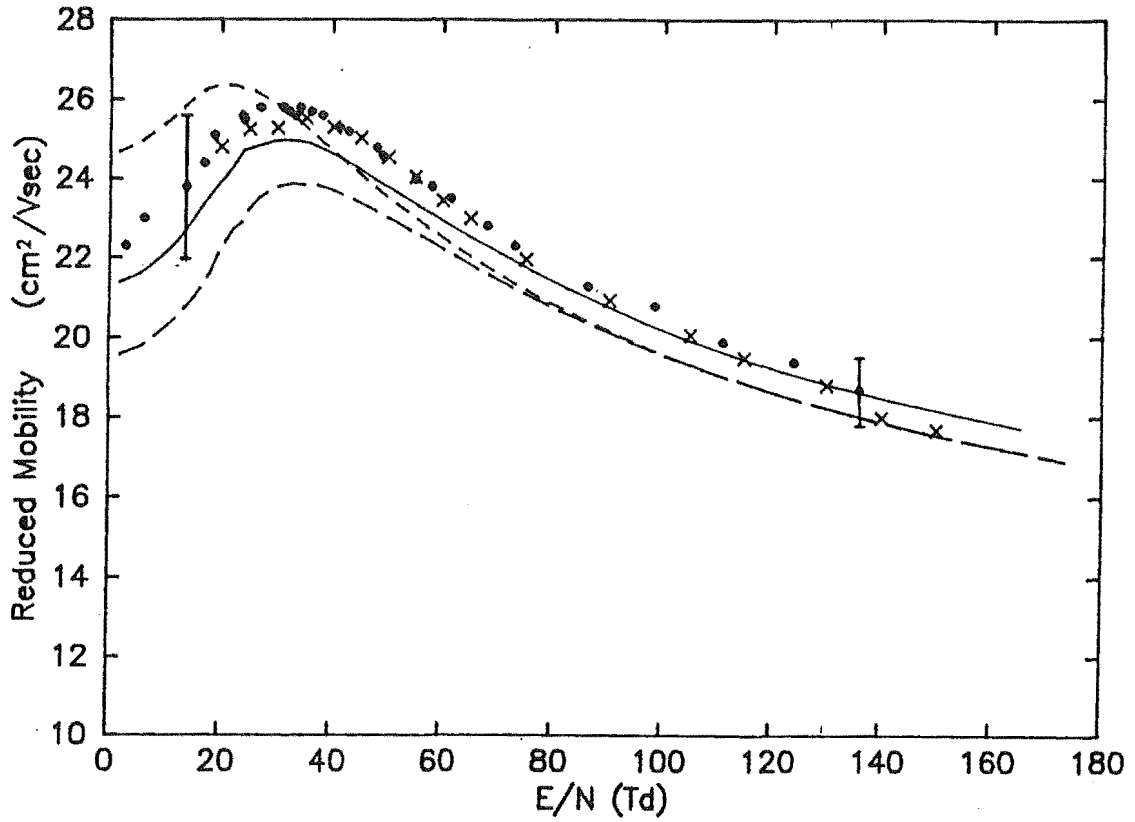

Figure 9.1 Reduced mobility of O^+ in helium. •, experimental values (Lindinger and Albritton, 1975); x, experimental values (Fhadil et al., 1982); ———, calculation using MP4SDQ potential (HeO^+ $^4\Sigma$); — — , calculation using VB potential (HeO^+ $^4\Sigma$); – – – , calculation using HF potential (HeO^+ $^4\Sigma$).

It can be seen in Table 9.4 that the well depth of the HF interaction potential is significantly less than the well depth of the other $^4\Sigma$ calculations. Low field reduced mobilities can be very sensitive to minor changes in the position, r_m and depth, ε of the interaction potential well, and a high level of theory is required to estimate these quantities accurately. A small change in r_m or ε may lead to a relatively large change in the long range part of the interaction potential, the region known to affect the calculated low field mobilities (Viehland et al., 1976a). In contrast, experimental mobilities for atomic ions measured at values of E/N above 30 Td can be reproduced within experimental error using the two-temperature theory of ion mobility with interaction potentials generated using ab-initio methods as shown in Chapter 7.

Initially, only the lowest energy molecular ion state, which dissociates to each of the three low energy states of O^+, was considered as being solely responsible for the experimental observations. This assumption is not correct for molecular states widely differing in energy. For this case a weighted average of ion drift velocities, calculated from each of the molecular states dissociating to a particular atomic state, is required. The weighting factor is the degeneracy of the molecular state involved and reflects the probability of collisions giving rise to that molecular state. This phenomenon is further illustrated in Chapter 10.

Valence bond calculations performed on the two low lying doublet states of HeO^+ were used to calculate the reduced mobility curves shown in Figure 9.2. It is immediately obvious that the mobility calculated using the HeO^+ $^2\Pi$ (^2P) interaction potential is remarkably close to the experimental values for the mobility of O^{+*} in helium except at low values of E/N. The correlation between the mobility calculated using the HeO^+ $^2\Pi$ (^2D) interaction potential and the experimental values is very poor and certainly well outside the maximum discrepancies expected from application of the second approximation of the two-temperature theory. From Table 9.4 it is not possible to account for the difference in the calculated mobilities of O^+ ^2P and O^+ ^2D on the basis of r_m and ε values. The difference between these two interaction potentials, which is responsible for the higher calculated mobility of O^+ ^2D than O^+ ^2P, appears to be a significantly 'harder' repulsive wall in the HeO^+ $^2\Pi$ (^2P) interaction potential as compared with the HeO^+ $^2\Pi$ (^2D) interaction potential. The third curve in Figure 9.2 was obtained by scaling the negative energies (relative to the separated atoms) of the HeO^+ $^2\Pi$ (^2P) curve by a factor of 2.4. This has the effect of decreasing the well depth by only 0.02 eV but has a dramatic effect on the low field reduced mobility. The effect of this scaling is insignificant above 40 Td. Figure 9.3 shows the drift velocity v_d of O^+ in helium as a function of E/N calculated for three low-lying states of O^+ considered in this study together with the experimental results for O^+ and O^{+*} drifting in helium. The conclusion from this work is that the O^{+*} ion observed in experiments (Rowe et al., 1980; Johnsen et al., 1982; and Fhadil et al., 1982) and assigned as O^+ ^2D is more likely due to the O^+ ^2P state.

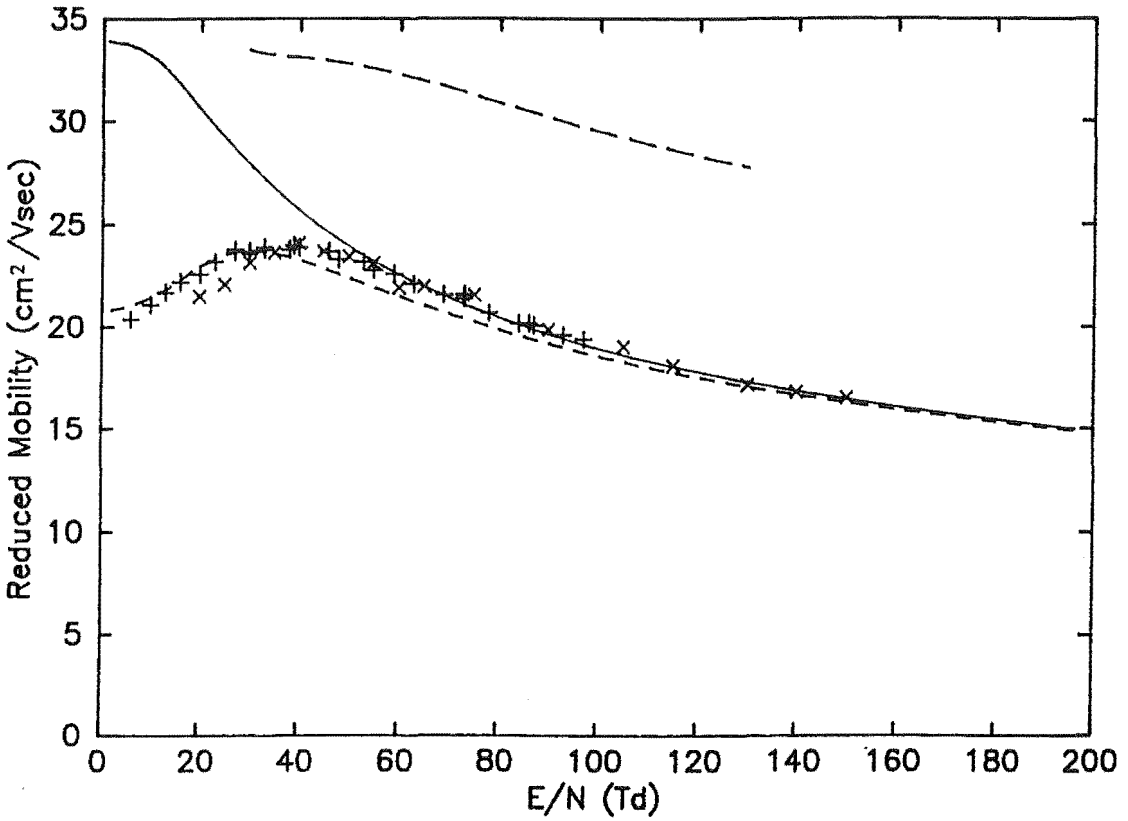

Figure 9.2 Reduced mobility of O^{+*} in helium. +, experimental values (Rowe et al., 1980); x, experimental values (Fhadil et al., 1982); ———, calculation using VB potential (HeO^+ $^2\Pi$ (^2P)); — —, calculation using VB potential (HeO^+ $^2\Pi$ (^2D)); – – –, calculation using VB potential (HeO^+ $^2\Pi$ (^2P))with the well increased in depth by 0.02 eV.

To further our confidence in this finding, three-temperature theory calculations, using the four doublet state interaction potentials, were carried out. The results of these calculations are summarised in Table 9.5. As shown in Table 9.5, both the $^2\Pi$ (^2P) and $^2\Sigma$ (^2P) interactions lead to very similar results for the mobility of O^+ ^2P in helium. This reinforces our earlier results because a weighted average of the results from these two states will be very similar to the mobility arising from the $^2\Pi$ (^2P) state alone. We can make no definitive comment on the expected mobility of O^+ ^2D because of a lack of information on the $^4\Sigma$ (^2D) state.

E/N (Td)	K_0 ($cm^2V^{-1}s^{-1}$)				
	Expt.	$^2\Pi$ (^2D)	$^2\Delta$ (^2D)	$^2\Pi$ (^2P)	$^2\Sigma$ (^2P)
20.	21.5	34.64	29.74	31.03	29.90
25.	22.1	34.13	28.18	29.74	28.32
30.	23.13	33.58	26.67	28.53	27.00
35.	23.65	33.28	25.74	27.40	25.86
40.	24.1	33.13	24.76	26.36	24.88
45.	23.7	33.02	23.90	25.45	24.02
50.	23.96	32.84	23.16	24.67	23.26
55.	23.13	32.67	22.49	23.91	22.91
60.	21.92	32.44	21.89	23.19	21.99
65.	22.00	32.21	21.35	22.57	21.44
75.	21.58	31.64	20.42	21.59	20.51
90.	19.87	30.68	19.29	20.27	19.36
105.	19.03		18.37	19.21	18.44
115.	18.10		17.86	18.61	17.92
130.	17.16		17.19	17.82	17.25
140.	16.80		16.80	17.36	16.86
150.	16.50		16.44	16.95	16.50

Table 9.5 Reduced mobilities calculated using the three-temperature theory with four doublet states of HeO^+. Experimental values from Fhadil et al., (1982).

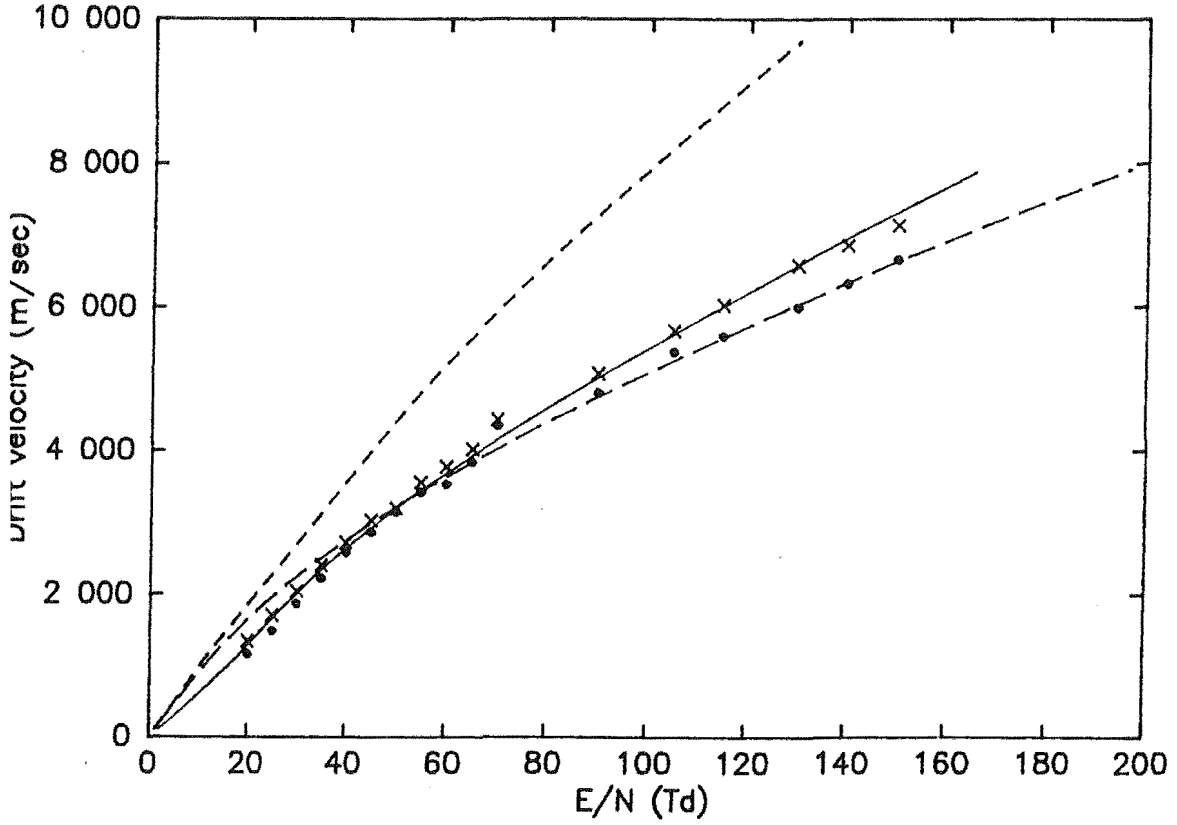

Figure 9.3 Drift velocity of O^+ and O^{+*} in helium. x, O^+ experimental values (Fhadil et al., 1982); o, O^{+*} experimental values (Fhadil et al., 1982); ———, calculation using MP4SDQ potential (HeO^+ $^4\Sigma$); — —, calculation using VB potential (HeO^+ $^2\Pi$ (^2P)); – – –, calculation using VB potential (HeO^+ $^2\Pi$ (^2D)).

Previous experimental evidence used in justifying the O^+ ^2D state assignment included comparison of photorelaxation lifetimes and energy levels for each possible state. However, a typical ion source producing O^{+*} will be forming both the ^2P and ^2D states as they are only 13650 cm^{-1} (1.7 eV) apart. Both states have photorelaxation lifetimes several orders of magnitude longer than flow-drift tube transit times so neither state will be significantly depleted by this process. The apparent state selection of O^+ ^2P can be explained in terms of the potential energy surface crossing between the $^2\Pi$ (^2D) state and the $^4\Sigma$ (^4S) ground state of HeO^+. This occurs at 2.2 bohr and is 0.8 eV above the energy of O^+ ^2D +He ^1S and 4.3 eV above the energy of O^+ ^4S +He ^1S. The presence of this curve crossing provides an effective channel for depletion of the $^2\Pi$ (^2D) state. There is no equivalent curve crossing from the $^2\Pi$ (^2P) state of

HeO^+ to lower lying surfaces. The presence of the $^2\Pi$ (^2D) state and $^4\Sigma$ (^4S) state curve crossing has been predicted (Augustin et al., 1973) to result in quenching of the ^2D state of O^+ by helium but not the ^2P state. This quenching process is written as follows:

$$He\ ^1S + O^+\ ^2D \rightarrow He\ ^1S + O^+\ ^4S \qquad (9.2)$$

The assignment of O^{+*} observed in flow tube studies to the ^2D state of O^+ is based upon limited evidence and is in direct conflict with some experimental results. Based upon our mobility calculations, using ab-initio interaction potentials, we believe that it is in fact O^+ (^2P) which has been observed. This can be explained since both O^+ (^2P) and O^+ (^2D) will be formed in an ion source producing O^{+*} but only the ^2D state of O^+ can be quenched by collision with helium.

Although we were unable, in this study, to obtain interaction potentials corresponding to all of the doublet molecular states which dissociate into $He\ ^1S + O^+\ ^2D$, we were able to show that the ^2P state of O^+ can account for the mobility of the experimentally observed excited oxygen ion.

Chapter 10

Mobility Calculations for Other Ion-Atom Systems

10.1 The Mobility of B^+ in Helium

The mobility of B^+ ions in helium has never been measured. An attempt to rectify this situation encountered considerable experimental obstacles. From our attempts, it appears that boron containing compounds have an adverse effect on the emission properties of thermionic filaments. The emission of both the ion source filament and the ion gauge filament was observed to drop markedly when a trace of a boron containing compound was admitted to the helium buffer gas in the drift tube, thus making arrival time distribution measurements impossible. This phenomenon occurred for filaments made of iridium or rhenium regardless of the boron compound, B_2H_6, BCl_3 or BF_3, used.

The difficulty in making experimental measurements has created the opportunity for ab-initio theoretical methods to provide the first prediction of the mobility of B^+ ions in helium.

The HeB^+ interaction potential was calculated using the GAUSSIAN82 program (Binkley et al., 1982) at the MP4SDQ/6-311+G(3df,3pd) level of theory, excluding core contributions to the correlation energy. The results of this calculation are given in Table 10.1.

This interaction potential was used in both the two- and three-temperature theory calculations of the mobility of B^+ ions in helium. The collision cross sections were calculated to 0.1% accuracy and the three-temperature theory calculation converged to within 0.8% for the mobility. The theoretical mobility of B^+ in helium, calculated using the three-temperature theory is shown in Figure 10.1.

r (Å)	E (hartree)	r (Å)	E (hartree)
1.50	-27.1546543	3.250	-27.1897326
1.75	-27.1745029	3.500	-27.1895900
2.00	-27.1839220	3.750	-27.1894691
2.25	-27.1879307	4.000	-27.1893749
2.50	-27.1894370	4.500	-27.1892472
2.75	-27.1898598	5.000	-27.1891684
2.875	-27.1898889	∞	-27.1890286
3.000	-27.1898608		

Table 10.1 Interaction potential energies for the ground state of HeB^+ calculated at the MP4SDQ/6-311+G(3df,3pd) level of theory.

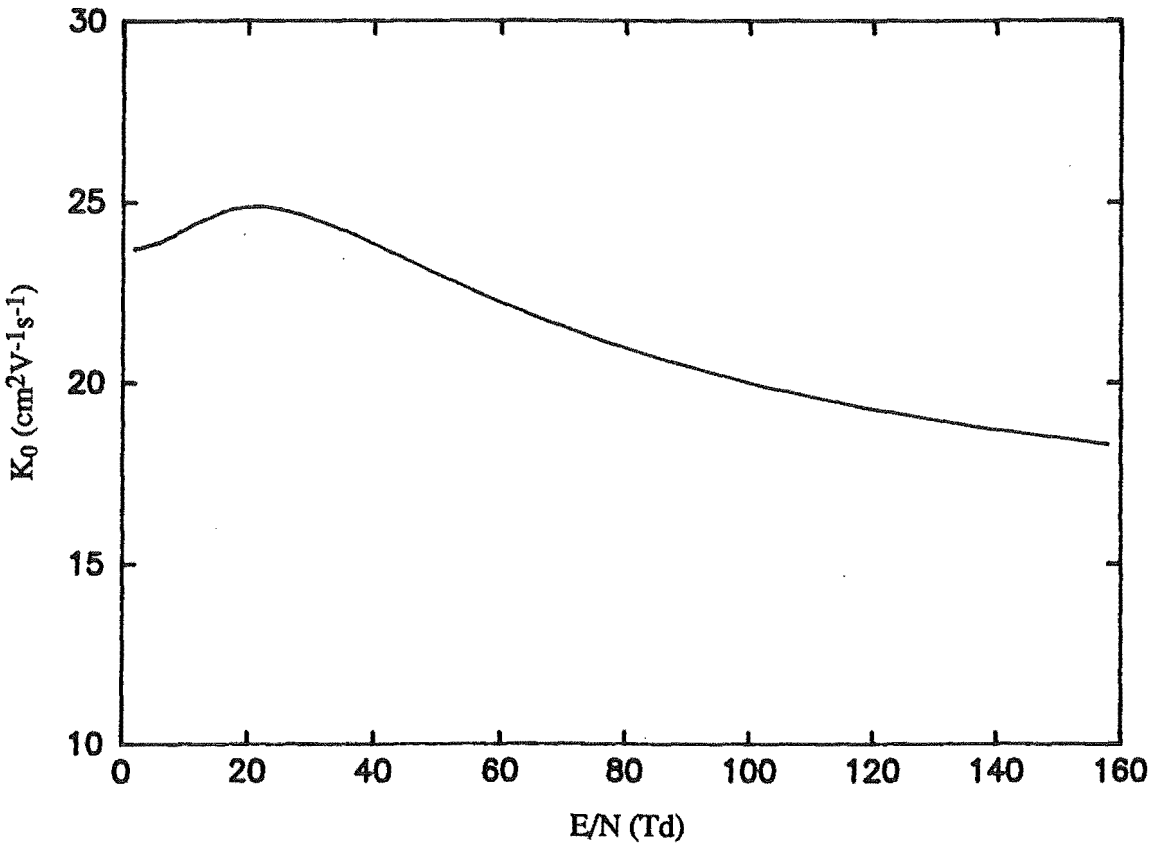

Figure 10.1 Calculated reduced mobility of B^+ in helium as a function of E/N.

10.2 The Mobility of Li^+ in Helium

Alkali ions have long been the focus of both experimental and theoretical research and Li^+ has been no exception. These studies provide a means of comparing and assessing the accuracy of various research methods, techniques and theories. Therefore, the previous investigations of the mobility of Li^+ in helium were of interest to us. In the last two-decades there have been several experimental measurements of the mobility of Li^+ in helium (Takata, 1975; Akridge et al., 1975; Gatland et al., 1977a; Kaneko et al., 1978) and several attempts at calculating the mobility (Gatland et al., 1977a, 1977b; Viehland, 1982, 1983). Of these, Gatland et al. (1977a) performed a two- and Viehland (1983) performed a three-temperature theory calculation using an ab-initio interaction potential. The interaction potential used in both those studies was the Coupled Electron Pair Approximation, CEPA, calculation by Hariharan and Staemmler (1976). Recently, the mobility of Li^+ in helium has been remeasured by Cassidy and Elford (1985), providing data at 294K and 80K. The accuracy of this data is estimated to be 0.6% at 294K increasing to 1.5% at 80K. The low temperature low field strength measurements are influenced predominantly by the long range part of the $He\text{-}Li^+$ interaction potential and thus provide a sensitive means of testing proposed ab-initio interaction potentials. We have performed three-temperature mobility calculations using three recently available ab-initio interaction potentials for the ground state ($^1\Sigma^+$) of $HeLi^+$ to compare the calculated reduced mobility with the best experimental values at both 294K and 80K. The collision cross-sections were calculated to 0.1% accuracy and the three-temperature theory calculation converged to 0.8%. The results are shown in Tables 10.2 and 10.3.

The results of this study show that at 294K all three interaction potentials tested gave very good agreement with the experimental values over the whole range of E/N. The maximum discrepancy between experiment and theory is 3% at this temperature.

At 80K, the difference between the calculated and experimental reduced mobilities,using any of the interaction potentials, was greater than the difference at 294K. However, the interaction potential calculated by Tatewaki et al. (1984) is slightly better at determining the mobility than the other interaction potentials, especially at very low E/N. This was expected since this interaction potential was also the most accurate for low field mobilities at 294K.

E/N (Td)	K_0 ($cm^2V^{-1}s^{-1}$)			
	expt.	A	B	C
3.00	22.81	22.87	22.96	23.16
4.00	22.88	22.96	23.03	23.24
5.00	22.94	23.07	23.14	23.30
6.00	23.06	23.21	23.27	22.68
8.00	23.35	23.60	23.66	24.12
10.00	23.77	24.21	24.27	24.25
12.00	24.26	24.84	24.79	24.85
13.00	24.56	25.18	25.08	25.15
14.00	24.91	25.57	25.40	25.53
15.00	25.32	25.97	25.76	25.90
16.78	26.09	26.78	26.50	26.58
17.90	26.65	27.47	26.96	27.00
18.00	26.70	27.50	27.00	27.04
20.00	27.55	27.89	27.82	27.80
25.00	29.62	30.09	30.09	29.85
30.00	31.18	31.53	32.07	31.50
35.00	32.13	32.13	32.84	32.46
40.00	32.47	32.28	33.49	32.79
50.00	32.35	31.81	33.09	32.59
60.00	31.72	31.11	32.30	31.88
70.00	31.35	30.19	31.46	31.05

Table 10.2 Comparison of calculated and experimental reduced mobilities for Li^+ in helium at 294K. Experimental measurements by Cassidy and Elford (1985). The interaction potentials used were: A, Tatewaki et al. (1984); B, Senff and Burton (1986); and C, Cooper et al. (1985).

Thus, we conclude from this work that the currently available interaction potentials for the $HeLi^+$ ion are sufficiently good to provide very accurate estimates of the reduced mobility of Li^+ in helium at 294K, but care must be taken when using these interaction potentials to calculate low temperature mobilities. This is a consequence of the sensitivity of mobility calculations at low temperature to the very small energies present in the long range part of the interaction potential. Very accurate ab-initio calculations, especially at large internuclear separation, are required to successfully calculate low field, low temperature ion mobilities.

	K_0 ($cm^2V^{-1}s^{-1}$)			
E/N (Td)	expt.	A	B	C
2.	19.63	19.54	20.45	20.27
4.	19.63	19.58	20.45	20.32
5.	19.64	19.61	20.47	20.36
6.	19.67	19.66	20.49	20.42
8.	19.79	19.85	20.71	20.55
10.	19.92	20.12	21.03	20.71
12.	20.10	20.64	21.23	21.27
14.	20.36	21.49	21.89	21.62
15.	20.54	21.92	22.23	21.94
16.	20.88	22.42	22.76	22.44
18.	21.58	22.85	23.55	23.29

Table 10.3 Comparison of calculated and experimental reduced mobilities for Li^+ in helium at 80K. Experimental measurements by Cassidy and Elford (1985). The interaction potentials used were: A, Tatewaki et al. (1984); B, Senff and Burton (1986); and C, Cooper et al. (1985).

10.3 The Mobility of N^+ in Helium

When the lowest state of N^+ (^3P) interacts with He (^1S) there are two possible molecular states which can arise:

$$N^+ \, ^3P + He \, ^1S \rightarrow HeN^+ \, ^3\Sigma$$
$$N^+ \, ^3P + He \, ^1S \rightarrow HeN^+ \, ^3\Pi \qquad (10.1)$$

Using the GAUSSIAN82 program (Binkley et al., 1982) we have calculated interaction potentials for both these molecular states at the MP4SDQ/6-311+G(3df,3pd) level of theory excluding core contributions to the correlation energy. The results of these calculations are given in Tables 10.4 and 10.5. The two interaction potentials are compared graphically in Figure 10.2. The only other calculation for this molecular ion was by Liebman and Allen (1970) who reported SCF calculations on some low energy states.

r (Å)	E (hartree)	r (Å)	E (hartree)
1.25	-56.7418894	3.00	-56.8766890
1.50	-56.8261409	3.25	-56.8765212
1.75	-56.8592355	3.50	-56.8763794
2.00	-56.8715204	4.00	-56.8761719
2.25	-56.8756437	5.00	-56.8759671
2.50	-56.8767291	6.00	-56.8759078
2.75	-56.8768324	∞	-56.8758654

Table 10.4 Interaction potential energies for the $^3\Pi$ state of HeN^+ calculated at the MP4SDQ/6-311+G(3df,3pd) level of theory.

r (Å)	E (hartree)	r (Å)	E (hartree)
0.875	-56.7662450	2.000	-56.8807184
0.9375	-56.8045083	2.125	-56.8799193
1.000	-56.8301483	2.500	-56.8781226
1.125	-56.8596567	3.000	-56.8769328
1.250	-56.8737459	3.500	-56.8764351
1.3125	-56.8776326	4.000	-56.8761848
1.375	-56.8801713	5.000	-56.8759717
1.500	-56.8825869	6.000	-56.8759098
1.625	-56.8829622	∞	-56.8758654
1.750	-56.8824249		

Table 10.5 Interaction potential energies for the $^3\Sigma$ state of HeN^+ calculated at the MP4SDQ/6-311+G(3df,3pd) level of theory.

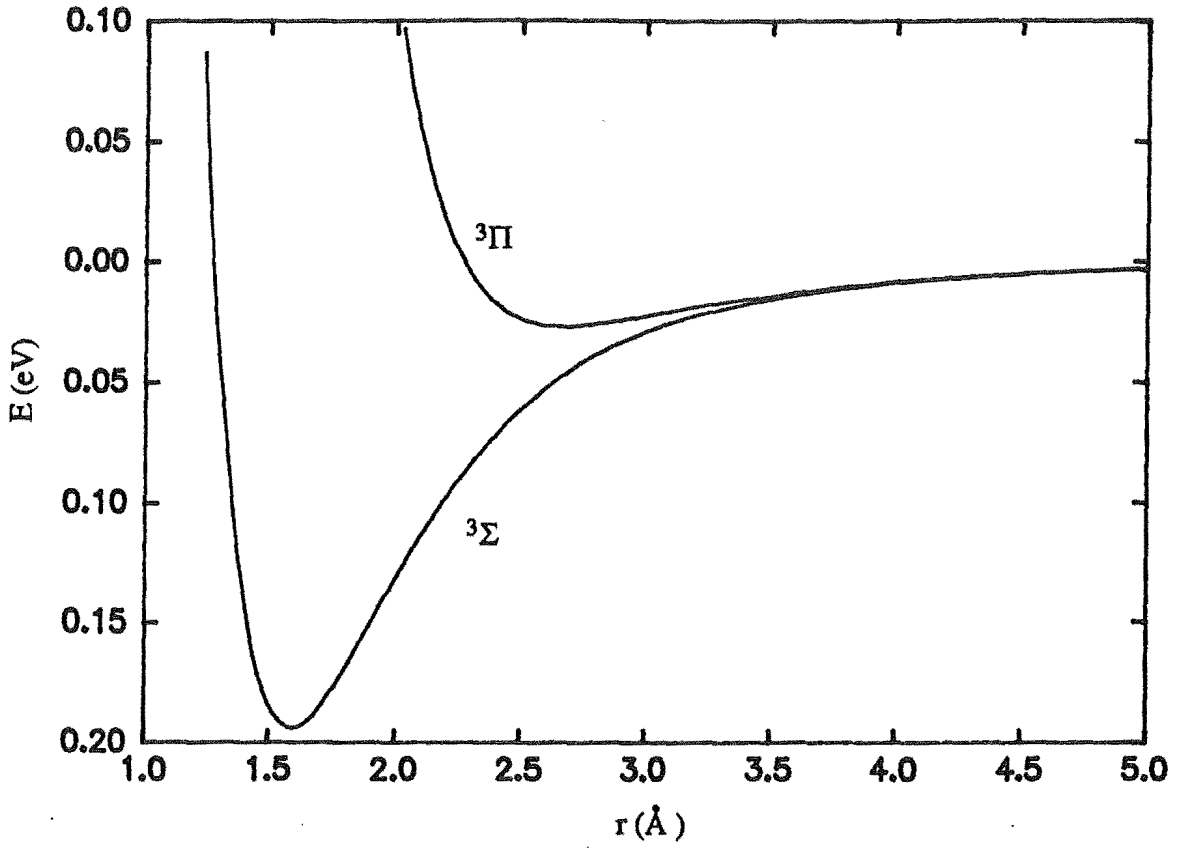

Figure 10.2 Interaction potentials for the $^3\Sigma$ and $^3\Pi$ states of HeN^+.

These interaction potentials were used to calculated the mobility for $N^+ {}^3P$ in helium at both the two- and three-temperature levels of theory. We expected the actual observed mobility of N^+ in helium to be a combination of the calculated mobilities for these two states as they differed widely in energy. The degeneracy of the molecular states is taken into account when calculating this average mobility. For example, Σ and Π molecular states have degeneracies of one and two respectively. Equation 10.2 shows how the average mobility is obtained from mobilities calculated for the two molecular states which can occur when $N^+ {}^3P$ collides with $He\ {}^1S$:

$$K_0(\text{averaged}) = \frac{1}{3}\left(2K_0({}^3\Pi) + K_0({}^3\Sigma)\right) \qquad (10.2)$$

The results of the two mobility calculations, using the three-temperature theory, together with the average mobility are shown in Figure 10.4. The mobility calculated for the $^3\Sigma$ state is unusual and reflects the physical behaviour occurring during collisions as a result of the 0.2eV deep well in the interaction potential. There is a critical ion temperature, below which ions are significantly slowed down by orbiting type collisions. Above this temperature, the ion has sufficient translational energy to avoid these situations and consequently attains a much higher drift velocity. For the $^3\Sigma$ state this temperature corresponds to an intermediate field strength and is reflected in a large rise in calculated mobility.

The average mobility shows an unexpected increase at around 70Td. In Figure 10.5 the average calculated reduced mobility is compared to the experimental observations. Initially we conducted an experimental investigation into the possibility that this calculated behaviour was a real phenomenon but found no evidence for this. Upon a re-examination of the interaction potentials and the calculated reduced mobility, it is possible that a small change in the depth or position of the well in the $HeN^+ {}^3\Sigma$ state would lead to a calculated average mobility that could more faithfully reproduce the experimental observations.

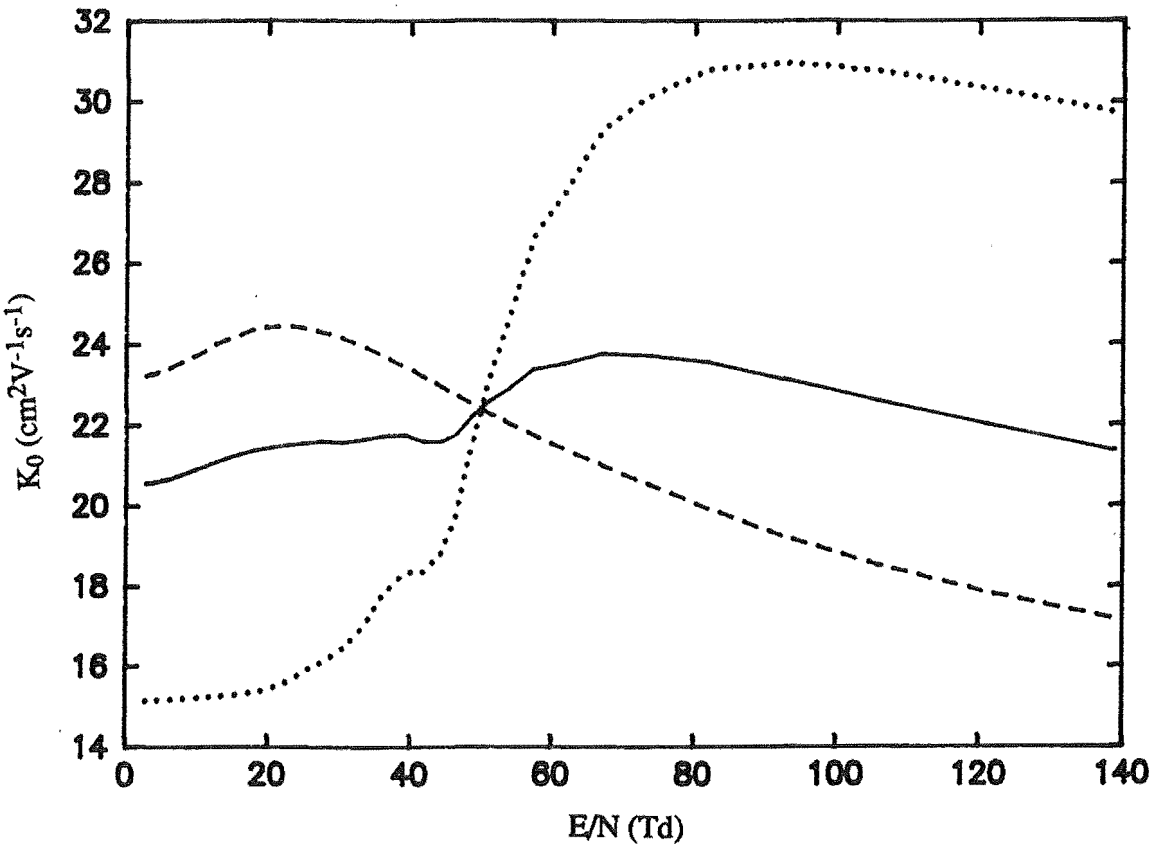

Figure 10.3 Calculated reduced mobility of N^+ in helium as a function of E/N arising from the $^3\Sigma$ (·····) and $^3\Pi$ (– – –) state of HeN^+ together with the average mobility (——).

We know of no other ab-initio mobility calculations which have attempted to solve the problem of a mobility arising from more than one molecular state. The classical description of the processes ocurring inside the drift tube is that in any collision between an ion and a neutral particle the scattering is determined by one of the possible molecular states which are accessible to the particles involved. The choice of state is probably determined by the relative orientation of the partners very early in the collision process. This phenomena has repercussions when mobility data is used to determine an interaction potential by an inversion process. The interaction potential obtained, from mobility data alone, would be some sort of average interaction potential and would not reflect the actual molecular states involved during the experiment. A modified inversion procedure could be developed to use experimental data and one ab-initio interaction potential to recover the second interaction potential. This could lead to

an iterative testing process where two ab-initio interaction potentials are successively compared to the results of this modified inversion procedure. Eventually, this would need to be extended to the general case of n possible molecular states.

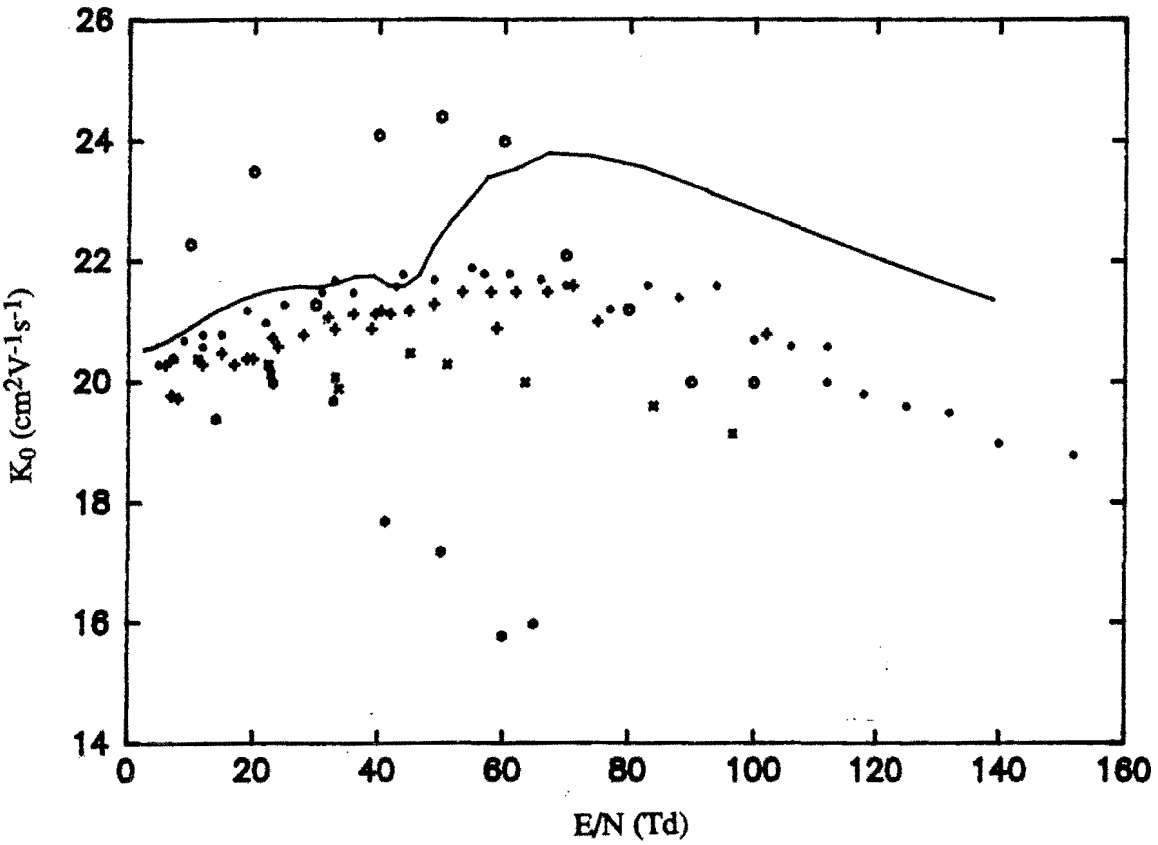

Figure 10.4 Calculated average and experimental reduced mobility of N^+ in helium as a function of E/N. ——, calculation; x, Johnsen et al., 1970; +, McFarland et al., 1973; *, Kaneko et al., 1978; •, Fahey et al., 1981; o, Fhadil et al., 1985.

10.5 The Mobility of F^+ in Helium

The interaction of F^+ ^3P with He ^1S is similar to the interaction of N^+ ^3P with He ^1S as there are two possible molecular states which can arise.

$$F^+ \, ^3P + He \, ^1S \rightarrow HeF^+ \, ^3\Sigma$$
$$F^+ \, ^3P + He \, ^1S \rightarrow HeF^+ \, ^3\Pi \qquad (10.3)$$

Using the GAUSSIAN82 program (Binkley et al., 1982) we have calculated interaction potentials for both these molecular states at the MP4SDQ/6-311+G(3df,3pd) level of theory excluding core contributions to the correlation energy. The results of these calculations are given in Tables 10.6 and 10.7. As for HeN^+, the only other calculation on this molecular ion was by Liebman and Allen (1970) who reported some SCF calculations. The interaction potentials they obtained were not suitable for accurate mobility calculations. The two interaction potentials we obtained are compared graphically in Figure 10.5.

r (Å)	E (hartree)	r (Å)	E (hartree)
0.875	-98.5349132	2.50	-98.8819235
0.9375	-98.6284798	2.75	-98.8814569
1.000	-98.6980978	3.00	-98.8810965
1.25	-98.8340632	3.25	-98.8806210
1.50	-98.9712385	4.00	-98.8803641
1.75	-98.8808589	4.50	-98.8802400
1.875	-98.8822213	5.00	-98.8801813
2.00	-98.8826510	6.00	-98.8801325
2.125	-98.8826374	∞	-98.8800905
2.25	-98.8824413		

Table 10.6 Interaction potential energies for the $^3\Pi$ state of HeF^+ calculated at the MP4SDQ/6-311+G(3df,3pd) level of theory.

These interaction potentials were used to calculated the mobility for F^+ ^3P in helium at both the two- and three-temperature levels of theory. Again, we expected the actual observed mobility of F^+ in helium to be a combination of the calculated mobilities for these two states as they also differed widely in energy. The results of the two mobility calculations, using the three-temperature theory, together with the average calculated mobility and the experimental values are shown in Figure 10.6. It is clear from this figure that we have successfully accounted for the observed mobility of F^+ in helium in terms of the mobilities arising from the two possible molecular states of the HeF^+ ion which can occur during collisions of F^+ ^3P and He ^1S.

r (Å)	E (hartree)	r (Å)	E (hartree)
1.50	-98.8234786	3.00	-98.8809559
1.75	-98.8633792	3.50	-98.8805930
2.00	-98.8762796	4.00	-98.8803508
2.50	-98.8810379	4.50	-98.8802319
2.625	-98.8811264	5.00	-98.8801768
2.75	-98.8811099	∞	-98.8800905

Table 10.7 Interaction potential energies for the $^3\Sigma$ state of HeF^+ calculated at the MP4SDQ/6-311+G(3df,3pd) level of theory.

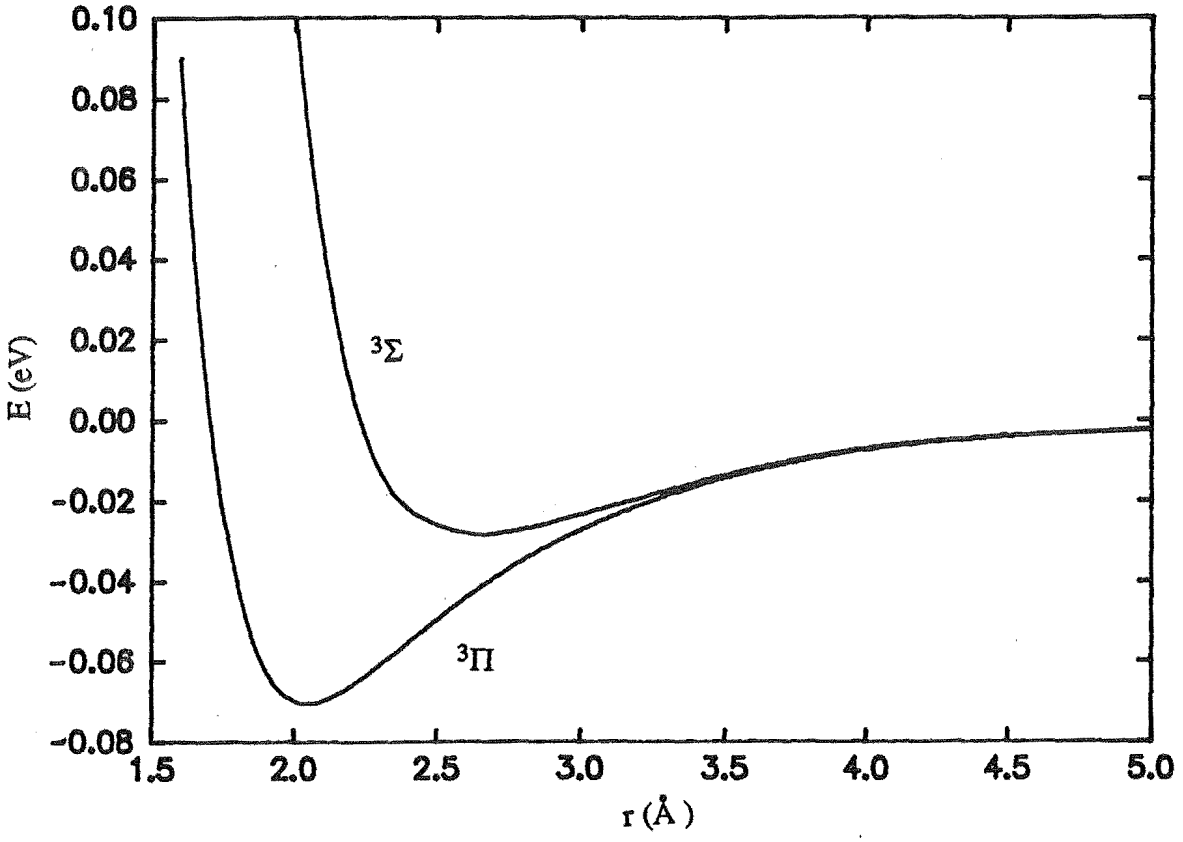

Figure 10.5 Interaction potentials for the $^3\Sigma$ and $^3\Pi$ states of HeF^+.

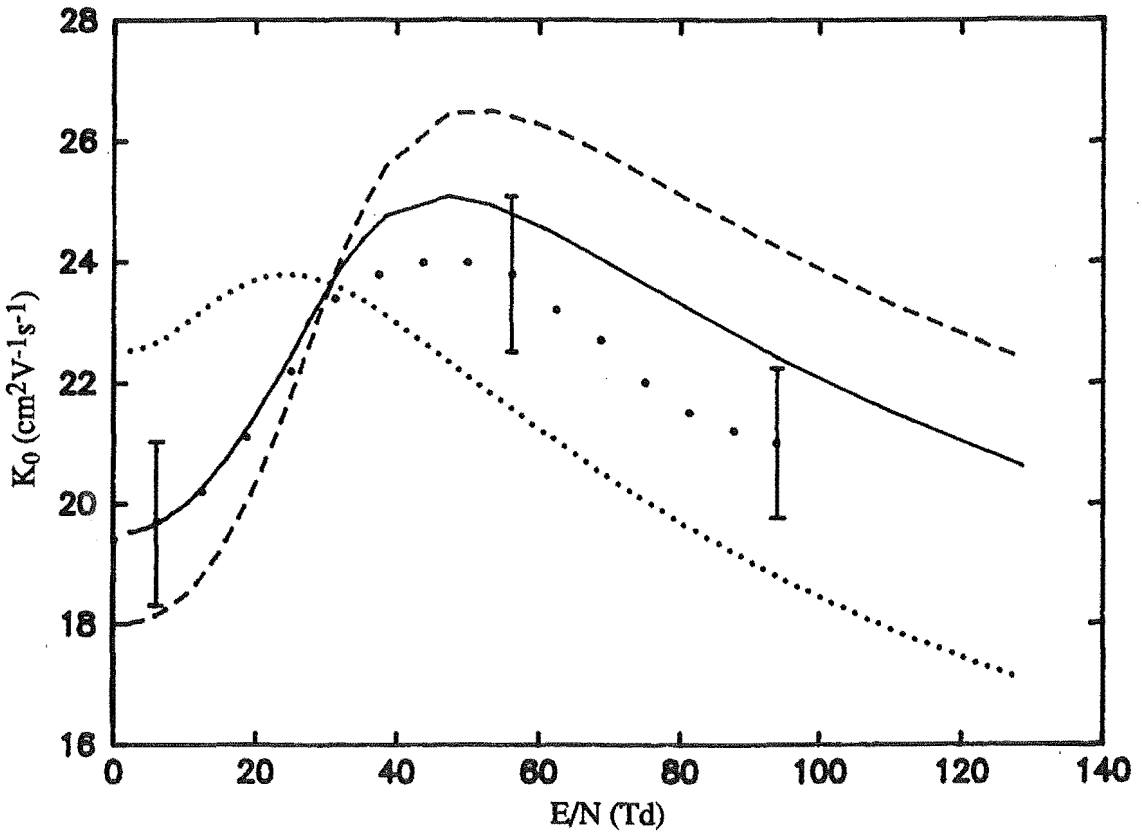

Figure 10.6 Calculated reduced mobility of F^+ in helium as a function of E/N arising from the $^3\Sigma$ (·····) and $^3\Pi$ (– – –) states of HeF^+ together with the average mobility (——) and the experimental values (●) (Hamdan and Birkinshaw, 1986).

Chapter 11

Conclusion

11.1 Overview

The original objectives of this work have been realised. Experimental and theoretical techniques have been applied to the study of gas phase ion mobility resulting in a better understanding of the effects of ion structure and the advantages and difficulties of purely ab-initio methods when calculating ion transport properties.

While the emphasis has been upon the application of experimental and theoretical methods to ion-helium systems which have not been satisfactorily studied previously, an appreciation has been developed of the subtleties of both techniques.

The computer programs which have been developed make routine, accurate mobility calculations feasible, and allow the analysis of large quantities of experimental mobility data to be performed quickly and efficiently.

Both valence bond and Møller-Plesset methods have been shown to be useful in calculating interaction potentials suitable for mobility calculations. However, there are limitations with these methods which need to be taken into account before they are used indiscriminately.

This study of theoretical and experimental aspects of ion transport and ion-molecule interactions has shown that there are many problems that need to be addressed, even for the simplest cases of first row ions drifting in helium. If this work has succeeded it is because it has not only tackled and solved some of these problems, it has also uncovered others.

11.2 Directions for Future Work

As with any project, the work is never finished. There are several areas in this project which could be further developed beyond the scope of the present work.

11.2.1 Interaction Potential Calculations

Although valence bond and Møller-Plesset methods have been used with success, other ab-initio techniques may prove more versatile and accurate at determining interaction potentials for use in mobility calculations. In particular, the Two-Configuration Self Consistent Field (TCSCF) method may be useful (Yamaguchi et al., 1986) as it provides the simplest qualitatively correct picture of electronic states. The general application of this technique is probably more feasible than multi-configuration methods (MCSCF). One method that appears promising for diatomic calculations is the two-dimensional, fully numerical Hartree-Fock method (Laaksonen et al., 1985) because this circumvents the problems encountered when using finite basis sets. This has only been developed for linear molecules but has been extended to a MCSCF method.

11.2.2 Mobility Calculations

The present work was (unintentionally) limited to studies of first row ions drifting in helium. The techniques developed could be applied to second row ions and non-helium buffer gases. It would be more difficult, but not impossible, to obtain interaction potentials for these systems of comparable accuracy to those determined for first row ions in helium. There have been very few mobility calculations for second row ions and non-helium buffer gases so this would naturally be a very fruitful area.

There are still many first row ion-helium systems for which mobility calculations have not been performed. Calculations have been started on the interaction potentials describing HeO^- which will lead to a calculation of the mobility of O^- in helium. Other systems, in this category, requiring study would be Li^-, B^-, He^-, N^-, C^+, C^-, Be^+, and Be^- ions in helium.

11.2.3 Mobility Measurements

The obvious experimental study inspired by this work is the measurement of the mobility of B^+ ions in helium. The experimental difficulties noted in Chapter 10 could be avoided by using ionising radiation from a radioactive source to form the B^+ ions. This would require redesigning the ion source in the drift tube mass spectrometer.

Acknowledgements

First and foremost I would like to thank my supervisors Dr P. W. Harland and Dr. R. G. A. R. Maclagan for their continual encouragement and interest throughout the course of this work and the University Grants Committee for providing financial assistance in the form of a postgraduate scholarship.

I am grateful to Dr H. O'Hara and Dr F. J. Smith, and Prof L. A. Viehland for supplying the programs ACQN and MOBDIF respectively. These programs were fundamental to the ion mobility calculations and I thank them for helping me in this way.

I would also like to thank Mr J. Harrison for assistance with the N^+ experimental work, Mr P. Sudkeaw for debugging the program MOBDIF, and Dr B. J. McIntosh for his efforts in organising the construction of the drift tube used in this study and for performing mobility measurements and accuracy assessments against which I could compare my own work.

The Chemistry Department technicians and the Computer Centre staff were also helpful. In particular I wish to thank Mr K. M. Gillard for modifying the drift tube, Mr D. MacDonald and Mr R. McGregor for glassblowing, and the late Mr G. Collins for maintaining the electronic equipment.

Finally, I would like to thank my parents Stanley and Shirley, and my friend Heather for their understanding, support and tolerance of me during this work, Derek for running or rock-climbing with me when I needed a break and David for being a source of inspiration.

References

Akridge, G. R., Ellis, H. W., Pai, R. Y., and McDaniel, E. W. (1975). *J. Chem. Phys.* **62**, 4578.

Anicich, V. G. and Huntress, W. T. (1986). *A Survey of Bimolecular Ion-Molecule Reactions for use in Modelling the Chemistry of Planetary Atmospheres, Cometary Comae, and Interstellar Clouds*, Jet Propulsion Laboratory Report.

Augustin, S. D., Miller, W. H., Pearson, P. K., and Shaefer, H. F. (1973). *J. Chem. Phys.* **58**, 2845.

Balint-Kurti, G. G. and Yardley, R. N. (1977). *Faraday Disc. Chem. Soc.* **62**, 77.

Barassin, J., Barassin, A., and Thomas, R. (1983). *Int. J. Mass Spec. Ion Phys.* **49**, 51.

Binkley, J. S., Whiteside, R. A., Raghavachari, K., Seeger, R., DeFrees, D. J., Schlegel, H. B., Frisch, M. J., Pople, J. A., and Kahn, L. R. (1982) *GAUSSIAN82*, Carnegie-Mellon University, Pittsburgh.

Bouma, W. J., McLeod, J. K., and Radom, L. (1978). *J. Chem. Soc., Chem. Comm.* 724.

Bouma, W. J., McLeod, J. K., and Radom, L. (1979). *J. Am. Chem. Soc.* **101**, 5540.

Cassidy, R. A. and Elford, M. T. (1985). *Aust. J. Phys.* **38**, 587.

Chapman, S. and Cowling, T. G. (1970). *The Mathematical Theory of Non-uniform Gases*, (3rd Ed.) Cambridge University Press, London.

Clark, T. (1985). *A Handbook of Computational Chemistry*, Wiley-Interscience, New York.

Conte, S. D. and de Boor, C (1980). *Elementary Numerical Analysis*, (3rd ed.) McGraw Hill, Tokyo.

Cooper, D. L. and Wilson, S. (1981). *Mol. Phys.* **44**, 161.

Cooper, D. L., Raimondi, M., and Gerratt J. (1985). *Mol. Phys.* **56**, 611.

Corderman, R. R., LeBreton, P. R., Butrill, S. E., Williamson, A. D., and Beauchamp, J. L. (1976). *J. Chem. Phys.* **65**, 4929.

Diercksen, G. H. F. and Sadlej, A. J. (1986). *Mol. Phys.* **59**, 889.

Dirac, P. A. M. (1929). *Proc. Roy. Soc. (London)* **123**, 714.

Dotan, I., Albritton, D. L., and Fehsenfeld, F. C. (1977). *J. Chem. Phys.* **66**, 2232.

Dotan, I., Fehsenfeld, F. C., and Albritton, D. L. (1979). *J. Chem. Phys.* **71**, 4762.

Ellis, H. W., McDaniel, E. W., Albritton, D. L., Viehland, L. A., Lin, S. L., and Mason E. (1978). *At. Data Nucl. Data Tables*. **22**, 179.

Ellis, H. W., Pai, R. Y., McDaniel, E. W., Mason, E. A., and Viehland L. A. (1976). *At. Data Nucl. Data Tables*. **17**, 177.

Ellis, H. W., Thackston, M. G., McDaniel, E. W., and Mason, E. A. (1984). *At. Data Nucl. Data Tables*. **31**, 113.

Fahey, D. W., Fehsenfeld, F. C., and Albritton, D. L. (1981). *J. Chem. Phys.* **74**, 2080.

Fehsenfeld, F. C., Albritton, D. L., Bush, Y. A., Fournier, P. G., Govers, T. R., and Fournier, J. (1974). *J. Chem. Phys.* **61**, 2150.

Ferguson, E. E., Fehsenfeld, F. C. and Albritton, D. L. (1971). Gas Phase Ion Chemistry **1**, 45.

Fhadil, H. A., Mathur, D., and Hasted, J. B. (1982). *J. Phys. B: At. Mol. Phys.* **15**, 1443.

Fhadil, H. A., Numan, A. T., Shuttleworth, T., and Hasted, J. B. (1985). *Int. J. Mas. Spec. Ion. Phys.* **65**, 307.

Franklin, J. L., Dillard, J. G., Rosenstock, H. M., Heron, T. J., and Draxl, K. (1969). *Natl. Stand. Ref. Data Ser. (U.S.)* **26**.

Gallup, G. A., Vance, R. L., Collins, J. R., and Norbeck, J. M. (1982). *Adv. Q.Chem.* **16**, 229.

Gatland, I. R. (1981). *Chem. Phys.* **75**, 4162.

Gatland, I. R., Morrison, W. F., Ellis, H. W., Thackston, M. G., McDaniel, E. W., Alexander, M. H., Viehland, L. A., and Mason, E. A. (1977a). *J. Chem. Phys.* **66**, 5121.

Gatland, I. R., Thackston, M. G., Pope, W. M., Eisele, F. L., Ellis, H. W., and McDaniel, E. W. (1978). *J. Chem. Phys.* **68**, 1775.

Gatland, I. R., Viehland, L. A., and Mason, E. A. (1977b). *J. Chem. Phys.* **66**, 537.

Gerratt, J. (1974). *Specialist Periodical Reports: Theoretical Chemistry*. Chemical Society, London. **1**, 60.

Hamdan, M. and Birkinshaw, K. (1986). *Int. J. Mass Spec. Ion Proc.* ***70***, 221.

Hariharan, P. C. and Staemmler, V. (1976). *Chem. Phys.* **15**, 409.

Harland, P. W. and McIntosh, B. J. (1983). *Int. J. Mass Spec. Ion Proc.* **54**, 217.

Harland, P. W. and McIntosh, B. J. (1984). *Int. J. Mass Spec. Ion Proc.* **57**, 283.

Harland, P. W. and McIntosh, B. J. (1985). *J. Chem. Soc. Faraday Trans. 2* **81**, 169.

Harrison, A. G., Finney, C. D., and Stark, J. A. (1971). *Org. Mass Spectrom.* **5**, 1313.

Hehre, W. J., Radom, l., Schleyer, P. v. R., and Pople, J. A. (1986). *Ab-Initio Molecular Orbital Theory*, Wiley-Interscience, New York.

Heimerl, J., Johnsen, R., and Bondi, M. A. (1969). *J. Chem. Phys.* **51**, 5041.

Heitler, H. and London, F. (1927). *Z. Phys.* **44**, 455.

Hirschfelder, J. O., Curtiss, D. F., and Bird, R. B. (1964). *Molecular Theory of Gases and Liquids*, (2nd ed.) Wiley, New York.

Holmes, J. L., Terlouw, J. K., and Lossing, F. P. (1976). *J. Phys. Chem.* **80**, 2860.

Hurley, A. C. (1960). *Rev. Mod. Phys.* **32**, 400.

Huxley, L. G. H., Compton, R. W., and Elford, M. T. (1966). *Bull. Instr. Phys. Physical Soc.* **17**, 251.

Huzinaga, S. and Arnau, C. (1970). *J. Chem. Phys.* **53**, 451.

Jans, R. and Maclagan, R. G. A. R. (1984). *Aust. J. Chem.* **37**, 2159.

Johnsen, R. and Biondi, M. A. (1980). *J. Chem. Phys.* **73**, 190.

Johnsen, R., Biondi, M. A., and Hayashi M. (1982). *J. Chem. Phys.* **77**, 2545.

Johnsen, R., Brown, H. L., and Biondi, M. A. (1970). *J. Chem. Phys.* **52**, 5080.

Kaneko, Y., Koizumi, T., and Kobayashi, N. (1978). *Mass Spec.* **26**, 35.

Kihara, T. (1953). *Rev. Mod. Phys.* **25**, 844.

Kirkpatrick, C. C. and Viehland, L. A. (1985). *Chem. Phys.* **98**, 221.

Koch, W. and Frenking, G. (1986). *J. Chem. Soc. Chem. Comm.* 1095.

Kosmider, R. G. and Hasted, J. B. (1975). *J. Phys. B: At. Mol. Phys.* **8**, 273.

Koutecky, J. and Bonacic, V. (1971). *J. Chem. Phys.* **55**, 2408.

Laaksonen, L., Sundholm, D., and Pyykkö, P. (1985). *Int. J. Q. Chem.* **27**, 601.

Lamm, D. R., Thackston, M. G., Eisele, F. L., Ellis, H. W., Twist, J. R., Pope, W. M., Gatland, I. R., and McDaniel, E. W. (1981). *J. Chem. Phys.* **74**, 3042.

Langevin, P. (1903). *Ann. Chim. Phys.* **2**, 289.

Langevin, P. (1905). *Ann. Chim. Phys.* **5**, 245. An English translation is given in App. II of McDaniel (1964).

Laudenslager, J. B., Huntress, W. T., and Bowers, M. T. (1974). *J. Chem. Phys.* **61**, 4600.

Levine, I. N. (1985). *Quantum Chemistry*, (3rd ed.) Allyn and Bacon, Boston.

Liebman, J. F. and Allen, L. C. (1970). *J. Am. Chem. Soc.* **92**, 3539.

Liebman, J. F. and Allen, L. C. (1971). *Int. J. Mass. Spec. Ion. Phys.* **7**, 27.

Lin ,S. L., Viehland, L. A., and Mason, E. A. (1979b). *Chem. Phys.* **37**, 411.

Lin, S. L. and Bardsley, J. N. (1977). *J. Chem. Phys.* **66**, 435.

Lin, S. L., Gatland, I. R. and Mason, E. A. (1979a). *J. Phys. B: At. Mol. Phys.* **12**, 4179.

Lin, S. N., Griffin, G. W., Horning, E. C., and Wentworth, W. E. (1974). *J. Chem. Phys.* **60**, 4994.

Lindinger, W. and Albritton, D. L. (1975). *J. Chem. Phys.* **62**, 3517.

Lindinger, W., Alge, E., Störi, H., Varney, R. N., Helm, H., Holzmann, P., and Pahl, M. (1979). *Int. J. Mass Spec. Ion. Phys.* **30**, 251.

Lischka, H. and Kohler, J. (1979). *Chem. Phys. Lett.* **63**, 326.

Maclagan, R. G. A. R. (1981). *Chem. Phys. Lett.* **82**, 501.

Maclagan, R. G. A. R. and Schnuelle, G. W. (1971). *J. Chem. Phys.* **55**, 5431.

MacNair, D. (1967). *Rev. Sci. Instrum.* **38**, 124.

Maitland, G. C., Mason, E. A., Viehland, L. A., and Wakeham, W. A., (1978). *Mol. Phys.* **36**, 797.

Mason, E. A. (1957). *J. Chem. Phys.* **27**, 75.

Mason, E. A. and Schamp, H. W. (1958). *Ann. Phys.* **4**, 233.

Mason, E. A., O'Hara, H., and Smith, F. J. (1972). *J. Phys. B: At. Mol. Phys.* **5**, 169.

McDaniel, E. W. (1964). *Collision Phenomena in Ionised Gases.*, Wiley, New York.

McDaniel, E. W. and Mason, E. A. (1973). *The Mobility and Diffusion of Ions in Gases*, Wiley, New York.

McDaniel, E. W. and Viehland, L. A. (1984). *Phys. Rep.* **110**, 333.

McFarland, M., Albritton, D. L., Fehsenfeld, F. C., Ferguson, E. E., and Schmeltekopf A. L. (1973). *J. Chem. Phys.* **59**, 6610.

McIntosh, B. J. (1984). *Ph. D. Thesis*, University of Canterbury, Christchurch, New Zealand.

Moore, C. (1971). *U.S. Dept. Comm., NBS Atomic Energy Levels* **45**.

Moseley, J. T., Gatland, I. R., Martin, D. W., and McDaniel, E. W. (1969). *Phys. Rev.* **178**, 234.

Møller, C. and Plesset, M. S. (1934). *Phys. Rev.* **46**, 618.

Neufeld, P. D. and Aziz, R. A. (1972). *Comp. Phys. Comm.* **33**, 269.

O'Hara, H. and Smith, F. J. (1970). *J. Comp. Phys.* **5**, 328.

O'Hara, H. and Smith, F. J. (1971). *Comp. Phys. Comm.* **2**, 47.

Ong, P. P. and Hasted, J. B. (1969). *J. Phys. B: At. Mol. Phys.* **2**, 91.

Oppenheimer, M., Constantinides, E. R., Kirby-Docken, K., Victor, G. A., and Dalgarno, A. (1977). *J. Geophys. Res.* **82**, 5485.

Parent, D. C. and Bowers, M. T. (1981). *Chem. Phys.* **60**, 257.

Patterson, P. L. (1972). *J. Chem. Phys.* **56**, 3943.

Pauling, L. (1960). *The Nature of the Chemical Bond*, (3rd ed.) Cornell University Press, New York.

Pople, J. A., Binkley, J. S., and Seeger, R. (1976). *Int. J. Q. Chem. Symp.* **10**, 1.

Press. W. H., Flannery, B. P., Teukolsky, S. A., and Vetterling. W. T. (1986). *Numerical Recipes*, Cambridge University Press, Cambridge.

Raimondi, M., Simonetta, M., and Tantardini, G. F. (1985). *Computer Phys. Rep.* **2**, 171.

Refeay, K. M. A. and Chupka, W. A. (1968). *J. Chem. Phys.* **48**, 5205.

Roos, B., Salez, C., Veillard, A., and Clementi, E. (1968). IBM *Research Laboratory*, San Jose.

Rosenstock, H. M., Draxl, K., Steiner, B. W., and Heron, T. J. (1977). *J. Phys. Chem. Ref. Data Suppl.* **1**, 6.

Rowe, B. R., Fahey, D. W., Fehsenfeld, F. C., and Albritton D. L. (1980). *J. Chem. Phys.* **73**, 194.

Russ. C., Barnhill III, M. V., and Woo, S. B. (1975). *J. Chem. Phys.* **62**, 4420.

Senff, U. E. and Burton, P. G. (1986). *Mol. Phys.* **58**, 637.

Skrezenek, F. L. and Harcourt, R. D. (1984). *J. Am. Chem. Soc.* **106**, 3934.

Smith, F. J. and Munn, R. J. (1964). *J. Chem. Phys.* **41**, 3560.

Snuggs, R. M., Voltz, D. J., Gatland, I. R., Schummers, J. H., Martin, D. W., and McDaniel, E. W., (1971). *Phys. Rev. A.* **3**, 487.

Staemmler, V., and Jaquet, R. (1985). *Chem. Phys.* **92**, 141.

Staley, R. H., Corderman, R. R., Foster, M. S., and Beauchamp, J. L. (1974). *J. Am. Chem. Soc.* **96**, 1260.

Stevens, R. M. (1971). *J. Chem. Phys.* **55**, 1725.

Takata, N. (1975). *J. Phys. B: At. Mol. Phys.* **8**, 2390.

Tatewaki, H., Tanaka, K., Ohno, Y., and Nakamura, T. (1984). *Mol. Phys.* **53**, 233.

Turner, A. G. (1974). *Methods in Molecular Orbital Theory*, Prentice-Hall, New Jersey.

Van de Sande, C. C. and McLafferty, F. W. (1975). *J. Am. Chem. Soc.* **97**, 4613.

Viehland, L. A. (1981). *Spec. Per. Rep.* **6**, 84.

Viehland, L. A. (1982). *Chem. Phys.* **70**, 149.

Viehland, L. A. (1983). *Chem. Phys.* **78**, 279.

Viehland, L. A. (1986). *Chem. Phys.* **101**, 1.

Viehland, L. A. and Lin, S. L. (1979). *Chem. Phys.* **43**, 135.

Viehland, L. A. and Mason, E. A. (1975). *Ann. Phys.* **91**, 499.

Viehland, L. A. and Mason, E. A. (1977). *J. Chem. Phys.* **66**, 422.

Viehland, L. A. and Mason, E. A. (1978). *Ann. Phys.* **110**, 287.

Viehland, L. A. and Mason, E. A. (1981). *Chem. Phys. Lett.* **83**, 298.

Viehland, L. A. and Mason, E. A. (1984). *J. Chem. Phys.* **80**, 416.

Viehland, L. A., Harrington, M. M., and Mason, E. A. (1976a). *Chem. Phys.* **17**, 433.

Viehland, L. A., Lin, S. L., and Mason, E. A. (1981b). *Chem. Phys.* **54**, 341.

Viehland, L. A., Mason, E. A., and Lin, S. L. (1981a). *Phys. Rev. A.* **24**, 3004.

Viehland, L. A., Mason, E. A., Morrison, W. F., and Flannery, M. R. (1975). *At. Dat. Nuc. Dat. Tab.* **16**, 495.

Viehland, L. A., Mason, E. A., Stevens, T. H., and Monchick, L. (1976b). *Chem. Phys. Lett.* **44**, 360.

Wang Chang, C. S., Uhlenbeck, G. E., and de Boer, J. (1964). *Studies in Statistical Mechanics*, (vol. 2) North Holland, Amsterdam.

Wannier, G. H. (1951). *Phys. Rev.* **83**, 281.

Wannier, G. H. (1952). *Phys. Rev.* **87**, 795.

Wannier, G. H. (1953). *Bell System Tech. J.* **32**, 170.

Whealton, J. H., Mason, E. A., and Vu, T. H. (1974). *Chem. Phys. Lett.* **28**, 125.

Williams, W. E. (1980). *Partial Differential Equations*, Oxford University Press, Oxford.

Yamaguchi, Y., Frisch, M. J., Lee, T. J., Schaefer, H. F., and Binkley, J. S. (1986). *Theo. Chim. Acta.* **69**, 337.

Publications Arising from this Work

Harland, P. W., McIntosh, B. J., Simpson, R. W., and Thomas, N. J. (1986). The effect of ion structure on gas-phase ion transport properties, *J. Chem. Soc., Farad. Trans. 2*, **82**, 2039.

Harland, P.W., Maclagan, R.G.A.R., and Simpson, R.W. (1987). *Ab-initio* calculation of the mobilities of ground state and electronically excited ions in the gas phase, *Proceedings of the 5th International Swarm Seminar*, Birmingham.

Harland, P.W., Maclagan, R.G.A.R., and Simpson, R.W. (1988). The dependence of zero-field ion-mobilities on the well depth, ε, and minimum position, r_m, in the ion-neutral interaction potential , *Aust. J. Phys.* (in press).

Maclagan, R. G. A. R. and Simpson, R. W. (1987). Valence-bond calculations on N_2 and isoelectronic species, *Int. J. Quant. Chem.*, **31**, 463.

Simpson, R. W., Maclagan, R. G. A. R., and Harland, P. W. (1987). *Ab-initio* calculation of the mobility of F^- in helium, *J. Phys. B: At. Mol. Phys.*, **20**, 2723.

Simpson, R.W., Maclagan, R.G.A.R., and Harland, P. W., (1987). Interaction potentials and mobility calculations for the HeO^+ system, *J. Chem. Phys.* (in press).

Appendix A

Definitions of Non-S.I. Units

Quantity	Name of Unit	Symbol for Unit	Definition
Dipole moment	Debye	D	3.33564×10^{-30} Cm
Distance	ångström	Å	10^{-10}m
E/N	Townsend	Td	10^{-21} Vm^2
Energy	atomic unit	hartree	4.35967×10^{-18} J
	electron volt	eV	1.602189×10^{-19} J
			96.486 kJmol^{-1}
Pressure	millibar	mbar	101.3 Pa
	torr	Torr	133.3 Pa

Physical Quantity Units

Quantity	Quantity Symbol	Common Units	S.I. Units
Diffusion Coefficient	D	cm^{2}s^{-1}	10^{-4} m^{2}s^{-1}
Mobility	K	cm^{2}V^{-1}s^{-1}	10^{-4} m^{2}V^{-1}s^{-1}
Rate constant	k	cm^{3}s^{-1}	1.66×10^{-18} m^{3}mol^{-1}s^{-1}
Gas number density	N	cm^{-3}	10^6 m^{-3}

Physical Constants

Quantity	Symbol	Value
Atomic mass unit	u	1.66057×10^{-27} kg
Avogadro constant	L	6.02205×10^{23} mol^{-1}
Bohr radius	a_0	0.529177×10^{-10} m
Boltzmann constant	k_B	1.38066×10^{-23} JK^{-1}
Charge of proton	q	1.60219×10^{-19} C
Gas number density	N_0	2.6872×10^{25} m^{-3}
Vacuum permittivity	ϵ_0	8.854188×10^{-12} J^{-1}C^{2}m^{-1}

Appendix B

Computer Program Listings

(i) Program TT.F77

The two-temperature theory program, TT.F77, calculates the reduced mobility of an ion in a buffer gas as a function of the parameter E/N at both the first and second approximation. It requires a tabulated interaction potential such as would be obtained from quantum mechanical calculations.

A modified version of the program ACQN (O'Hara and Smith, 1970, 1971) is used to calculate the collision integrals required; that is, a set of $(T^*,\Omega^{(l,s)}(T^*))$ values. Below are listings of the routines which deal with the interaction potential; converting the discrete values into a continuous function, and with the final phase of the calculation; performing the two-temperature theory calculation. These routines are interfaced with ACQN to give a single program, TT.F77.

The subroutine VRFIT reads in a tabulated interaction potential containing and, as described in Chapter 4, fits a cubic spline through them by calling subroutine CSFIT. Extrapolating functions are then fitted to match two points at each end of the spline. The interaction potential can have the distance in atomic units (bohr) or in angstroms (Å), and the energy in atomic units (hartree) or electron volts (eV), and also can tend too some limiting value other than zero if required. This flexibility allows interaction potentials taken from the literature to be typed directly into the input file. The cubic spline and extrapolating function details are stored in a COMMON block where they can be accessed by other subprograms.

```
      SUBROUTINE VRFIT(V,T,S,W,N)
C     fits a cubic spline to a tabulated interaction potential
      IMPLICIT REAL*8 (A-H,O-Z), INTEGER*4 (I-N)
      REAL*8 V(N),T(N),S(N,N),W(N+1,N+1),X(60),Y(60),CS(60,6),NL,NH
      REAL*8 MIN,MAX,M1,M2
      INTEGER*4 M
      COMMON/FLAGS/IFLAG(10)
```

```
      COMMON/POT/CS,MIN,MAX,AL,BL,NL,AH,BH,NH,M
      COMMON/IO/IIN,IOUT
      COMMON/SCALE/VRM,VEP
1     FORMAT ('FLAGS',12X,' ._________1_________________0________.'
     #       /'distance',I7,'    |       r in bohr       | r in Angstroms |'
     #       /'energy',I9,'    | energy in hartrees |  energy in eV  |'
     #       /'asymptote',I5,'    |   read E(r=rinf)    |   E(r=inf)=0   |'
     #       /'temperature',I4,'    |   generate Teff     |  read all Teff |'
     #       /'interpolation',I2,'    |  x(2) --> x(n-1)    |  x(1) --> x(n)'
     #       ,' |'/15X,'   ''-------------------------------------'''')
2     FORMAT (3D20.9)
3     FORMAT (/I3,'pts',6X,'r /A',10X,'V(r) /eV')
4     FORMAT (2F15.8)
6     FORMAT (2F15.8,4D20.9)
7     FORMAT (/3X,2F15.8,' low and high inverse powers')
8     FORMAT (/3X,2F15.8,' scale factors Rmin and epsilon')
9     FORMAT (I3,2F15.8)
10    FORMAT (/'DETERMINE CUBIC SPLINE'/)
11    FORMAT (/'COLLISION INTEGRAL AND MOBILITY CALCULATION')
12    FORMAT ('not possible to fit top section')
      WRITE (8,1) (IFLAG(I),I=1,5)
      READ (IIN,4) (X(I),Y(I),I=1,N)
      M1=1.
      M2=1.
      YINF=0.
      IF (IFLAG(1).EQ.1) M1=0.529177
      IF (IFLAG(2).EQ.1) M2=27.2107
      IF (IFLAG(3).EQ.1) READ (IIN,4) YINF
      READ (IIN,4) NL,NH,VRM,VEP
      RMV=1./VRM
      EPV=1./VEP
      DO 13 I=1,N
         X(I)=X(I)*RMV*M1
         Y(I)=(Y(I)-YINF)*EPV*M2
13    CONTINUE
      WRITE (8,3)N
      WRITE (8,9)(I,X(I),Y(I),I=1,N)
      WRITE (8,7)NL,NH
      WRITE (8,8)VRM,VEP
      M=N-1
      CALL CSFIT(X,Y,CS,V,T,S,W,N)
      SL=CS(1,5)
      DX=X(N)-X(M)
      SU=3.*CS(M,3)*DX*DX+2.*CS(M,4)*DX+CS(M,5)
      AL=-SL*(X(1)**(NL+1.))/NL
      BL=Y(1)-(AL/(X(1)**NL))
      IF ((DABS(Y(N))-DABS(Y(N-1))).GE.0.) THEN
      WRITE (8,12)
      CALL CPU
      END IF
      YK=(Y(N)/Y(N-1))**(1./NH)
      AH=(YK*X(N)-X(N-1))/(YK-1.)
      BH=0.5*(Y(N)*((X(N)-AH)**NH)+Y(N-1)*((X(N-1)-AH)**NH))
      MIN=CS(1,1)
      MAX=CS(M,2)
      IF (IFLAG(5).EQ.1) THEN
      MIN=CS(2,1)
      MAX=CS(M-1,2)
      END IF
      WRITE (8,10)
      WRITE (8,6)((CS(I,J),J=1,6),I=1,M)
      WRITE (8,2)AL,BL,NL
      WRITE (8,2)AH,BH,NH
      CALL VRTEST
      WRITE (8,11)
      RETURN
```

```
      END
```

The routine VRTEST steps through each sub-interval spanned by the cubic spline and checks for the presence of any critical points and notes any axis crossing. The information obtained is used to identify oscillations in the cubic spline which may upset the integral calculations, and is also useful as it provides estimates for $V(r=\sigma) = 0$ and $V(r=r_m) = \varepsilon$

```
      SUBROUTINE VRTEST
C     tests cubic spline to find local critical points in each sub-interval
      IMPLICIT REAL*8 (A-H,O-Z), INTEGER*4 (I-N)
      REAL*8 CS(60,6),NL,NH,MIN,MAX
      INTEGER*4 M
      COMMON/POT/CS,MIN,MAX,AL,BL,NL,AH,BH,NH,M
      COMMON/SCALE/VRM,VEP
 1    FORMAT(/41X,'x',11X,'y',11X,'y'''',10X,'y"')
 2    FORMAT ('local  minimum  in sub-interval ',I2,'  at',4F12.7)
 3    FORMAT ('local  maximum  in sub-interval ',I2,'  at',4F12.7)
 4    FORMAT ('inflexion point in sub-interval ',I2,'  at',4F12.7)
 5    FORMAT ('potential = 0  in  sub-interval ',I2,'  at',4F12.7)
      EPS=1.D-6
      WRITE (8,1)
      DO 6 I=1,M
         X1=CS(I,1)
         X2=CS(I,2)
         U=X2-X1
         A=CS(I,3)
         B=CS(I,4)
         C=CS(I,5)
         D=CS(I,6)
         Y1=D
         Y2=((A*U+B)*U+C)*U+D
C check for y=0
         IF (Y1*Y2.LE.0.) THEN
 7          X3=(X1+X2)*0.5
            X=X3-CS(I,1) Y3=((A*X+B)*X+C)*X+D
            IF ((DABS(X3-X2).LT.EPS).AND.(DABS(Y3).LT.EPS)) THEN
               D1=(3.*A*X+2.*B)*X+C
               D2=6.*A*X+2.*B
               WRITE (8,5) I,X3,Y3,D1,D2
            ELSE
               IF (Y3*Y2.LT.0.) THEN
                  Y1=Y3
                  X1=X3
               ELSE
                  Y2=Y3
                  X2=X3
               END IF
               GO TO 7
            END IF
            X1=CS(I,1)
            X2=CS(I,2)
         END IF
         E=4.*B*B-12.*A*C
C y'=0
         IF (E.GE.0.) THEN
            R1=X1+(-2.*B+DSQRT(E))/(6.*A)
            R2=X1+(-2.*B-DSQRT(E))/(6.*A)
            F1=6.*A*(R1-X1)+2.*B
```

```
            F2=6.*A*(R2-X1)+2.*B
            IF ((R1.GE.X1).AND.(R1.LE.X2)) THEN
               X=R1-X1
               Y1=((A*X+B)*X+C)*X+D
               D1=(3.*A*X+2.*B)*X+C
               D2=6.*A*X+2.*B
               IF (F1.GT.0.) WRITE (8,2) I,R1,Y1,D1,D2
               IF (F1.LT.0.) WRITE (8,3) I,R1,Y1,D1,D2
            END IF
            IF ((R2.GE.X1).AND.(R2.LE.X2)) THEN
               X=R2-X1
               Y2=((A*X+B)*X+C)*X+D
               D1=(3.*A*X+2.*B)*X+C
               D2=6.*A*X+2.*B
               IF (F2.GT.0.) WRITE (8,2) I,R2,Y2,D1,D2
               IF (F2.LT.0.) WRITE (8,3) I,R2,Y2,D1,D2
            END IF
         END IF
C y"=0
         R3=X1-B/(3.*A)
         IF ((R3.GE.X1).AND.(R3.LE.X2)) THEN
            X=R3-X1
            Y3=((A*X+B)*X+C)*X+D
            D1=(3.*A*X+2.*B)*X+C
            D2=6.*A*X+2.*B
            WRITE (8,4) I,R3,Y3,D1,D2
         END IF
 6    CONTINUE
      RETURN
      END
```

The function VF uses the interpolating function found in VRFIT to find the interaction energy, V, at internuclear separation r.

```
      DOUBLE PRECISION FUNCTION VF(R)
      IMPLICIT REAL*8 (A-H,O-Z), INTEGER*4 (I-N)
      REAL*8 CS(60,6),MIN,MAX,AL,BL,NL,AH,BH,NH,R1,X1
      INTEGER*4 M,I
      COMMON/POT/CS,MIN,MAX,AL,BL,NL,AH,BH,NH,M
      R1=R
      IF (R1.LT.MIN) VF=AL*(R1**(-NL))+BL
      IF (R1.GT.MAX) VF=BH*((R1-AH)**(-NH))
      IF ((R1.GE.MIN).AND.(R1.LE.MAX)) THEN
      DO 1 I=1,M
         IF ((CS(I,1).LE.R1).AND.(CS(I,2).GE.R1)) GO TO 2
 1    CONTINUE
      PRINT *,'ERROR IN VF'
      CALL1+CS(I,5))*X1+CS(I,6)
      END IF
      RETURN
      END
```

The function VD uses the interpolating function found in VRFIT to find the first derivative of the interaction energy, $\frac{dV}{dr}$, at nuclear separation r.

```
      DOUBLE PRECISION FUNCTION VD(R)
      IMPLICIT REAL*8 (A-H,L,BL,NL,AH,BH,NH,M
      R1=R
      IF (R1.LT.MIN) VD=-NL*AL*(R1**(-NL-1))+BL
      IF (R1.GT.MAX) VD=-NH*BH*((R1-AH)**(-NH-1))
      IF ((R1.GE.MIN).AND.(R1.LE.MAX)) THEN
      DO 1 I=1,M
         IF ((CS(I,1).LE.R1).AND.(CS(I,2).GE.R1)) GO TO 2
1     CONTINUE
      PRINT *,'ERROR IN VD'
      CALL EXIT
2     X1=R1-CS(I,1)
      VD=(3.*CS(I,3)*X1+2.*CS(I,4))*X1+CS(I,5)
      END IF
      RETURN
      END
```

This subroutine, CSFIT, fits a cubic spline through $\{(x_i,y_i), i=1,n\}$ and returns full spline information in array CS. The end point behaviour of the spline is set so that the second derivatives at x_1 and x_n are linear extrapolations of the second derivatives at x_3 and x_2, and at x_{n-2} and x_{n-1} respectively.

```
      SUBROUTINE CSFIT(X,Y,CS,V,T,S,W,N)
C     GENERAL NATURAL CUBIC SPLINE FITTING
C     X and Y contain coordinates to be fitted
C     CS is returned with the spline parameters
C     array dimensions are U(N-1),V(N),T(N),S(N,N),W(N+1,N+1)
      IMPLICIT REAL*8 (A-H,O-Z), INTEGER*4 (I-N)
      REAL*8 X(60),Y(60),U(60),V(N),T(N),S(N,N),W(N+1,N+1),CS(60,6)
      INTEGER*2 NI,NP,IERR
      COMMON/IO/IIN,IOUT
      NP=N+1
      NI=N
      M=N-1
      DO 12 I=1,M
         U(I)=X(I+1)-X(I)
12    CONTINUE
      DO 11 I=1,N
      DO 11 J=1,N
11    S(I,J)=0.0
      DO 2 I=2,M
         S(I,I-1)=U(I-1)
         S(I,I)=2.0*(U(I-1)+U(I))
         S(I,I+1)=U(I)
         V(I)=((Y(I+1)-Y(I))/U(I))-((Y(I)-Y(I-1))/U(I-1))
         V(I)=V(I)*6.0
2     CONTINUE
      S(1,1)=U(2)
      S(1,2)=-U(1)-U(2)
      S(1,3)=U(1)
      S(N,N-2)=U(M)
      S(N,M)=-U(M)-U(N-2)
      S(N,N)=U(N-2)
      V(1)=0.0
      V(N)=0.0
```

```
      CALL DLINEQ(T,V,S,W,NI,NP,IERR)
      IF (IERR.NE.0) THEN
         WRITE (6,4) IERR
 4       FORMAT ('crashed in DLINEQ',I9)
         CALL CPU
      END IF
      DO 13 I=1,M
         CS(I,1)=X(I)
         CS(I,2)=X(I+1)
         CS(I,3)=(T(I+1)-T(I))/6.0/U(I)
         CS(I,4)=T(I)*0.5
         CS(I,5)=(Y(I+1)-Y(I))/U(I)-(2.0*U(I)*T(I)+U(I)*T(I+1))/6.0
         CS(I,6)=Y(I)
 13   CONTINUE
      RETURN
      END
```

The cubic spline interpolation routine, CSEVAL, is used to get a set of interpolated values from a cubic spline. Using this routine the spline interpolation of calculated reduced mobility, K_0, verses E/N can be compared with experimental reduced mobilities measured at various E/N values.

```
      SUBROUTINE CSEVAL(CS,M,EN,N,YY)
C     SPLINE INTERPOLATION ROUTINE
C     for spline parameters stored in CS(M,6)
C     we interpolate to find the y-values corresponding to x-values
C     stored in EN(N). Results returned in YY(N)
      IMPLICIT REAL*8 (A-H,O-Z), INTEGER*4 (I-N)
      REAL*8 CS(60,6),MIN,MAX,EN(60),YY(60)
      INTEGER*4 M,N
      MIN=CS(1,1)
      MAX=CS(M,2)
      DO 2 K=1,N
         R=EN(K)
         IF ((R.LT.MIN).OR.(R.GT.MAX)) THEN
            Y=0.
         ELSE
            DO 1 I=1,M
               IF ((CS(I,1).LE.R).AND.(CS(I,2).GE.R)) J=I
 1          CONTINUE
            X1=R-CS(J,1)
            Y=((CS(J,3)*X1+CS(J,4))*X1+CS(J,5))*X1+CS(J,6)
         END IF
         YY(K)=Y
 2    CONTINUE
      RETURN
      END
```

Subroutine ALBET calculates both the first and second approximations of the two temperature theory. The reduced collision integrals and corresponding reduced temperatures required are passed from the O'Hara-Smith collision integral calculation program via a COMMON

block. The information printed after the calculation includes, for each effective temperature, T_{eff}; the the collision integral $\Omega^{(1,1)}(T_{eff})$ and collision integral ratios A^*, B^* and C^*; the correction terms α and β; and the E/N value, drift velocity, v_d and reduced mobility, K_0, for both approximations. Also determined, if required, are a set of reduced mobilities at a specific set of E/N values.

```
      SUBROUTINE ALBET(V,T,S,W,N)
C     first and second approximation two-temperature theory calculation
C     of K0 and Vd as a function of E/N
      IMPLICIT REAL*8 (A-H,O-Z), INTEGER*4 (I-N)
      REAL*8 V(N),T(N),S(N,N),W(N+1,N+1)
      REAL*8 TEFF(60),OM(60),A(60),B(60),C(60),TRED(60)
      REAL*8 EN1(60),EN2(60),VD1(60),VD2(60),CS(60,6),EN(60)
      REAL*8 ALPHA(60),BETA(60),K01(60),K02(60),YV1(60),YK1(60),YV2(60)
      REAL*8 YK2(60),EXK(60),OM2(60),MION,MNEUT,M1,K1,K6,K9,K10,KEV,KJ
      COMMON/AB/TRED,OM,A,B,C
      COMMON/IO/IIN,IOUT
      COMMON/SCALE/RM,EP
 1    FORMAT (8F15.6)
 2    FORMAT (/'INTERPOLATED MOBILITY'//
      15X,'      first approx.      second approx.'//
      25X,'E/N      K0      VD      K0      VD'/
      3(F10.3,2(F12.6,F12.4)))
 3    FORMAT (2F15.0)
 4    FORMAT (I3)
 6    FORMAT (//'interpolated values'//26X,'first approx.',19X,
     #'second approx.'//5X,'E/N      K0(expt)    K0(calc)   dK0 %',
     #'    Vd(calc)    K0(calc)   dK0 %    Vd(calc)')
 7    FORMAT(F10.3,F12.6,2(F12.6,F8.2,F12.4))
 5    FORMAT (/6X,'Teff (K)',8X,'om(1,1)',8X,'T*',12X,'om(1,1)*'
     #      ,8X,'A*',13X,'B*',13X,'C*'//(F11.2,4X,6F15.8/
     #      F11.2,4X,6F15.8/F11.2,4X,6F15.8/F11.2,4X,F15./
     #      F11.2,X,6F15.8/))
 10   FORMAT (/22X,'first approx.',61X,'second approx.'//6X,'E/N (Td)'
     #      ,7X,'VD (m/s)',7X,'K0 (cm2/Vs)',6X,'alpha',10X,'beta',9X,
     #      'E/N (Td)',7X,'VD (m/s)',7X,'K0 (cm2/Vs))'//
     #      (8F15.6/8F15.6/8F15.6/8F15.6/8F15.6/))
 9    FORMAT (/'mass of ion      ',F10.3,' amu,  mass neutral ',F10.3,
     #      ' amu,  experimental temperature ',F10.3,' K')
      READ (IIN,1) TEXP,MION,MNEUT
      PI=3.141592653589793
      PR2=PI*RM*RM
      KEV=8.617335D-5
      KJ=1.38066D-23
      M1=1.66057D-27
      MN2=MNEUT**2
      MI2=MION**2
      MTM=MION*MNEUT
      MPM=MION+MNEUT
      MMM=MION-MNEUT
      K1=3.*KJ/MNEUT/M1
      K6=DSQRT(MION*MNEUT/(MION+MNEUT))*2.01079D-5
      K9=0.37221
      K10=EP/KEV
      NP=N+1
      NI=N
      N1=N-1
      DO 19,I=1,N
         TEFF(I)=K10*TRED(I)
```

```
          OM2(I)=PR2*OM(I)
          VD1(I)=DSQRT(K1*(TEFF(I)-TEXP))
          EN1(I)=OM2(I)*VD1(I)*DSQRT(TEFF(I))*K6
          K01(I)=VD1(I)*K9/EN1(I)
          DYDX=(6.*C(I)-5.)*(TEXP-TEFF(I))/TEFF(I)
          DYDX=DYDX/(1.-DYDX)
          BETA(I)=(MTM*(5.-2.*A(I))/(5.*(MI2+MN2)+4.*MTM*A(I))*DYDX)
          ALPHA(I)=MION*MPM*(10.*MPM/(5.*MION+3.*MNEUT*A(I))-(5.*MMM+
     #    4.*MNEUT*A(I))/MPM)*DYDX/(5.*(3.*MI2+MN2)+8.*MTM*A(I))
          VD2(I)=DSQRT(K1*(TEFF(I)-TEXP)/(1.+BETA(I)))
          EN2(I)=OM2(I)*VD2(I)*DSQRT(TEFF(I))*K6/(1.+ALPHA(I))
          K02(I)=VD2(I)*K9/EN2(I)
 19    CONTINUE
C       print out results
       WRITE (8,5) (TEFF(I),OM2(I),TRED(I),OM(I),A(I),B(I),C(I),I=1,N)
       WRITE (8,10) (EN1(I),VD1(I),K01(I),ALPHA(I),BETA(I),
     #       EN2(I),VD2(I),K02(I),I=1,N)
       WRITE (8,9) MION,MNEUT,TEXP
C      interpolate to get results at experimental E/N's
       READ (IIN,4)NE
       IF (NE.NE.0) THEN
          READ (IIN,3)(EN(I),EXK(I),I=1,NE)
          CALL CSFIT(EN2,VD2,CS,V,T,S,W,N)
          CALL CSEVAL(CS,N1,EN,NE,YV2)
          CALL CSFIT(EN2,K02,CS,V,T,S,W,N)
          CALL CSEVAL(CS,N1,EN,NE,YK2)
          CALL CSFIT(EN1,VD1,CS,V,T,S,W,N)
          CALL CSEVAL(CS,N1,EN,NE,YV1)
          CALL CSFIT(EN1,K01,CS,V,T,S,W,N)
          CALL CSEVAL(CS,N1,EN,NE,YK1)
          IF (EXK(1).EQ.0.) THEN
             WRITE (8,2)(EN(I),YK1(I),YV1(I),YK2(I),YV2(I),I=1,NE)
          ELSE
             WRITE (8,6)
             DO 11 I=1,NE
                DK1=100.*(YK1(I)-EXK(I))/EXK(I)
                DK2=100.*(YK2(I)-EXK(I))/EXK(I)
                WRITE (8,7) EN(I),EXK(I),YK1(I),
     #             DK1,YV1(I),YK2(I),DK2,YV2(I)
 11          CONTINUE
          END IF
       END IF
       RETURN
       END
```

(ii) Program ATD.F77

This program will calculate an arrival time distribution for a primary or secondary ion drifting in a buffer gas at experimental conditions and compare it with the actual arrival time distribution found by experiment. If the agreement is good then the values found for the mobility and rate constants required for the fitting procedure should be accurate. Comments are either prefixed by a 'c' in column 1 or '/*' anywhere on a line.

```
      PROGRAM ATD
C     Calculating and fitting an Arrival Time Distribution (ATD) to
C     experimental data.  The input required is read from ATD.INPUT
C     and is of the form
C
C     1                     number of calculations to be performed
C     ATD.131087.1          name of experimental data file
C     4.,4.,14.             mass of buffer, primary and secondary ions
C     8.0,21.0              primary and secondary ion reduced mobilities
C     1.6D-9,2              rate of loss of the primary ion and
C     1.D-13,2              loss of the secondary ion with reaction order
C     .01,T                 proportion of reactant and secondary ion flag.
C
C     The relevant experimental data is found in file ATD.DATA which is
C     similar to the following:
C
C     ATD.131087.1                      name ATD.<DDMMYY>.<run number>
C     3.67                              drift distance
C     19.39                             maximum in arrival time distribution
C     6.39285124                        electric field in V/cm
C     .2                                pressure in Torr
C     302.15                            temperature in K
C     6                                 start time in clock cycles
C     30                                finish time in clock cycles
C     1                                 increment
C     HE+  13/10/87    09-27 am         heading
C     23                                6 cc ion signal
C     71                                7
C     146                               8
C     537                               9
C     783                               10
C     .                                 .
C     .                                 .
C     687                               25
C     436                               26
C     257                               27
C     140                               28
C     62                                29
C     25                                30 cc ion signal
C
C     The output is written to file ATD.OUTPUT.
C     Routines SMOOFT,REALFT,FOUR1,QSIMP and TRAPZD are taken from
C     'Numerical Recipes' (Press et al., 1986)
C
      IMPLICIT REAL*8 (A-H,O-Z), INTEGER*4 (I-N)
      CHARACTER*13 NAME
C
```

```
      REAL*8 DIST,SIGM,E,EN,PRES,TEMP              /* input
      INTEGER*4 TI,TF,STEP,ISIG(100),NUM
      COMMON /D/ DIST,SIGM,E,EN,PRES,TEMP,TI,TF,STEP,ISIG,NUM
C
      REAL*8 MA,K0A,D0A,DTA,DLA,VDA,KA,AA          /* primary ion
      COMMON /A/ MA,K0A,D0A,DTA,DLA,VDA,KA,AA
C
      REAL*8 MB,K0B,D0B,DTB,DLB,VDB,KB,AB          /* secondary ion
      COMMON /B/ MB,K0B,D0B,DTB,DLB,VDB,KB,AB
C
      REAL*8 MBUF,KLOSA,KLOSB,CLOCK,TIME(100),SIG(100),CSIG(100),IB,IA
      INTEGER*4 NCALC,OLOSA,OLOSB
      LOGICAL SEC
C
      OPEN (5,FILE='ATD.INPUT',STATUS='OLD')              /* input file
      OPEN (6,FILE='ATD.OUTPUT',STATUS='UNKNOWN')         /* output file
      CLOCK=0.97752D-6                                    /* clock speed (s)
      READ (5,*) NCALC                                    /* number of calcs
C
      DO 11 I=1,NCALC
         WRITE (6,14) I                                /* header
 14      FORMAT ('-----------------------------------------------'/
     #           'CALCULATION   #',I2/'================')
         READ (5,5) NAME                               /* get exptl file name
 5       FORMAT (A13)
         CALL INPUT(NAME)                              /* get exptl details
         DENS=3.535D16*(273.15/TEMP)*PRES
         READ (5,*) MBUF,MA,MB,K0A,K0B,KLOSA,OLOSA,
     #               KLOSB,OLOSB,PROP,SEC
 25      CONTINUE
         WRITE (*,5) NAME
         WRITE (6,12)
 12      FORMAT(/19X,'mass   K0 cm2/Vs   K  cm2/Vs   vd   cm/s  ',
     #                    ' D0  cm2/s   DL  cm2/s   DT  cm2/s  ')
C                                                     /* primary ion
         AA=KLOSA*PROP*(DENS**(OLOSA-1))              /* coll. freq. A --> B
         K0A=K0A*1.D-4                                /* cm2/Vs --> m2/Vs
         KA=K0A*(TEMP/273.15)*(760./PRES)             /* unreduced mobility
         VDA=KA*E                                     /* drift velocity (m/s)
         CALL DIFF(KA,E,MA,MBUF,TEMP,D0A,DLA,DTA)     /* diff coeffs
         NAME='primary ion  '
         WRITE (6,7) NAME,MA,K0A*1.D4,KA*1.D4,VDA*1.D2,
     #               D0A*1.D4,DLA*1.D4,DTA*1.D4
C
         IF (SEC) THEN                                /* secondary ion
            AB=KLOSB*PROP*(DENS**(OLOSB-1))
            K0B=K0B*1.D-4
            KB=K0B*(TEMP/273.15)*(760./PRES)
            VDB=KB*E
            CALL DIFF(KB,E,MB,MBUF,TEMP,D0B,DLB,DTB)
            NAME='secondary ion'
            WRITE (6,7) NAME,MB,K0B*1.D4,KB*1.D4,VDB*1.D2,
     #                  D0B*1.D4,DLB*1.D4,DTB*1.D4
         END IF
C
         NAME='buffer       '
         WRITE (6,7) NAME,MBUF
 7       FORMAT (A13,'  : ',F6.2,6D12.3)
         WRITE (6,9) PROP*100.
 9       FORMAT (/'reactant       : ',F4.1,' %')
         WRITE (6,13)
 13      FORMAT (/18X,'rate const         coll. freq')
         IF (SEC) THEN
            NAME='pri. --> sec.'
            WRITE (6,8) NAME,KLOSA,3*OLOSA-3,AA
            NAME='sec. -->  ?  '
```

```
            WRITE (6,8) NAME,KLOSB,3*OLOSB-3,AB
         ELSE
            NAME='pri. -->  ?  '
            WRITE (6,8) NAME,KLOSA,3*OLOSA-3,AA
         END IF
 8       FORMAT (A13,'  : ',D10.3,' cm',I1,'/s   ',D10.3,' /s')
C
         DO 1 J=1,NUM
            SIG(J)=DBLE(ISIG(J))                          /* real counts
            TIME(J)=(DBLE(TI)+DBLE(STEP*(J-1)))*CLOCK     /* actual time (s)
            TIME(NUM)=(DBLE(TI)+DBLE(STEP*(NUM-1)))*CLOCK  /* actual time
(s)
            IF (SEC) THEN
               CSIG(J)=IB(TIME(J))                     /* calculated signal
            ELSE
               CSIG(J)=IA(TIME(J))                     /* calculated signal
            END IF
 1       CONTINUE
C
         CALL SMOOFT(SIG,NUM,2.)                       /* smooth exptl signal
         CALL MAXMIN(SIG,NUM,XMAX,YMAX,YMIN)           /* exp. max and min
         CALL MAXMIN(CSIG,NUM,CXMAX,CYMAX,CYMIN)       /* calc max and min
         XMAX=(XMAX+DBLE(TI-1))*CLOCK                  /* true max time
         CXMAX=(CXMAX+DBLE(TI-1))*CLOCK
         TDIFF=XMAX-CXMAX                              /* difference in tmax
C
         DO 3 J=1,NUM
            IF (SEC) THEN
               CSIG(J)=IB(TIME(J)-TDIFF)               /* shifted calculation
            ELSE
               CSIG(J)=IA(TIME(J)-TDIFF)               /* shifted calculation
            END IF
 3       CONTINUE
         CALL MAXMIN(CSIG,NUM,CXMAX,CYMAX,CYMIN)       /* calc max and min
C
         DO 6 J=1,NUM
            SIG(J)=(SIG(J)-YMIN)/(YMAX-YMIN)*100.      /* scaled expt.
            CSIG(J)=(CSIG(J)-CYMIN)/(CYMAX-CYMIN)*100.  /* scaled calc.
 6       CONTINUE
C
         WRITE (6,2) (TI+STEP*(J-1),TIME(J)*1.D6,ISIG(J),
     #               SIG(J),CSIG(J),SIG(J)-CSIG(J),J=1,NUM)
 2       FORMAT(/' time     usec  signal    scaled     calc.     diff.'
     #         /(   I5 ,    F9.2 ,  I8 ,    F10.2 ,    F10.2 ,  F10.3))
         WRITE (6,4) XMAX*1.D6,TDIFF*1.D6
 4       FORMAT (/'maximum after',F6.2,'  usec'
     #           /'calculation shifted by',F6.2,'  usec')
C
       WRITE (*,26)
 26    FORMAT (/'new KLOSA,K0B')
       READ (*,*) KLOSA,K0B
       IF (KLOSA.LT.0.) THEN
          GO TO 11
       ELSE
          WRITE (6,27)
          WRITE (*,27)
 27       FORMAT('- - - - - - - - - - - - - - - - - - - - - - - -')
          K0A=K0A*1.D4
          GO TO 25
       END IF
 11    CONTINUE
       CLOSE (5,STATUS='KEEP')
       CLOSE (6,STATUS='KEEP')
       STOP
       END
```

```
      DOUBLE PRECISION FUNCTION IB(T)
C     calculate the secondary ion flux through an axial aperture
C     produced by reaction from primary ions during drift tube transit
      IMPLICIT REAL*8 (A-H,O-Z), INTEGER*4 (I-N)
      REAL*8 TIME,VAL
      EXTERNAL BI                                   /* integrand function
      COMMON /C/ TIME
      TIME=T
      CALL QSIMP(BI,0.,TIME,VAL)                    /* Simpson's integration
      IB=VAL
      RETURN
      END

      DOUBLE PRECISION FUNCTION BI(U)               /* integrand function
      IMPLICIT REAL*8 (A-H,O-Z), INTEGER*4 (I-N)
C
      REAL*8 Z,SIGM,E,EN,PRES,TEMP                  /* input
      INTEGER*4 TI,TF,STEP,ISIG(100),NUM
      COMMON /D/ Z,SIGM,E,EN,PRES,TEMP,TI,TF,STEP,ISIG,NUM
C
      REAL*8 MA,K0A,D0A,DTA,DLA,VDA,KA,AA           /* primary ion
      COMMON /A/ MA,K0A,D0A,DTA,DLA,VDA,KA,AA
C
      REAL*8 MB,K0B,D0B,DTB,DLB,VDB,KB,AB           /* secondary ion
      COMMON /B/ MB,K0B,D0B,DTB,DLB,VDB,KB,AB
C
      REAL*8 U,T,A,B,C,D,PI,R0,ZMC
      COMMON /C/ T
C
      R0=2.D-3                                      /* radius of source ap.
      PI=3.141592653589793
      A=4.*DTA*T-4.*(DTA-DTB)*U
      B=4.*DLA*T-4.*(DLA-DLB)*U
      C=VDA*T-(VDA-VDB)*U
      D=AA*T-(AA-AB)*U
      ZMC=Z-C
      BI = 1./DSQRT(PI*B) * (2.*DLB*ZMC/B+VDB)
     #     * DEXP(-D-ZMC*ZMC/B) * (1.-DEXP(-R0*R0/A))
      RETURN
      END

      DOUBLE PRECISION FUNCTION IA(T)               /* primary ion flux
      IMPLICIT REAL*8 (A-H,O-Z), INTEGER*4 (I-N)
C
      REAL*8 Z,SIGM,E,EN,PRES,TEMP                  /* input
      INTEGER*4 TI,TF,STEP,ISIG(100),NUM
      COMMON /D/ Z,SIGM,E,EN,PRES,TEMP,TI,TF,STEP,ISIG,NUM
C
      REAL*8 MA,K0A,D0A,DTA,DLA,VDA,KA,AA           /* primary ion
      COMMON /A/ MA,K0A,D0A,DTA,DLA,VDA,KA,AA
C
      REAL*8 T,PI,R0
C
      R0=2.D-3                                      /* radius of source ap.
      PI=3.141592653589793
      IA = 0.25/DSQRT(PI*DLA*T) * (VDA+Z/T)
     #   * DEXP(-AA*T-((Z-VDA*T)**2)/(4.*DLA*T))
     #   * (1.-DEXP(-R0*R0/(4.*DTA)))
      RETURN
      END

      SUBROUTINE DIFF(K,E,MI,MN,T,D0,DL,DT)
C     This routine calculates the diffusion coefficient D0 from the
C     Einstein equation and then estimates the longitudinal and
C     transverse diffusion coefficients at electric field strength E
C     K is the ion mobility, MI and MN are the masses of the ion and
```

```
C     buffer gas particles in amu and T is the temperature in K.
      IMPLICIT REAL*8 (A-H,O-Z), INTEGER*4 (I-N)
      REAL*8 K,E,MI,MN,T,D0,DL,DT,VD,Q,KB,X,MASS
      MASS=1.66D-27
      Q=1.6022D-19
      KB=1.38066D-23
      VD=K*E
      D0=KB*T*K/Q
      X=MASS*MN*(VD**3)/(3.*(MN+1.908*MI)*Q*E)
      DL=D0+(MN+3.72*MI)*X
      DT=D0+(MN+MI)*X
      RETURN
      END

      SUBROUTINE MAXMIN(Y,N,XMAX,YMAX,YMIN)
C     Finds the maximum and minimum values a function stored as discrete
C     values in array Y.  YMAX is found from quadratic interpolation
C     about the maximum.  XMAX is the position of the maximum 1<XMAX<N
      IMPLICIT REAL*8 (A-H,O-Z), INTEGER*4 (I-N)
      REAL*8 Y(N),XMAX,YMAX,YMIN
      INTEGER*4 N,NMAX
      YMIN=+1.D37
      YMAX=-1.D37
      NMAX=0
      DO 1 I=1,N
         IF (Y(I).GT.YMAX) THEN
            YMAX=Y(I)
            NMAX=I
         END IF
         IF (Y(I).LT.YMIN) YMIN=Y(I)
 1    CONTINUE
      IF ((NMAX.EQ.1).OR.(NMAX.EQ.N)) THEN
         XMAX=DBLE(NMAX)
         YMAX=Y(NMAX)
         RETURN
      END IF
      A=0.5D0*(Y(NMAX+1)-2.*Y(NMAX)+Y(NMAX-1))
      B=Y(NMAX)-Y(NMAX-1)-A
      C=Y(NMAX-1)
      XMAX=-B/(2.*A)
      YMAX=(A*XMAX+B)*XMAX+C
      XMAX=XMAX+DBLE(NMAX-1)
      RETURN
      END

      SUBROUTINE INPUT(NAME1)
C     finds the relevant experimental details from ATD.DATA
C     corresponding to experiment NAME1
      IMPLICIT REAL*8 (A-H,O-Z), INTEGER*4 (I-N)
      CHARACTER*13 NAME1,NAME2
      CHARACTER*10 TITLE(3)
C
      REAL*8 DIST,SIGM,E,EN,PRES,TEMP
      INTEGER*4 TI,TF,STEP,ISIG(100),NUM
      COMMON /D/ DIST,SIGM,E,EN,PRES,TEMP,TI,TF,STEP,ISIG,NUM
C
      REAL*8 MA,K0A,D0A,DTA,DLA,VDA,KA,AA          /* primary ion
      COMMON /A/ MA,K0A,D0A,DTA,DLA,VDA,KA,AA
C
      OPEN (8,FILE='ATD.DATA',STATUS='OLD')        /* data file
 5    READ (8,6,END=7) NAME2
 6    FORMAT(A13)
      IF (NAME1.EQ.NAME2) GO TO 8                  /* find data
      GO TO 5
 7    WRITE (6,9) NAME1
 9    FORMAT ('arrival time data for ',A13,' has not been found')
```

```
      STOP
8     READ (8,*) DIST,SIGM,E,PRES,TEMP,TI,TF,STEP
      E=E*100.                                        /* V/cm --> V/m
      DIST=DIST+0.57                                  /* true geometric distance
      DENS=3.535D16*PRES*(273.15/TEMP)
      EN=E /DENS*1.D15                                /*  in Td
      READ (8,2) (TITLE(I),I=1,3)
2     FORMAT(3A10)
      NUM=(TF-TI)/STEP+1
      READ (8,*) (ISIG(I),I=1,NUM)
      WRITE (6,1) NAME1,(TITLE(I),I=1,3),DIST,EN,E*0.01,PRES,DENS,TEMP
1     FORMAT (/'data file       : ',1X,A13
     #        /'details         : ',1X,3A10
     #        /'drift distance  : ',1X,F5.2,' cm'
     #        /'E/N             : ',1X,F5.1,' Td'
     #        /'electric field  : ',F6.2,' V/cm'
     #        /'pressure        : ',1X,F5.3,' Torr'
     #        /'number density  : ',D10.3,' /cm3'
     #        /'temperature     : ',F5.0,' K')
      DIST=DIST*0.01
      CLOSE (8,STATUS='KEEP')
      RETURN
      END
```

(iii) ATD

This program collects the arrival time distribution of an ion in the drift tube. It scans through a range of drift times and accumulates the ion signal at each time. The scanning finishes when 'ESC' pressed during a scan. If noise spikes or other anomalies occur which render the current scan invalid it can be lost by pressing 'A'. To begin scanning again 'B' can be pressed during execution.

```
 10  REM ATD.PROGRAM
 16  TEXT : HOME
 18  REM ----------------------
 20  GOSUB 700
 22  REM PIA SETUP
 24  REM ----------------------
 26  GOSUB 600
 28  REM DECLARATIONS
 30  REM ----------------------
 38  GOSUB 300
 40  REM EXPT. DETAILS
 42  REM ----------------------
 48  GOSUB 100
 50  REM COLLECT DATA
 52  REM ----------------------
 54  GOSUB 200
 56  REM LAGRANGE INTERPOLATION
 58  REM ----------------------
 60  GOSUB 400
 62  REM PRINT RESULTS
 64  REM ----------------------
 66  GOSUB 500
 68  REM DRAW GRAPH
 70  REM ----------------------
 72  GOSUB 900
 74  REM SAVE DATA
 76  REM ----------------------
 77  PRINT :
     PRINT  CHR$(4); "OPEN K,D1" : PRINT  CHR$(4); "CLOSE K" :
     PRINT
 78  RUN
 80  END
100  REM ------------------------------------------------------------------
102  REM SCAN LOOP
104  POKE -16368,0 : PRINT : PRINT "hit any key to begin"; : GET K$ : PRINT
106  NS=1
108  POKE -16368,0 : REM CLEAR KEY BUFFER
110  PRINT  CHR$(4); "BLOAD PULSEMC,A$6000,D1"
112  POKE 24813,CY : REM  $60ED
114  EP=24611+INT((MX-3.999)/2) :
     POKE EP,76 : POKE EP+1,221 : POKE EP+2,96 : REM JMP $60DD
116  HOME : PRINT F$; "  "; : INVERSE : PRINT "SCAN "; NS : NORMAL : PRINT
   : PRINT "time   sig.    acc.    last"
118  FOR DP=MN TO MX STEP T
120     DI=INT(DP/2) : CA=24600+DI
```

```
122      RESTORE :
         FOR I=CA TO CA+8 :
            READ D
124         POKE I,D :
         NEXT I
126      DATA 140,10,199,234,234,234,141,10,199
128      REM  STY $C70A  NOP NOP NOP STA $C70A
130      IF DI*2 < > DP THEN  POKE 24797,234 : POKE 24602,72 : GOTO 134
132      POKE 24602,234 : POKE 24797,72
134      PRINT  FN F(DP); TAB( 8);
136      CALL 24576
138      FOR I=CA TO CA+8 : POKE I,234 : NEXT : REM NOP'S
140      IS(DP)=IS(DP)+CNT(DP)
142      CNT(DP)=65536*PEEK(P2)+256*PEEK(P3)+PEEK(P1)
144      PRINT CNT(DP); TAB( 16); CNT(DP)+IS(DP); TAB( 24); IS(DP)
146   NEXT DP
148   AK=PEEK(-16384) : IF AK=155 THEN POKE -16368,0 : GOTO 154
149   IF AK=194 THEN
         FOR DP=MN TO MX STEP T :
            CNT(DP)=0 : IS(DP)=0 :
         NEXT :
      GOTO 106
150   IF AK=193 THEN NS=NS-1 :
         FOR DP=MN TO MX STEP T :
            CNT(DP)=0 :
         NEXT
152   NS=NS+1 : GOTO 108
154   FOR DP=MN TO MX STEP T
156      IS(DP)=IS(DP)+CNT(DP)
158      IF IS(DP)=0 THEN IS(DP)=.1
160      SS(DP)=IS(DP)
162   NEXT DP
164   PRINT : PRINT
166   DP=DP-1 : T2=2*T
199   RETURN
200   REM ----------------------------------------------------------------
201   REM SMOOTH SIGNAL
202   REM LAGRANGE INTERPOLATION
208   FOR I=MN+T2 TO DP-T2 STEP T
210      SS(I)=(-3*IS(I-T2)+12*IS(I-T)+17*IS(I)+12*IS(I+T)-3*IS(I+T2))/35
212   NEXT I
213   REM FIND MAX IN SMOOTHED SIGNAL
214   FOR I=MN+T2 TO DP-T2 STEP T
215      IF SS(I) > LS THEN LS=SS(I) : IM=I
216   NEXT I
217   REM ACCURATE MAXIMUM
218   I=IM-.75*T : LM=0
220   LB= FN LB(I) : IF LB > LM THEN LM=LB : I=I+.05*T : GOTO 220
221   I=I-.05*T
224   SM= FN F(I)
226   VD=DR /(CC*1E-6*I)
228   PC=PR/760*273.15/TK
230   RM=VD*PC/E
231   REM FIND MINIMUM
232   MS=9E37
233   FOR I=MN TO DP STEP T
234      IF SS(I) < MS THEN MS=SS(I)
235   NEXT
299   RETURN
300   REM ----------------------------------------------------------------
301   REM EXPT DETAILS
302   INPUT "run number? "; RN : GOSUB 340 :
      F$="ATD."+LEFT$(DA$,2)+MID$(DA$,4,2)+RIGHT$(DA$,2)+"."+STR$(RN)
304   HOME
306   PRINT F$ : PRINT
308   INPUT "ion details        > "; ID$
```

```
309  ID$=ID$+"  "+DA$+"  "+WD$+"  "+TI$
310  INPUT "pressure    (Torr) > "; PR
311  INPUT "temperature     (C) > "; TC
312  INPUT "source pos.    (mm) > "; DD
313  REM  DRIFT TUBE VOLTAGES
314  TK=TC+273.15 : DR=(100-DD)/10+.67
315  INPUT "E/N           (Td) > "; EN
317  POKE -16368,0 :
     PRINT "any changes (Y/N)  > "; : GET K$ : PRINT K$ :
     IF K$="Y" THEN  PRINT : GOTO 308
319  E=EN*96.58*PR/TK : PRINT
320  PRINT "V(gradient)       = "; FN G(E); " V/cm"
321  PRINT "V(rings)          = "; FN G(10.5*E); " V"
322  PRINT "2V(source-sleeve) = "; FN G(E*2*.67); " V"
323  PRINT "V(tracking)       = "; FN G((DR-.63)*E)
324  PRINT
329  INPUT "min. time >=6 us   > "; MN : IF MN < 6 OR MN > 370 THEN 329
330  INPUT "max. time =<371 us > "; MX : IF MX > 370 THEN 330
331  TC=(MX+50)/1E6
332  INPUT "time increment us  > "; T
333  IF  INT((MX-MN)/T) < 4 THEN 329
334  INPUT "sample time s      > "; CY : TT=CY : CY=CY/TC
335  CY= INT(CY/256) : IF CY=0 THEN  PRINT "Too short" : GOTO 334
336  IF CY > 255 THEN  PRINT "Too long" : GOTO 334
337  POKE -16368,0 :
     PRINT "any changes(Y/N)   > "; : GET K$ : PRINT K$ :
     IF K$="Y" THEN 324
338  RETURN
339  REM READING THE REALTIME CLOCK
340  A=49362 : B=A-1
341  I=0 : POKE B,16 :
     FOR EE=44 TO 32 STEP -1 :
        POKE A,EE : X(I)= PEEK(A) : I=I+1 :
     NEXT EE
342  IF F > 7 THEN P$=" "
343  IF X(4) > 3 THEN X(4)=X(4)-4
344  F=X(7)
345  IF F > 7 THEN P$=" "
346  IF X(7) > 7 THEN X(7)=X(7)-8
347  IF F < 8 AND X(7) < 4 THEN P$="am"
348  IF F < 8 AND X(7) > 3 THEN P$="pm"
349  IF X(7) > 3 THEN X(7)=X(7)-4
350  DA$= STR$(X(4))+STR$(X(5))+"/"+STR$(X(2))+STR$(X(3))
        +"/"+STR$(X(0))+STR$(X(1)) : REM DATE
351  TI$= STR$(X(7))+STR$(X(8))+"-"+STR$(X(9))+STR$(X(10))
    +" "+P$ : REM TIME
352  POKE B,0
399  RETURN
400  REM ------------------------------------------------------------------
401  REM PRINT RESULTS
402  IF PO THEN  PRINT O$
403  PRINT F$; "  "; ID$ : PRINT
404  PRINT "temperature          "; TK-273.15; " C"
405  PRINT "pressure             "; PR; " Torr"
406  PRINT "E/N                  "; INT(EN+.5); " Td"
412  PRINT "drift distance       "; DR; " cm"
413  PRINT NS; " scan(s) with "; TT; " second counting time"
415  PRINT "signal max after     "; SM; " us"
418  PRINT "drift velocity       "; INT(VD); " cm/s"
421  PRINT "reduced mobility     "; RM; " Td" : PRINT
422  PRINT "V(gradient)       = "; FN G(E); " V/cm" :
     PRINT "V(rings)          = "; FN G(10.5*E); " V"
423  PRINT "2V(source-sleeve) = "; FN G(E*2*.67); " V" :
     PRINT "V(tracking)       = "; FN G((DR-.63)*E)
424  PRINT :
     PRINT "time   exp sig   smooth sig   norm. sig"
```

```
427  FOR I=MN TO DP STEP T :
        PRINT  FN F(I); TAB( 8); FN H(IS(I)); TAB( 18); FN H(SS(I));
430     PRINT  TAB( 31) INT(SS(I)/LS*1000+.5) :
     NEXT I
433  PRINT OF$ : PRINT
499  RETURN
500  REM ----------------------------------------------------------------
502  REM DRAW GRAPH
503  POKE -16368,0 : GF$="PULSEPIC" : D$="D1" :
     PRINT "custom picture? "; : K$="N" : PRINT K$
504  IF K$="Y" THEN  POKE -16368,0 : PRINT "are you sure? "; :
        GET K$ : PRINT K$ :
        IF K$="Y" THEN  INPUT "file,drive no. "; GF$,DN :
     D$="D"+STR$(DN)
505  HGR2 : HCOLOR=3
506  PRINT :
     PRINT  CHR$(4); "BLOAD"; GF$; ",A$4000,"; D$
508  FOR I=MN TO DP STEP T
509     GY=(SS(IM)-SS(I)) /(SS(IM)-MS)*159+11
510     GX=257 *(I-MN) /(DP-MN)+21
511     G2=(SS(IM)-IS(I)) /(SS(IM)-MS)*159+11
512     IF GY < 191 AND GY > 0 THEN
           HPLOT GX-1,GY TO GX+1,GY :
           HPLOT GX,GY-1 TO GX,GY+1 : HCOLOR= 0 :
           HPLOT GX,GY : HCOLOR= 3
514     IF G2 < 192 AND G2 > =0 THEN  HPLOT GX,G2
516  NEXT I
518  TEXT : PRINT
522  IF PO THEN  PRINT O$ : PRINT  CHR$(9); "G2"
524  PRINT "Drift time from "; FN F(MN); " us to "; FN F(DP); " us"
526  PRINT "in steps of "; T*CC; " us"
529  PRINT  CHR$(12) : PRINT OF$
599  RETURN
600  REM ----------------------------------------------------------------
602  REM DECLARATIONS
604  DEF FN F(X)=INT(100*X*CC+.5)/100-.4
606  DEF FN G(X)=INT(100*X+.5)/100
608  DEF FN H(X)=INT(10*X+.5)/10
610  CC=.97752 : REM CLOCK CYCLE us
612  DIM IS(371),SS(371),CNT(371),X(13),Y$(7)
614  DIM X$(255)
616  DEF FN L4(X)=((X-IM-T) *(X-IM) *(X-IM+T)
                   *(X-IM+T2))/24*T
618  DEF FN L3(X)=((X-IM-T2) *(X-IM) *(X-IM+T)
                   *(X-IM+T2))/-6*T
620  DEF FN L2(X)=((X-IM-T2) *(X-IM-T) *(X-IM+T)
                   *(X-IM+T2))/4*T
622  DEF FN L1(X)=((X-IM-T2) *(X-IM-T) *(X-IM)
                   *(X-IM+T2))/-6*T
624  DEF FN L0(X)=((X-IM-T2) *(X-IM-T) *(X-IM)
                   *(X-IM+T))/24*T
626  DEF FN LB(X)= FN L0(X)*SS(IM-T2)+FN L1(X)*SS(IM-T)
                  +FN L2(X)*SS(IM)+FN L3(X)*SS(IM+T)
                  +FN L4(X)*SS(IM+T2)
634  PO=1
636  O$= CHR$(4)+"PR#1"
638  OF$= CHR$(4)+"PR#0"
699  RETURN
700  REM ----------------------------------------------------------------
702  REM PIA SETUP
704  HOME : INVERSE
706  PRINT "  PULSED DRIFT-TUBE OPERATION  "
708  PRINT "                               "
710  PRINT "ION DRIFT VELOCITY MEASUREMENTS" : NORMAL : PRINT : PRINT
714  P1=50948 : Q1=50950 : P2=50952 : Q2=50954 : P3=50956 :
     Q3=50958 : P4=50964 : Q4=50966 : P5=50968 : Q5=50970
```

```
716  POKE P1+1,0 : POKE P1,0   : POKE P1+1,4
718  POKE P2+1,0 : POKE P2,0   : POKE P2+1,4
720  POKE P3+1,0 : POKE P3,0   : POKE P3+1,4
722  POKE P4+1,0 : POKE P4,0   : POKE P4+1,4
724  POKE P5+1,0 : POKE P5,255 : POKE P5+1,4
726  POKE Q1+1,0 : POKE Q1,0   : POKE Q1+1,4
728  POKE Q2+1,0 : POKE Q2,255 : POKE Q2+1,4
730  POKE Q3+1,0 : POKE Q3,255 : POKE Q3+1,4
732  POKE Q4+1,0 : POKE Q4,255 : POKE Q4+1,4
734  POKE Q5+1,0 : POKE Q5,255 : POKE Q5+1,4
799  RETURN
800  REM ------------------------------------------------------------------
802  REM DATA RECOVERY
806  PRINT : INPUT "filename > "; F$ : PRINT
808  PRINT  CHR$(4); "OPEN"; F$",D2"
810  PRINT  CHR$(4); "READ"; F$
812  INPUT DR,SM,E,PR,TK,MN,DP,T,ID$ :
     T2=2*T : DD=(10.67-DR)*10 : EN=E*TK/PR/96.58
814  FOR I=MN TO DP STEP T
816     INPUT IS(I)
817     SS(I)=IS(I)
818  NEXT I
820  PRINT  CHR$(4); "CLOSE"; F$
822  POP : GOTO 54
899  RETURN
900  REM ------------------------------------------------------------------
902  REM SAVE DATA
904  POKE -16368,0 : PRINT "do you want to store the data on disk? "; :
     GET K$ : PRINT K$ : IF K$="N" THEN 940
906  IF K$ <  > "Y" THEN 904
907  ONERR  GOTO 960
908  PRINT  CHR$(4); "OPEN"; F$",D2"
910  PRINT  CHR$(4); "WRITE"; F$
912  PRINT DR : PRINT SM
914  PRINT E : PRINT PR
916  PRINT TK : PRINT MN
918  PRINT DP : PRINT T
920  PRINT ID$
922  FOR I=MN TO DP STEP T
924  PRINT IS(I)
926  NEXT I
928  PRINT  CHR$(4); "CLOSE"; F$
935  RETURN
940  POKE -16368,0 : PRINT "are you sure? "; : GET K$ : PRINT K$ :
     IF K$="Y" THEN 999
950  GOTO 908
960  Y= PEEK(222) : IF Y=8 THEN  PRINT "I/O ERROR "; : GOTO 962
961  IF Y=9 THEN  PRINT "DISK FULL ";
962  PRINT "insert another disk and press any key"
963  POKE -16368,0 : GET K$
964  GOTO 900
999  RETURN
```

(iv) PULSEMC

The disassembled source code for the program PULSEMC is given below. This code is responsible for generating pulses and the time delay between. Before this routine is called, part of the code is overwritten to give the correct time delay. The code below is what would be set up for a delay of 11 clock cycles (10.75μs) between the pulses. The first computer pulse is active when low but the second is active when high. These correspond to bits seven and six of the PIA at hexadecimal address $C70A. The cycle counter is first set to zero then the ion counter is reset by setting bit four of the PIA to one. The PIA is rendered inactive (7hi, 6lo) before the X- and Y- registers are loaded with the first pulse and the second pulse only values respectively. When first loaded from disk the machine language instructions contain two hundrer NOP (No Operation) codes. The machine codes for enabling the second pulse are inserted by the BASIC program ATD to give the minimum time delay required. The minimum time possible correspondes to six clock cycles since four are used by the `STY $xxyy` command and at least one NOP taking two clock cycles is also required. After the second pulse is disabled another series of NOP's fills in time until the jump instruction is reached. This instruction is also inserted by the BASIC program and is positioned to allow the maximum time delay required between pulses to be used without overwritting the jump code. The sixteen bit counter formed by `v` and `v+1` is then incremented and compared to a value POKEd from the BASIC program corresponding to the required sampling time request. If cycling is completed the ion counts are latched through to the counter PIA's and control returns to BASIC. The machine code program is then reconfigured to correspond to the next time interval specified and the process repeated. The whole sequence from minimum to maximum time is be repeated until a satisfactory arrival time has been collected.

```
                                P2B=$C70A          ;6821 PIA Bit7=1st pulse
                                V = $48            ;Number of cycles
6000        A9 00         INIT LDA #$00           ;Initialize cycle count
6002        85 48              STA V
6004        85 49              STA V+1
6006        A9 90              LDA #%10010000     ;Reset ion count
6008        8D 0A C7           STA P2B
600B        A9 80              LDA #%10000000     ;Both pulses inactive
600D        8D 0A C7           STA P2B
6010        A2 C0              LDX #%11000000     ;1st pulse active (HI)
6012        A0 00              LDY #%00000000     ;2nd pulse active (LO)
6014        8E 0A C7    PULSE  STX P2B            ;Reset system
6017        8D 0A C7           STA P2B            ; and start 1st 4017
601A        48                 PHA                ; 3 clock cycles
601B        EA                 NOP                ; 2   "     "
601C        EA                 NOP                ; 2   "     "
601D        8C 0A C7           STY P2B            ; 4   "     " . Enable
6020        EA                 NOP                ;2nd 4017 for 10us.
6021        EA                 NOP                ;This code moved by BASIC
6022        EA                 NOP                ;calling program
6023        8D 0A C7           STA P2B
6026        EA                 NOP
6027        EA                 NOP
6028        EA                 NOP
6029        EA                 NOP
602A        EA                 NOP
602B        4C DD 60           JMP DLYEND         ;JUMP after delay
602E        EA                 NOP
602F        EA                 NOP
60DD        EA          DLYEND NOP
60DE        68                 PLA
60DF        18                 CLC
60E0        A5 48              LDA V
60E2        69 01              ADC #$01           ;Increment number of cycles
60E4        85 48              STA V
60E6        A5 49              LDA V+1
60E8        69 00              ADC #$00
60EA        85 49              STA V+1
60EC        C9 37              CMP #$37           ;Data POKEd here from BASIC
60EE        F0 05              BEQ NEXT
60F0        A9 80              LDA #%10000000     ;Both off state
60F2        4C 14 60           JMP PULSE          ;Pulse again
60F5        A9 A0         NEXT LDA #%10100000     ;Latch ion count
60F7        8D 0A C7           STA P2B
60FA        A9 90              LDA #%10010000
60FC        8D 0A C7           STA P2B
60FF        60                 RTS
```

Documented 6502 assembly language listing for PULSEMC.